# TURBULENCE AND FLAME INTERACTION FOR CONTROL OF FLAME LOCATION IN DIFFUSER COMBUSTOR

A Dissertation

by

Ibrahim Thamer Nazzal Nazzal

Submitted to the

Graduate School of Sciences and Engineering
In Partial Fulfillment of the Requirements for
the Degree of

Doctor of Philosophy

in the
Department of Mechanical Engineering

Özyeğin University

August 2018

# TURBULENCE AND FLAME INTERACTION FOR FLAME LOCATION CONTROL IN DIFFUSER COMBUSTOR

Approved by:


Asst. Prof. Dr. Özgür Ertunç, Advisor,

Department Mechanical Engineering

*Özyeğin University*

Prof. Dr. M. Pınar Mengüç

Department of Mechanical Engineering

*Özyeğin University*

Asst. Prof. Altuğ Başol Department of

Department of Mechanical Engineering

*Özyeğin University*

Prof. Dr. Bedii Özdemir

Department of Mechanical Engineering

*Istanbul Technical University*

Prof. Dr. Ali Koşar

Department of Mechatronics Engineering

*Sabanci University*


Date Approved: 3 August 2018

*To my family,*

*To my children (Abdullah, Yamamah, and Mohammed) and my wife,*

*& to my parents, my brothers and my sister*

# ABSTRACT

Achieving an appropriate flame location is desirable in many combustion system applications especial in the design of the combustion system. Given that the characteristics of turbulent flows influence flame behavior and the design of combustion systems, flame location can be controlled within desirable levels without distorting the design of the combustor geometry by selecting suitable characteristics. A feedback control method utilizes the characteristics of turbulent flows to stabilize the flame location within the desirable level. The primary objective of this study is to introduce a strategy for flame location control using characteristics of turbulence flow. Turbulence intensity and length scale are among the main parameters of turbulent flow. Therefore, the secondary goal of this study is to investigate the influence of turbulence intensity and length scale on flame location.

The investigation of the dependency of flame location on turbulence is based on selecting suitable combustor geometry. For this purpose, the axisymmetric diffuser form is used to reveal the response of the flame location of a turbulent premixed flame that has been exposed to various turbulence intensities and length scales. The diffuser is selected because the flow slows down along the direction. Thus, the flame is expected to propagate towards the inlet when the flame speed increases. In this manner, the effect of turbulence can be studied without changing the thermal power. In addition, the diffuser combustor is used to avoid blow-off and flame extinction because the flow slows along the combustor. Two types of diffuser combustors are selected for this study. The first combustor is a cylindrical diffuser, while the second one is a cylindrical diffuser with a conical insert. Numerical simulations are applied to the diffuser combustor for turbulent premixed propane flames by using a coherent flame model integrated to the Reynolds-averaged Navier–Stokes flow model with k-epsilon turbulence model.

Firstly, the influence of turbulence on flame location in a diffuser-type combustor is studied under steady-state conditions. Results show that the flame location moves towards the inlet of the diffuser combustor with the increase in turbulence intensity for moderate- and high-turbulence length scales. The behavior of flame location is different in the low-turbulence length scale. The flame location initially decreases with the increase in turbulence intensity and subsequently stabilizes. Furthermore, the flame area density influences the flame location with the increase in turbulence intensity and turbulence length scale. Turbulence intensity and length scale simultaneously influence the flame area density, flame shape, and flame location.

Secondly, the results of the unsteady simulations indicate that turbulence intensity, length scale, and flow separation exert a significant effect on the flame location of the premixed turbulent combustion. The flame front moves toward the diffuser inlet as a result of the increase in turbulence intensity and length scale. The flame location drops to the middle of the diffuser for the high turbulence intensity. However, the effect of turbulence intensity is more visible than that of turbulence length scale within the tested range. An increase in turbulent length scale at a constant turbulence intensity causes a decrease in flame location. It is observed that the combustion and inlet turbulence cause a flow separation mainly downstream of the flame front. Consequently, the secondary flow structures influence the flame topology and location. Therefore, the flame location and shape are influenced by the flow separation and the turbulence intensity and length scale.

Thirdly, a conical insert is placed in the middle of a diffuser-type combustor to eliminate the flow separation. The influence of turbulence on flame location in two diffuser-type combustors (with and without conical insert) is studied and compared. Results indicate that the flame moves towards the inlet of the diffuser with the increase in turbulence intensity and length

scale in the two diffuser-type combustors. At a high-turbulence length scale, the flame rapidly drops at the inlet of the diffuser with a conical insert with the increase in turbulence intensity, whereas the flame drops to an intermediate level when the diffuser is not used with a conical insert. Moreover, a similarity was observed in the trends of the flame location at low turbulence intensities in both cases. Results show that the Taylor-scale Reynolds number is the influential parameter of flame location and not turbulence intensity and length scale. An increase in the Taylor-scale Reynolds number leads the flame location to move towards the combustor inlet. The flame drops to the inlet of the combustor at a high-turbulence Taylor-scale Reynolds number. Flow separation is observed in the diffuser without a conical insert, and flow separation is eliminated by using the conical insert.

Finally, the control of the flame location in the diffuser combustor is studied under various turbulent flow characteristics. A control strategy is suggested for this purpose. Control algorithm written as a Java macro is implemented to a commercial CFD software, namely STAR CCM+. This framework is utilized to perform all the simulations for the premixed turbulent flame under unsteady-state controlled conditions. The algorithm is built to adjust the turbulent kinetic energy and turbulent dissipation rate. Feedback control is introduced to stabilize the flame location at the desired level. Results indicate that control of the turbulent kinetic energy at the inlet control the flame location within the targeted level. In addition, it is observed the flame location moved to a low level for high turbulent kinetic energy whilst it moved to the high level for low turbulent kinetic energy.

# ÖZETÇE

Uygun alev konumu, yanma sistemlerinin uygulamalarında, özellikle yanma sistemlerinin tasarımında talep edilir. Sınır koşulları, yanma odası geometrisi ve türbülans akış geometrisi gibi birçok parametre alev davranışını etkiler. Verilenlere göre türbülans akışlarının özellikleri, alev davranışını ve yanma sisteminin tasarımını etkiler. Alev konumu, yanma odasının geometrisinin uygun özelliklerin seçimi ile tasarımı bozmadan istenilen seviyeler içinde kontrol edilebilir. Bir geri bildirim kontrol yöntemi alev konumunu istenilen seviyelerde kararlı hale getirmek için türbülans akışın özelliklerinden yararlanır. Bu çalışmanın esas amacı türbülans akışın özelliklerini kullanarak alev konum kontrolü için bir strateji ortaya koymaktır. Türbülans şiddeti ve uzunluk ölçüsü, türbülanslı akışın ana parametreleri arasındadır. Bu yüzden, bu çalışmanın ikinci amacı alev konumunda türbülans şiddeti ve uzunluk ölçüsünün etkilerini araştırmaktır.

Alev konumunun türbülansa bağlılığının araştırılması, uygun bir yanma odası geometrisinin seçilmesine dayanır. Bu amaçla, simetrik eksenli difüzör şekli türbülanslı değişik türbülans şiddetlerine ve uzunluk ölçülerine maruz kalmış önceden hazırlanmış alevin alev konumunu ortaya çıkarmak için kullanılır. Akışın yön boyunca yavaşlaması nedeniyle difüzör seçildi. Bu nedenle, alev hızı arttığı zaman alevin içeri doğru yayılması beklenilir. Bu şekilde, Termal güç değişimi olmadan türbülans etkisi çalışılabilir. Ek olarak, yanma odası boyunca yavaşlayan akış nedeniyle, alev sönmesi ve boşaltmadan kaçınmak için difüzör yakıcı kullanılır. Bu çalışma için iki tip yakıcı difüzör seçildi. Birinci yakıcı silindirik bir difüzör iken ikincisi konik eklemeli silindirik difüzördür. Türbülanslı önceden karıştırılmış propan alevleri için difüzör yakıcıya, Reynolds-ortalamalı Navier-Stokes akış modeline k-epsilon türbülans modeli ile entegre edilmiş uyumlu bir alev modeli kullanılarak sayısal simülasyonlar uygulanmıştır.

İlk olarak, bir difüzör tipli yanıcıdaki türbülansın alev konumu üzerindeki etkisi kararlı durumlar altında çalışıldı. Sonuçlar, alev konumunun, orta ve yüksek türbülans uzunluk ölçüleri için türbülans yoğunluğundaki artışla birlikte difüzör yanma odasının girişine doğru hareket ettiğini göstermektedir. Düşük türbülans uzunluk ölçülerinde alev konumu davranışları farklıdır. Alev konumu türbülans şiddetindeki artışla beraber başlangıçta azalır ve sonra kararlı hale gelir. Ayrıca, alev alanı yoğunluğu türbülans şiddeti ve türbülans uzunluk ölçüsündeki artış ile birlikte alev konumunu etkiler. Türbülans şiddeti ve uzunluk ölçüsü aynı zamanda alev alanı yoğunluğu, alev şekli ve alev konumunu etkiler.

İkinci olarak, kararsız simülasyonların sonuçları, türbülans şiddeti, uzunluk ölçüsü ve akış ayrımı önceden karıştırılmış türbülans yanmasının alev konumu üzerindeki önemli bir etki uyguladığını belirtir. Türbülans şiddeti ve uzunluk ölçüsündeki artışın sonucu olarak alevin ön tarafı difüzörün içine doğru hareket eder. Alev konumu yüksek türbülans şiddeti için difüzörün ortasına düşer. Bununla birlikte, test aralığında türbülans şiddetinin etkisi türbülans uzunluk ölçüsünün etkisinden daha görünebilirdir. Sabit türbülans şiddetinde türbülans uzunluk ölçüsündeki artış, alev konumunda azalmaya sebep olur. Yanma ve giriş türbülansının, esas olarak alev ön tarafında akış yönünde bir akış ayrımına neden olduğu gözlenmiştir. Sonuç olarak, ikincil akış yapıları alev topolojisi ve konumunu etkiler. Bu nedenle, akış konumu ve şekli; akış ayrımı, türbülans şiddeti ve uzunluk ölçüsünden etkilenir.

Üçüncü olarak, akış ayrımını ortadan kaldırmak için difüzör tipli yakıcının ortasına bir konik ek yerleştirildi. İki tip difüzörün (konik ekli ve eksiz) alev konumu üzerindeki türbülansın etkisi çalışıldı ve karşılaştırıldı. Sonuçlar, alev, iki difüzör tipli yakıcıda türbülans şiddeti ve

uzunluk ölçüsündeki artışla difüzörün girişine doğru hareket ettiğini gösterir. Yüksek türbülans uzunluk ölçüsünde, alev, türbülans şiddetindeki artışla konik bir ekleme ile difüzörün girişinde hızla düşer, oysa difüzör konik bir ek ile kullanılmadığında alev bir orta seviyeye düşer. Dahası, her iki durumda da düşük türbülans şiddetinde alev konumunun eğilimlerinde bir benzerlik gözlendi. Sonuçlar, Taylor-scale Reynolds sayısı türbülans şiddeti ve uzunluk ölçüsünün değil alev konumunun etkili parametresi olduğunu gösterir. Taylor-scale Reynolds sayısındaki bir artış alev konumun yanma odasının girişine doğru hareket etmesine neden olur. Yüksek türbülans Taylor-scale Reynolds sayısında alev yanma odasının girişine düşer. Akış ayırımı konik ekin olmadığı difüzörde gözlendi ve konik ek kullanılarak akış ayırımı ortadan kaldırıldı.

Son olarak, difüzör yakıcıda alevin kontrolü farklı türbülanslı akış özellikleri altında çalışıldı. Bu amaç için bir kontrol stratejisi önerildi. Java makro olarak yazılan kontrol algoritması, ticari bir CFD yazılımına, yani STAR CCM + 'ya uygulanır. Bu yapı iskeleti, kararlı hal kontrollü koşullar altında önceden karıştırılmış türbülanslı alev için tüm simülasyonları gerçekleştirmek için kullanılır. Algoritma türbülans kinetik enerjisini ve türbülans dağılım oranını ayarlamak için yapıldı. Alev yerini istenen seviyede sabitlemek için geri besleme kontrolü uygulanır. Sonuçlar girişteki türbülanslı kinetik enerjinin kontrolü, hedeflenen seviyedeki alev yerini kontrol ettiğini gösterir. Buna ek olarak, düşük türbülanslı kinetik enerji için yüksek seviyeye hareket ederken, alev bölgesinin yüksek türbülanslı kinetik enerji için düşük bir seviyeye taşındığı gözlenmektedir.

# ACKNOWLEDGMENTS

Firstly, I would like to thank God Almighty for giving me the strength and determination to complete my Ph.D. thesis.

Secondly, I would like to express my gratitude to my advisor, Assistant Prof. Dr. Ozgur Ertunc, for his constant support, advice and guidance during my study, which have been instrumental in the preparation and arrangement of this thesis.

I would like to express my thanks to the committee members, Dr. Bedii Ozdemir, Dr. M. Pinar Menguc, Assistant Professor Altuğ Başol and Professor Dr. Ali Koşar. I am very grateful to Prof. Dr. Bedii Ozdemir for offering many suggestions for my work. I am also veey grateful to colleague Alireza Razeghi.

I acknowledge the financial support provided by the Ministry of Higher Education in Iraq for my Ph.D. study and my stay in Istanbul, Turkey. I would also like to acknowledge the Scientific and Technological Research Council of Turkey (TÜBİTAK) for providing financial support for this research with the 114C113 project.

I would like to express my gratitude to my parents, sister and brothers for supporting and encouraging me during the study. Special thanks go to my wife and children for always being there for me. They have given up a lot to give me the opportunity to complete this work.

TABLE OF CONTENTS

**ABSTRACT** ..... iv
**ÖZETÇE** ..... vii
**ACKNOWLEDGMENTS** ..... x
**LIST OF TABLES** ..... xiv
**LIST OF FIGURES** ..... xv
**NOMENCLATURE** ..... xx
**CHAPTER I** ..... 1
**1 INTRODUCTION** ..... 1
***1.1 Introduction*** ..... 1
***1.2 Review of literature on turbulence and combustion interaction*** ..... 3
***1.3 Review of literature on combustor and flame configurations*** ..... 16
***1.4 Review of the combustion control*** ..... 18
***1.5 Review on the flame models*** ..... 23
***1.6 Review of turbulence models*** ..... 31
***1.7 Motivation*** ..... 35
***1.8 Methodology*** ..... 36
***1.9 Novel aspects*** ..... 39
***1.10 Research objectives*** ..... 39
***1.11 Structure of the thesis*** ..... 40
**CHAPTER II** ..... 43
**2 MATHEMATICAL MODEL** ..... 43
**2.1 *Fundamentals of turbulent premixed flame*** ..... 43
**2.1.1 Introduction** ..... 43
**2.1.2 Physical phenomena and simplification** ..... 43
**2.1.3 Turbulence** ..... 52
**2.1.4 Turbulence scales** ..... 54
**2.1.5 Taylor scale Reynolds number** ..... 56
**2.1.6 Flame thickness** ..... 57
**2.1.7 Laminar flame speed** ..... 58
**2.2 *Modeling strategies*** ..... 60
**2.2.1 Introduction** ..... 60
**2.2.2 Conservation governing equations** ..... 60

**2.3** ***Reynold - averaged Navier - Stokes equations*** ..... 63
**2.4** ***Flame model*** ..... 68
**CHAPTER III** ..... 72
**3 COMBUSTOR DESIGN AND NUMERICAL SIMULATIONS** ..... 72
***3.1 Introduction*** ..... 72
***3.2 Combustor design and numerical simulations*** ..... 73
**CHAPTER IV** ..... 83
**4 STEADY SIMULATIONS OF FLAME IN DIFFUSER COMBUSTOR** ..... 83
**4.1** ***Introduction*** ..... 83
**4.2** ***Effect of turbulence on the flame location*** ..... 83
**4.3** ***Turbulent kinetic energy*** ..... 88
**4.4** ***Flame area density*** ..... 92
**CHAPTER V** ..... 95
**5 UNSTEADY STATE SIMULATIONS OF FLAME IN DIFFUSER COMBUSTOR** .. 95
***5.1 Introduction*** ..... 95
***5.1 The Effect of turbulence on the flame location*** ..... 97
***5.2 The effect of secondary flow structures*** ..... 100
***5.3 Flame area density*** ..... 103
**CHAPTER VI** ..... 106
**6 UNSTEADY SIMULATIONS OF FLAME IN DIFFUSER COMBUSTOR WITH A CONICAL INSERT** ..... 106
***6.1 Introduction*** ..... 106
***6.2 The Effect of turbulence on the flame location*** ..... 107
***6.3 The effect of secondary flow structures*** ..... 111
***6.4 The effect of the Taylor Reynolds number*** ..... 117
***6.5 Turbulent kinetic energy*** ..... 122
***6.6 Flame area density*** ..... 126
**CHAPTER VII** ..... 130
**7 CONTROL OF FLAME LOCATION** ..... 130
***7.1 Control algorithm*** ..... 130
***7.2 Control of the flame location*** ..... 133
**CHAPTER VIII** ..... 141
**7.1 CONCLUSION AND FURTURE WORK** ..... 141

*8.1 Conclusions* ..... 141
**8.2** ***Future Work*** ..... 146
**APPENDIX** ..... 148
***Control algorithm*** ..... 148
**REFERENCES** ..... 163
**VITA** ..... 184

# LIST OF TABLES

Table 3-1 The physical simulations of the test, which is applied to the diffuser combustor..... 79

Table 3-2 Test cases at various turbulence intensities and length scales in the inlet of the combustor..... 81

Table 3-3 Test cases at various turbulence intensities and length scales in the inlet of the combustor..... 82

Table 5-1 The values of fluctuation velocities for different turbulence intensities and 5 cm length scale..... 96

# LIST OF FIGURES

Figure 1-1 Regime diagram for turbulent premixed combustion. ..... 4

Figure 1-2 The block diagram of the open-loop controller..... 19

Figure 1-3 The block diagram of the closed-loop controller. ..... 19

Figure 1-4 The types of the flame modeling scenarios. ..... 24

Figure 2-1 The interaction between radiation – turbulence and soot in the combustion process. 44

Figure 2-2 Instantaneous velocity via time. ..... 54

Figure 2-3 The temperature in Laminar flame speed..... 59

Figure 2-4 Fixed infinitesimal control volume $\Delta x1\ \Delta x2\ \ \Delta x3$ through which a fluid is flowing.61

Figure 3-1 Geometry of the diffuser combustor and boundary conditions. ..... 74

Figure 3-2 Number of cells of the mesh for 5% turbulence intensity and 1 cm turbulence length scale for the diffuser without conical insert. ..... 75

Figure 3-3 Flame location with the number of mesh cells for TI = 5% and $\ell$ = 1 cm. ..... 76

Figure 3-4 Geometry of the diffuser combustor with conical insert and boundary conditions. ... 77

Figure 3-5 the cross-section of the generated mesh and the upper and lower sections of the mesh diffuser with conical insert to clearly indicate the section of the mesh diffuser. The number of mesh cells is 506,387. ..... 78

Figure 3-6 Flame location with the number of mesh cells for TI = 5% and $\ell$ = 1 cm for steady state conditions..... 79

Figure 4-1 Locations of the flames in the turbulent combustion regime. ..... 84

Figure 4-2 Temperature contours with various turbulence intensities and turbulence length scales at the inlet of the diffuser. ..... 85

Figure 4-3 Flame location on the axial centerline of the diffuser combustor with various turbulence intensities and turbulence length scales. ..... 87
Figure 4-4 TKE along the axial centerline of the diffuser combustor at various turbulence intensities and at 1 cm turbulence length scale. ..... 89
Figure 4-5 TKE in the axial centerline of the diffuser at various turbulence intensities and at 5 cm turbulence length scale. ..... 90
Figure 4-6 Variation in TKE along the axial centerline of the diffuser combustor at various turbulence intensities for the 10 cm turbulence length scale. ..... 92
Figure 4-7 Maximum flame area density $FAD_{max}$ along the axial centerline of the diffuser with various turbulence intensities and length scales values. ..... 93
Figure 4-8 Integrated flame area over the diffuser for various turbulence intensities and length scales values. ..... 94
Figure 5-1 Flame locations on the premixed turbulent combustion regime (Borghi diagram) for all cases. ..... 97
Figure 5-2 Contours of temperature at different TI and $\ell$. ..... 98
Figure 5-3 Flame location normalized with the length of the diffuser at different TI and $\ell$. ..... 99
Figure 5-4 Contours of the line integral convolution (flow streamline). ..... 101
Figure 5-5 Turbulent kinetic energy along the axial direction of the diffuser combustor with various turbulence intensities and at 10-cm turbulent length scale. ..... 103
Figure 5-6 Profile of the flame area density for various TI and $\ell$. ..... 104
Figure 6-1 the location of the flame within the regimes of the turbulent premixed combustion. ..... 107

Figure 6-2 Temperature contours with various turbulence intensities and turbulent length scale on the diffuser without conical insert (left picture) and diffuser with conical insert (right picture) respectively. ..... 109

Figure 6-3 Flame location with various turbulence intensities and turbulent length scales for both diffusers (with and without conical insert). ..... 110

Figure 6-4 Contours of the line integral convolution (flow streamline) for the two cases (TI = 20 and ℓ = 10) and (30% and ℓ = 10) for the diffuser with conical insert and the diffuser without the conical insert. ..... 113

Figure 6-5 Temperature along the axial centerline for both diffusers (with and without conical insert) for (TI = 20% & ℓ= 10 cm) and (TI =30% & ℓ= 10 cm). ..... 114

Figure 6-6 The mean velocity along the axial centerline direction for both diffusers (with and without conical insert) for (TI = 20% & ℓ= 10 cm) and (TI =30% & ℓ= 10 cm)..... 115

Figure 6-7 The static pressure along the axial centerline direction for both diffusers (with and without conical insert) for (TI = 20% & ℓ= 10 cm) and (TI =30% & ℓ= 10 cm)..... 116

Figure 6-8 TKE along the axial direction for both diffusers (with and without conical insert) for (TI = 20% & ℓ= 10 cm). ..... 117

Figure 6-9 Temperature contours via Taylor-scale Reynolds number ($Re_{\lambda b}$) at the beginning of combustion for the diffuser combustor with conical insert. ..... 118

Figure 6-10 Flame location via $Re_{\lambda i}$ and $Re_{\lambda ib}$ for the diffuser combustor with conical insert. .. 119

Figure 6-11 the velocity along the X –axis from the centerline of the diffuser to the wall for the level 0.2 m from the inlet of the diffuser. ..... 120

Figure 6-12 the velocity along the X –axis from the centerline of the diffuser to the wall for the level 0.3 m from the inlet of the diffuser. ..... 121

Figure 6-13 the velocity along the X –axis from the centerline of the diffuser to the wall for the level 0.32 m from the inlet of the diffuser. ..... 121
Figure 6-14 TKE along the axial direction of the current diffuser with conical insert for various turbulence intensities and at 1-cm turbulent length scale. ..... 123
Figure 6-15 TKE along the axial direction of the current diffuser with conical insert for various turbulence intensities and at 5-cm turbulent length scale. ..... 124
Figure 6-16 TKE along the axial direction of the current diffuser with conical insert for various turbulence intensities and at 10-cm turbulent length scale. ..... 125
Figure 6-17 TKE along the axial centerline of the diffuser with conical insert for different Taylor-scale Reynolds number (the number on the curve is the values of $Re_{\lambda b}$). ..... 126
Figure 6-18 Contour of the flame area density via $Re_{\lambda b}$ for the diffuser combustor with conical insert. ..... 128
Figure 6-19 The comparison of the integrated flame area density (IFAD) over the axial direction of the diffuser combustor with conical insert for various TI and ℓ ..... 128
Figure 7-1 The scatter of turbulent kinetic energy, turbulent dissipation rate and fame location data and the model values. ..... 131
Figure 7-2 The schematic view of the control system that considers at the combustor inlet section. ..... 133
Figure 7-3 Flame Location Sensitivity to URF ..... 134
Figure 7-4 The flame location and TKE with physical time for the URF = 0.20. ..... 135
Figure 7-5 The flame location and TKE with physical time for the URF = 0.15. ..... 136
Figure 7-6 FL and TKE versus the physical time for the URF = 0.15 and at the flame location 0.34 m. ..... 137

Figure 7-7 FL and TKE versus the physical time for the URF = 0.15 and at the flame location 0.48 m. ..... 137

Figure 7-8 FL with physical various flame locations. ..... 138

Figure 7-9 TKE with physical various flame locations. ..... 138

Figure 7-10 The flame area density distribution on the diffuser for different flame location. ... 140

# NOMENCLATURE

| | |
|---|---|
| A | Area [$m^2$] |
| b | Progress reaction variable |
| $C_{EBU}$ | Constant of eddy break model [-] |
| $C_3 H_8$ | Propane [KPa] |
| $C_p$ | Specific heat at constant pressure [kJ/kg-K] |
| $CO_2$ | Carbon oxide [-] |
| D | Diameter [m] |
| Da | Damekohler [-] |
| $D_t$ | Mass diffusivity [$m^2$/s] |
| FL | Flame location [m] |
| FAD | Flame area density [m2/kg] |
| $FAD_{max}$ | Maximum flame area density [m2/kg] |
| IFA | Integrated flame area [$m^2$] |
| K | Turbulent kinetic energy [kj / kg. k] |
| Ka | Karlovitz number [chemical time scale / Kolmogorov time scale] |
| $K_t$ | Flame stretch [1/s] |
| $K_u$ | Thermal conductivity [W/m-K] |
| $Ka_\delta$ | Second Karovitz number [ reaction zone thickness * Ka ] |
| h | Enthalpy [kJ/kg] |
| $\ell$ | Turbulent length scale [m] |
| $\ell_f$ | Flame thickness [m] |

| | |
|---|---|
| M | Mass diffusivity |
| $N_2$ | Nitrogen [-] |
| NOx | Nitrogen oxides [-] |
| $\dot{m}$ | Mass flow rate [ $kg/m^3$] |
| $P_o$ | Pressure [KPa] |
| Pr | Laminar Prandtl number of the burnt gas [$C_p\ \mu / k_u$] |
| $P_o$ | Reference pressure [KPa] |
| $P_u$ | Pressure of the unburned gas [KPa] |
| $O_2$ | oxygen [-] |
| $Re_t$ | Turbulent Reynolds number [-] |
| Sc | Schmidt number [$\upsilon_t / D_t$]- |
| $S_L$ | Laminar flame speed [m/sec] |
| $S_L{}^0$ | Laminar flame speed [m/sec] |
| $S_{L0}{}^0$ | Reference laminar flame speed [m/sec] |
| $S_t$ | Turbulent flame speed [m/sec] |
| $u$ | Velocity [m/sec] |
| U | Mean Velocity [m/sec] |
| $T_o$ | Reference Temperature [K] |
| $T_u$ | Temperature of the unburned gas [K] |
| TKE | Turbulent kinetic energy [kJ/kg] |
| $u'$ | Fluctuation velocity [m/sec] |
| $u''$ | Fluctuation velocity with respect to the Favre-averaging [m/sec] |
| V | Volume [$m^3$] |

| | |
|---|---|
| x | Coordinate component [m] |
| Y | Axial direction along the diffuser [m] |
| $Y_{ft}$ | Mass fraction of unburnt gas [%] |
| $Y_f$ | Mass fraction [%] |
| $Y_{res}$ | Residual of fuel mass fraction [%] |
| $W$ | Constant of laminar flame speed |
| $Z$ | Constant of laminar flame speed |

**GREEK SYMBOLS**

| | |
|---|---|
| $\delta_l$ | The thermal boundary layer [m] |
| $\varepsilon$ | Turbulent dissipation rate [$m^2/s^3$] |
| $\eta$ | Constant of laminar flame speed [-] |
| $\Lambda$ | Constant of laminar flame speed [-] |
| $\lambda$ | Air – fuel ratio actual to stoichiometric [-] |
| $\lambda_r$ | Taylor microscale |
| $\mu_b$ | Molecular viscosity the burnt gas |
| $\upsilon_t$ | Kinematic viscosity [m/s] |
| $\eta_k$ | Small length scale [m] |
| $\xi$ | Constant of laminar flame speed [-] |
| $\rho$ | Density [kg/ $m^3$] |
| $\rho_u$ | Density of the unburned [$kg/m^3$] |
| $\Sigma$ | Flame area density per volume [$m^2$ /$m^3$] |

| | |
|---|---|
| $\sigma$ | Flame area density per mass [$m^2$ /kg] |
| $\theta$ | quantity [-] |
| $\psi$ | Constant of laminar flame speed [-] |
| $\tau$ | the ime scale of eddy beak model [sec] |
| $\eta_k$ | Kolmogorov microscale |
| $\tau$ | Time scale |

***ABBREVIATIONS***

| | |
|---|---|
| $A$ | Constant of the Turbulent flame closure |
| $\tilde{c}$ | Un-normalized reaction variable |
| B | Model parameter |
| BML | Bray–Moss–Libby |
| CFD | Computational fluid dynamic |
| CFM | Coherent flame model |
| CV | Control volume |
| $C_\mu$ | Constant of renormalization $k$- $\varepsilon$ model |
| $C_{\varepsilon 2}$ | Constant of dissipation in the $k$- $\varepsilon$ model |
| diffloc | The difference between the goal flame location and current flame location |
| DNS | Direct numerical simulation |
| EBU | Eddy break model |
| LES | Large eddy simulation |
| PCFM | Partially coherent flame model |

| | |
|---|---|
| PDF | Probability density function |
| PEBU | Premixed Eddy break model |
| PPDF | Persumed Probability density function |
| RANS | Reynolds-Averaged Navier-Stokes |
| RNG | renormalization |
| RMS | Root-mean-square |
| S | Source term |
| SF | Sensitivity factor |
| $S_f$ | Source term in terms of fuel mass fraction |
| $S_\Sigma$ | Source term in terms of a flame area density |
| TDR | Turbulent dissipation rate |
| TKE | Turbulent kinetic energy |
| TI | Turbulence intensity |
| TFC | Turbulent flame closure |
| TFM | Turbulent flame model |
| $\alpha$ | The constant parameter of the CFM model |
| $\beta$ | The constant parameter of the CFM model |
| $\Gamma_k$ | The ratio of the flame stretch to the k – epsilon |
| $\Gamma_p$ | The flame production due to the stretch |
| $\Gamma_q$ | The flame quench due to the stretch |
| $\phi$ | Any quantity |
| $\Omega$ | Any quantity |
| $\widetilde{....}$ | The Favre property |

$\overline{...}$ $\overline{...}$ The averaged property

... ...″ The Favre property with fluctuation

# CHAPTER I

# 1 INTRODUCTION

## *1.1 Introduction*

A large portion of the energy used for household heating and electricity production is generated from the combustion of fossil fuel. Combustion converts the chemical energy of fuel into heat energy. Combustion processes play a significant role in the design of combustion devices, such as gas turbines in power plants and spark ignition engines in transportation vehicles, rocket engines and furnaces [1-4]. However, some combustion products, such as NOx, are harmful to the environment and cause pollution. In recent years, the legislative restrictions for the protection of the environment have increased and have motivated researchers to focus on the development of combustion devices. Most studies on combustion systems aim to enhance the combustion process and reduce emission pollution. Many parameters influence the combustion process and its pollutions, such as combustor design, fuel type, and turbulent flow characteristics. Turbulent flow characteristics are one of the main parameters that influence flame behavior and the design of combustion systems. Contrary to the laminar flow, which occurs with no fluctuation between layers, fluctuations occur in the turbulent flow for the quantities of fluid motion, such as the velocity and pressure components with the time and location [5-8]. The mixing of the mixture, heat transfer, drag, and energy dissipation increases with the turbulence. In the combustion process, turbulence increases the mixing of fuel and air, thereby enhancing the burning of the flame.

The interaction between turbulence and combustion complicates the combustion process [9, 10]. However, turbulent combustion can be premixed, non-premixed or partially premixed, depending on the manner of air intake into the fuel flow. The fuel and the oxidizer are usually mixed before they enter the combustion chamber in premixed combustion. Meanwhile, the fuel remains separate from the air until it burns in non-premixed combustion where the reactants must diffuse towards each other before they react, which leads to the diffusion of flames. In a partially premixed flame, the mixing of air and fuel is incomplete [3]. Premixed combustion systems are preferred over non-premixed systems for their superiority in reducing pollutants. Turbulent premixed combustion is widely used in industrial applications in fields that involve thermal energy and power generation. In addition, lean turbulent premixed combustion can reduce pollution [3, 11].

The main problems in lean premixed combustion include flashback, flame blow-off and instability [12, 13]. Flashbacks occur when the flame propagates backward because the mixture velocity is lower than the flame velocity [14]. Flame stability is one of the main parameters in the design of combustion chambers, especially in lean premixed combustors, because of its strong effect on combustion conditions. Flame instability can extinguish the flame as the lean limit is approached. Therefore, most research on the interaction between premixed flame and turbulence focused on the main problems in combustion, such as flame instability and air pollution [12-15]. Previous studies also indicated that many parameters influence flame stability, such as combustor geometry, turbulent flow characteristics and NOx emissions.

A desirable flame location level is crucial in many applications to avoid blow-off and stabilize the flame. In addition, the blow-off limits need to be studied because they indicate the operation safety in any combustion system. Therefore, a smart control strategy for flame location

is crucial in keeping the flame at a desirable level and avoiding flashback. This chapter presents a review of the literature on turbulence and combustion interaction, control, the motivation and objectives of this study.

## *1.2 Review of literature on turbulence and combustion interaction*

Most problems in combustion include the strong coupling between turbulence and flame. The interactions between turbulence and flame play a role in the design of combustion systems, especially in the stabilization of flame. Many factors influence the stability and behavior of flames, such as turbulent flow characteristics, which include the turbulent Reynolds number, flame stretch, vorticity, turbulence intensity and length scale. In turn, heat release, which is the result of chemical reactions, changes fluid flow properties, such as density, flow velocity, and viscosity, thereby influencing the burning rate. Therefore, the interactions between the premixed flame and turbulent flow are divided into two parts: the influence of turbulence on the flame and the influence of flame on turbulent flow [3, 9, 10, and 16].

The studies of turbulent flame generally depend on the physical characteristics of the turbulent - flame interaction, especially the various values of time and length scales. Therefore, the effect of the dimensionless numbers, the time and length scales on the combustion process should be understood. Damkohler [17] was the first to address the effect of large-scale turbulence on the wrinkled flame in his pioneering work. In the turbulent flow processes, the time and length scales affect the premixed combustion process. Thus, researchers represented the time and length scales and others dimensionless numbers in terms of map regimes. Several researchers [18-20] introduced regimes for premixed turbulent combustion depending on the scales of the turbulence and the velocities ratio, which help researchers understand the effect of

turbulence on combustion [18, 21 and 22]. These regimes are essential in studies on turbulent combustion modeling. However, Borghi was the first to present the diagram of premixed turbulent combustion, as shown in Figure **1-1**. Researchers utilized the ratio of velocity scales over the ratios of length scales to build a diagram of premixed turbulent combustion. They identified the laminar flame region and four regions for the premixed turbulent flame that involves the regimes of wrinkled flamelets, corrugated flamelets, distributed reaction zones and a well-stirred reactor. The second and third regimes are more important because they describe the combustion–turbulence interaction [23, 24].

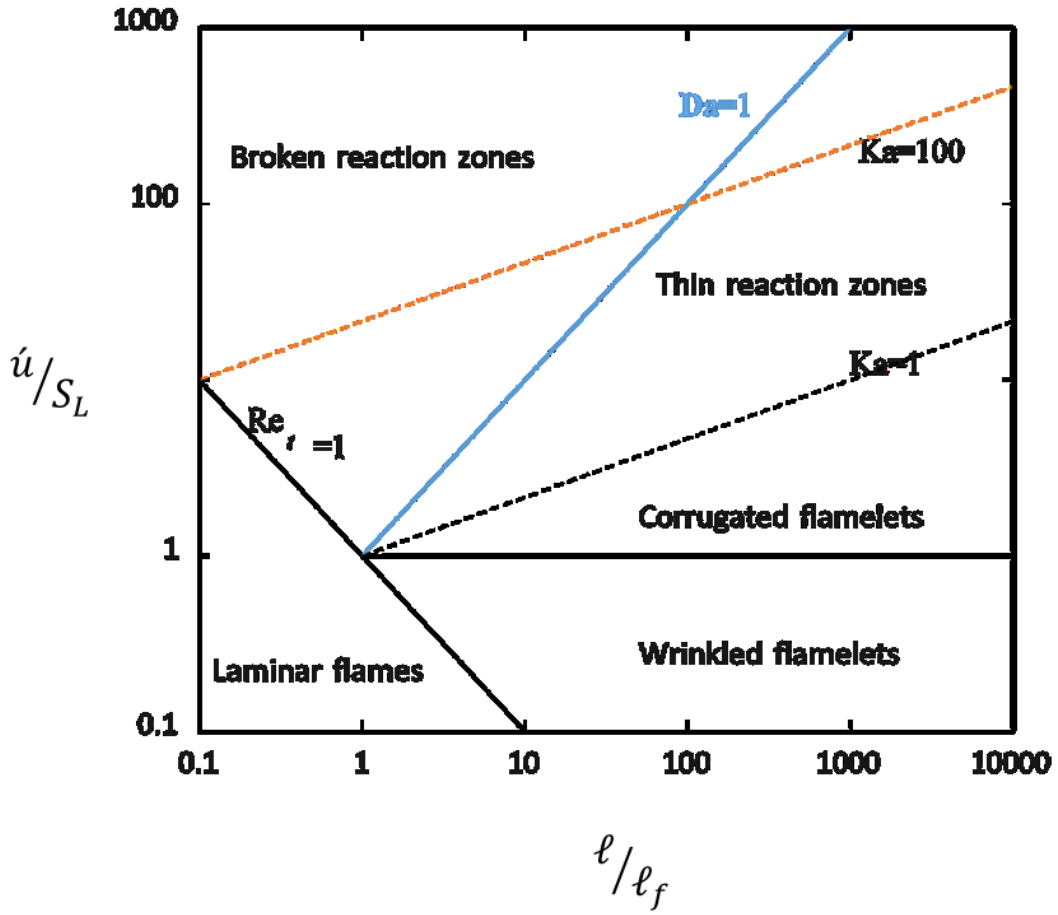


Figure 1-1 Regime diagram for turbulent premixed combustion.

Dimensionless numbers, which include the turbulent Reynolds number, ratio of the length scale to the flame thickness and the Karovoltiz number equal to the chemical time scale to smallest time scale, separate these regimes. The ratio of inertia to viscosity characterizes the turbulent flow that is represented by the turbulence Reynolds number ($Re_t$). The turbulence Karlovitz number, Ka, is a key in the diagram of premixed turbulent combustion that compares the ratio of laminar flame chemical timescale to the Kolmogorov timescale (smallest scale). The flow is laminar when the turbulent Reynolds number is less than the unity. Four other turbulent regimes exist if the Re > 1 region. In the wrinkled regime, the laminar flame speed is less than the fluctuation velocity.

In the flamelet regimes, the flame surface separates the unburnt and burned phases. The laminar flame propagation is wrinkled by turbulence in the wrinkled flamelet regime. The wrinkle in the flame surface increases with the turbulence intensity as pockets are created on the flame surface of this region of corrugated flamelets. In the flamelet regime, the Karlovitz number is less than 1, which means that the laminar flame scales are the smaller relevant scales of turbulence. Therefore, turbulent eddies wrinkle laminar flame. The line on the diagram is the Klimov–Williams line at Ka = 1, which separates the corrugated flamelet and the thin reaction zone. When the Karvoltiz number is greater than unity, the flame is transferred to the thin reaction zone [24]. The flame within the thin reaction zone enters the reactive diffusion flame structure when the smallest scale (Kolmogorov) is less than the flame thickness.

For high Karlovitz numbers, the flame enters the broken reaction zone. In this zone, the smallest scale (Kolmogorov) is less than the flame thickness but higher than the reaction thickness. Thus, the regimes of the premixed turbulent combustion are essential to the study of

the effect of turbulence on the flame. However, many studies have investigated the interaction between turbulence and flame.

Clavin and Joulin [25] studied premixed flames in a large-scale, high-intensity turbulent flow. They observed that the flame stretch might control the flame shape and motion of the front. Where the flame stretch is a quantity to measure the stretch in the surface of the flame because of the curvature and because of the strain of the outer velocity field. Furthermore, they found that the stretch is divided into two parts, strain tensor rates and mean curvature.

Aldredge and Williams [26] studied the effect of the wrinkled premixed flame dynamics of a large-scale, low-intensity turbulent flow. They observed that several parameters, including the influence of gas expansion, the phenomena of diffusive - thermal within the flame, buoyancy and the Lewis (the ratio of thermal diffusivity to mass diffusivity) and Prandtl numbers (the ratio of momentum diffusivity to thermal diffusivity), should be considered for large Zel'dovich numbers. Where the Zel'dovich number is a dimensionless number, which provides a quantitative value for the activation energy of a chemical reaction which appears in the Arrhenius exponent). They calculated the variations in parts of the turbulent flame and found a substantial change in the turbulence kinetic energy (TKE) components through the hydrodynamic regions. They observed that the root-mean-square (RMS) pressure oscillations are the highest near the flame, and the ratios of density are higher in the burnt zone than in the unburnt zone. They observed that the flame dynamics do not affect the vorticity field in the upstream hydrodynamic region. They found the longitudinal component of vorticity unmodified across the flame. They also observed that the flame increases the RMS transverse vorticity oscillation for realistic magnitudes of the gas expansion ratio. Finally, they found that when the

influences of the hydrodynamic regions are fully considered, the flame influences the anisotropy in the initially isotropic turbulence.

Zuhang and Rutland [27] used direct numerical simulation (DNS) to investigate the impact of premixed flame on turbulence and on the mean and fluctuation pressure. They examined the TKE budget for the influence of premixed flame on the turbulence within the fame brush. They compared the TKE within the flame brush with the non-reacting turbulence. They found that heat release strongly influences the turbulent flow and the high impact at high heat release. They also indicated that mean dilation and dissipation are considered the mean sink of turbulence. The pressure fluctuation terms remain the main source of turbulence at high heat release rates.

Giacomazzi et al. [28] introduced a study on simulating a bluff-body premixed flame that is anchored in a straight channel to test the fractal model applicability. They assumed in their model that chemical reactions occur only at the dissipating scales of turbulence, i.e. the instance near the so-called eddy dissipation. They calculated the local spatial dissipating scale using the model that considers the growth effect due to heat release. They analyzed both cases (cold flow and reacting) and for both two-dimensional and three-dimensional. They validated the simulation results with the experimental data and found that the recirculation zone downstream of the bluff body and the entraining fresh mixture into the hot recirculating region are periodically shortened by the 3D vortex structures. They found that the periodic boundary conditions could not capture the various impacts of sidewalls, such as the shortening of the re-circulation zone and the flow acceleration downstream. Their comparison of the kinetic energy spectral densities in the non-reacting and reacting cases indicated that large-scale fluctuations can suppress the latter and a fast chemical reaction causes a high-frequency energy peak.

Yuan et al. [29] studied the influence of turbulence and flame instability on flame front evolution. They performed their investigation at Lewis numbers 1.0 and 0.7, which was computationally achieved by using a sixth-order scheme of central differences for non-reflective boundary conditions. They changed the turbulence intensity from 1% to 50% and found that the turbulent flames are in the thin wrinkled flame region of the Borghi diagram. They observed that for low turbulence intensities, hydrodynamic instability dominates the growth of the flame cells. Meanwhile, for the high turbulence intensity is 50%, the turbulent motion wrinkles the flame front and dominates the evolution process. They also observed that the curvature stretch dominates the total stretch rate for flames with either low or high turbulence intensities.

Tang and Chan [30] examined the impact of turbulence on flame area density (FAD) and flame brush thickness in a rod-stabilized V-shaped flame. They compared the flame area densities using two models and indicated that the discrepancy between the two models becomes increasingly obvious with the increase in turbulence intensity.

Gulder and Smallwood [31] analyzed the effect of medium and high turbulence intensities on the FAD of a turbulent premixed flame in a Bunsen burner. They found the largest FAD at the highest turbulence intensity. Furthermore, they observed that turbulence intensity does not influence the integrated flame surface density across the flame brush significantly.

Han and Huh [32] investigated the role of displacement speed in the evolution of flame surface density with different Lewis numbers and turbulence intensities. They observed a high turbulence burning velocity at high turbulence intensity. They concluded that the turbulent flame speed increases with the total mean consumption speed. They observed that the flame surface

density is influenced by propagation flame and tangential strain. They also found that the mean strain changes linearly with the turbulence intensity.

Hartung et al. [33] experimentally examined the influence of heat release on the turbulence and scalar-turbulence interaction in premixed combustion. They used the bluff body to stabilize the flames in the thin region zones. They also used simulation OH- planar laser-induced fluorescence and stereoscopic particle pre-image velocimetry techniques in their study. They used a Canny edge detection algorithm to track the flame front. They focused on the effect of heat release on different mean turbulence quantities, such as integral length scale, fluctuations velocity and the probability density functions (PDFs) of the eigenvectors of the strain rate components. They indicated that heat release influences the size, shape, and characteristics of the recirculation region behind the bluff body. They observed that TKE is increased by the spatial intermittency in the flame front. In addition, the vortices of velocity fluctuations within the flame brush were larger than the magnitudes of the corresponding cold flow due to the intermittency of the flame front region. They also reported that heat releases are affected by the increase in the length and time scales of the turbulence. Heat releases increase the length and time scales of the turbulence. The acceleration of local flow by the flame front increases the skewness velocity gradients and the kurtosis of the PDFs of the strain rate tensor components.

Lipatnikov and Chomiak [34] studied the impact of premixed flames on turbulence and turbulent scalar transport. They utilized DNSs and experimental data to study the response of premixed combustion towards the change in basic characteristics, such as the fluctuating velocity field and the direction of scalar fluxes in a turbulent flow. They used different ways to modeling these phenomena and they emphasized the lack of a well-elaborated and widely validated

predictive method. They found that premixed flames may substantially influence a fluctuating velocity and the direction and value of turbulent scalar fluxes.

Fru et al. [35] investigated a premixed flame with various equivalence ratios under high turbulence intensities by using DNS. They investigated the effect of turbulence on the physical properties of the flame for the range of integral Reynolds numbers up to 4513. They concluded that consumption speed initially increases linearly, then, a bending zone emerges before the consumption speed decreases (quenching limit) with the increase in turbulence intensity. They observed that the fuel consumption rate increases with the turbulence intensity and that a correlation exists between the root-mean velocities and the laminar velocity. Their results indicated that for low-turbulence regions, the initial consumption speed increases linearly and then levels off (bending zone) before decreasing again (quenching limit) for highly intense turbulence. Finally, they observed that additional factors must be considered in the phenomenological expressions associated with two quantities (root-mean velocity to laminar velocity and consumption speed/laminar velocity) when the consumption speed/laminar velocity changes with the mixture equivalence ratio of the constant magnitude of the root-mean velocity to the laminar velocity.

Minamoto et al. [36] used DNS to simulate the turbulent combustion of the stoichiometric hydrogen-air mixture and dealt with complex chemical kinetics. They applied the simulation to freely propagating V-flames stabilized behind a hot rod. They studied the effect of a two-flame configuration on the turbulence–scalar interaction. This interactive process is not affected by these flame configurations. They found that the normal flame is aligned with the most extensive strain in the region of intense heat release. They also found that stabilized flame is a flamelet, and the Taylor theory of turbulent diffusion combustion represents the combustion in the rod

when the flame brushes are non-interacting. Finally, they observed that the thickness is saturated when the flame brushes interact.

Poludnenko and Oran [37] investigated the mechanisms for estimating the turbulent flame speed in the thin reaction zone regime. They conducted their study using DNSs of the premixed flame that interacts with the driven, subsonic, homogeneous, isotropic and Kolmogorov-type turbulence in an unconfined system. They used Athena-RFX and fully compressible, high-order, dimensionally unsplit, reactive-flow code and assumed one-step Arrhenius kinetics to simplify the reaction-diffusion model that represents a stoichiometric $H_2$–air mixture under the assumption of a Lewis number of 1. They drew many conclusions, which involve the structure of the peak reaction rate region represents the best global characterizations of the turbulent flame. In addition, they found that the increase in the surface area of the turbulent flame predominantly determines the TFS in the thin reaction zones regime that is caused by turbulence. Furthermore, on these conclusions, the increase in the speed turbulence relative to the speed laminar exceeds the related increase in the surface area of the turbulent flame relative to the surface area of the planar laminar flame. They observed in the cusps, the local flame speed substantially exceeds its laminar magnitude.

Hamlington et al. [38] studied the turbulence–flames interactions in the stoichiometric $H_2$-air premixed reacting flows for the ranges of turbulence intensities by using a scalar mass fraction, vortices, strain rate and scalar gradient. They used the reconstruction method for the internal stretch of flame by using the average condition of mass fraction. They found that for low-level turbulence, the flame structure is the same as that of the laminar flame and relatively little flame wrinkling exists. In addition, heat release captures the values of vortices and the strain rate for low turbulence intensity. The preheat zone is broadened and the alignment of the

local flame becomes increasingly isotropic as the turbulence intensity increases. Moreover, the orientation and the interactions between the local flame orientation, vortices and eigenvalues of the strain rates differ from those found in the non-reacting turbulence flow, particularly in the reaction zone of the low turbulence intensity. In their study, the effect of the strain rates on the flame width is the same as those found in the laminar flames of the low turbulence intensity. Finally, the interaction between the vortices, the strain rate components and the local flame orientation are the same as those found in non-reacting turbulence for high turbulence intensity.

Matalon and Creta [39] examined the turbulent flame speed of wrinkled premixed flames. They extended the asymptotic results to a fully nonlinear zone, which allows the systematic extraction of scaling laws for the turbulent flame speed that is based on the turbulence scale and intensity, thermal expansion and components of the mixture. They used the hybrid Navier–Stokes/front-capturing methodology that consisted of the asymptotic model. They dealt with the flame as a surface of density discontinuity that divides the unburned and burned zones. They simplified the model from 3D models to 2D turbulence by removing some 3D features. They discussed the conformations for the subcritical and supercritical where the critical defined respect to the good conditions which associated with laminar setting, therefore, they defined the subcritical. Conditions, the Flame stays planar on the average and for the super-critical, the flame was corrugated. They observed the existence of various scaling laws for both conditions (sub-critical and super-critical). They found that flame is highly correlated with increasingly sharp crests that point towards the burned zone for super-critical conditions. They observed for sub-critical conditions that the flame stays statistically planar. Finally, they observed that the various structures of the turbulent flame brush in these zones are characterized by their distinct statistical distributions.

Steinberg et al. [40] used high-repetition-rate stereoscopic particle image velocimetry to study the statistics and dynamics of the orientation strain rate and flame surfaces in the air–methane premixed combustion. They found that the statistics of the principal strain rate that is related to the turbulence are preferentially aligned more perpendicular than parallel to the normal flame surface direction. They observed a difference between the mean turbulence–flame alignments for various flames and found that stronger flames exhibit stronger preferential alignment. They also observed the greatest preferential alignment on the reactant side of the mean flame brush. They found that the orientation of the turbulence structure influences the flame surface. Finally, they found a decrease in the mean change in orientation from the unburnt to the burnt side of the flame brush that appears to be affected by the overall flame shape.

One of the first high-speed particle image velocimetry measurements was introduced by Chaudhuri et al. [41]. They used the technique to quantify the flame–turbulence interaction in central-ignited constant-pressure premixed flames. They indicated the mean flow velocity and fluctuation of flow velocity measurement for a range of conditions in the absence and presence of flame. In addition, they provided a range distribution of stretch rate. They observed that the non-Gaussian PDF could display normal straining tails, whereas tangential straining is near the Gaussian behavior. They also indicated that the expanding flame pushes the unburnt gases, generating a mean radially outward flow over the closeness of the flame for the multitude pressures and velocities of the fan. They compared stretch rate PDFs, especially tangential strain and normal strain, and indicated that a Gaussian distribution is followed by tangential strain, whereas stretched Gaussian profiles are followed by a normal strain with long tails. In addition, they found that the persistence/integral time scales that are related to stretch rate by pure

curvature is twice that of the tangential strain for the case of a 2D flame surface particle tracking method.

Bagdanavicius et al. [42] investigated the influence of stretch rate on flame surface densities in a turbulent premixed flame with a temperature and pressure of up to 673 K and 1.25 MPa, respectively. They derived a new overall correlation between the probability of the burning factor in terms of strain rate and the Markstein number at different Karlovitz numbers. They observed that the area that is related to turbulent burning velocity normalizes the wrinkling on the flame surface.

Aspden et al. [43] studied chemistry–turbulence interaction with 3D high-resolution DNSs in lean premixed hydrogen combustion at an equivalence ratio of 0.4, with a Karlovitz range of 1 to 36 for the turbulence levels. They found that the fuel consumption is greatly enhanced in regions of positive curvature, whilst heat is released in the region of negative curvature, which is adjacent to the fuel consumption region. They observed that the flame burned more intensely in the high Karlovitz range than in the low Karlovitz range as they analyzed the heat release by individual reactants. In addition, they observed that the radical pool is enriched throughout the entire flame when Karlovitz is increased. Finally, they recognized that high molar concentrations of radicals at low temperatures drive three reactions that are responsible for the high levels of heat release away from the regions of fuel consumption.

Kerl  et al. [44] used a quad-plane particle image velocimetry technique to study the behavior of flame curvature and flame displacement speed. They compared 3D and 2D planar measurements. They stabilized the flame in a diffuser with an annular swirling flow at its inlet They found that the results of 2D measurements are consistent with the real situation. They

observed that alignment could never be obtained because of the fluctuations that occur from turbulence in turbulent combustion. They presented three flame shapes (hyperbolic, parabolic and elliptic) in a diffuser combustor with an annular swirling flow at its inlet.

McGarry et al. [45] studied the interaction between the flame and turbulence of laminar premixed combustion. They examined the demand for high combustion and pressure gain combustion performances. They induced turbulence using a fluidic jet and generated the flame–turbulence interaction using the mechanisms of the jet, including flame-flow restriction, jet entrainment, turbulent transport and recirculation. They compared the interaction of the traditional flame–turbulence with the interaction generated by solid obstacles. They used high-speed PIV and chemiluminescence measurements to test the flame structural dynamics. They observed a high flame acceleration at the fluidic jet that is related to the obstacle. Finally, they found that the flame–turbulence interaction of the jet turbulence is dominated by the mechanism of a cross-stream high turbulence. Meanwhile, the flame–turbulence interaction for the obstacle is dominated by the Rayleigh–Taylor and Kelvin–Helmholtz instabilities.

Wang and Abraham [46] studied the influence of Karlovitz number on the flame surface using DNS in a lean premixed combustion at a mixture pressure of 20 bar and a temperature of 810 K. They changed the Karlovitz number within 1.1–49.4 and the Damköhler number within 0.26–3.2. They found that the shape factor of the local surface does not change with the Karlovitz number. They also found that the strain rate is a function of the Karlovitz number for the flame in the thin reaction regime. They also indicated that the Karlovitz number and the shape weakly affect the curvature of the mean flame displacement speed. The outcomes of the physical insights derived from the analysis are applied in the FAD model.

The findings of previous studies associated with the turbulent–combustion interaction indicate that turbulence significantly affects flame; thus, flame influences the flow. In all previous studies, despite considerable continuing efforts in the field of turbulence–flame interaction, we must still consider controlling the flame location using turbulence flow characteristics in an extensive investigation, where only turbulence properties are controlled. Therefore, a literature review on the control method will be submitted in the next sections. The investigation of the dependency of flame location on turbulence is based on selecting the suitable the geometry of the combustor. For this purpose, a review of the combustor and flame configurations will be discussed.

## *1.3 Review of literature on combustor and flame configurations*

A desirable limit of flame location is important in many combustion system applications. Flame stabilization is one of the main parameters in the design and configuration of a combustion system. Previous studies on the behavior and stability of flames focused on the parameters for preventing blow-off and extinction. In addition, NOx pollution depends on flame stabilization, especially for the lean premixed combustion. Many researchers have defined flame stabilization. For instance, Krikunova et al. [47] indicated that stabilization occurs in the flame at specific conditions when a dynamic equilibrium occurs between the tendency of the mixture to blow off the jet flame in the reaction zone and the flame to move to the fresh mixture.

Previous studies on flame stabilization also indicated that the flame configurations and the geometry of the combustor are among the many factors that influence the stability of the flame. In addition, the boundary condition influences the behavior and stability of the flame [48]. Many researchers investigated the flame stability on the basis of geometry configurations that

involve a Bunsen, V-, conical, spherical or stagnant flame. Bunsen burner is one of the combustor types used in classical experiments on premixed turbulent combustion. The Bunsen burner [49, 50] was first introduced by Bunsen, who found that premixing flammable gas with air decreases smoke and increases the temperature of combustion. The Bunsen burner has three types: blue flame, safety flame and roaring blue flame. The Bunsen burner [51, 52] has a hollow metal barrel or a metal tube that opens at the base to let the air in. Gas is normally injected at the base and mixes with the air, generating the flame at the top of the barrel. The V-shaped flame [53, 54] of the turbulent premixed flame is another flame configuration that is utilized to stabilize the flame with the rod or hot wire. Swirling Cheng [55] and bluff-body stabilization are among the main widespread methods that have been used in flame stabilization. Sattler et al. [56] studied the turbulent V-flame. To stabilize flame, Frank et al. [57] used the Bunsen burner, Soika et al. [58] used wire and Most et al. [59] utilized a bluff-body. Counterflow is also used to stabilize flat flame [60, 61].

Each flame stabilization mechanism has advantages and disadvantages. In addition, these stabilization mechanisms add complexity in the analysis of the flame and the implication of the results. These stabilization mechanisms have been utilized to study flame behavior and are crucial to controlling the flame location. The flame location must be controlled to stabilize the flame and avoid blow-off. Numerous studies have investigated the interaction between turbulence and flame in different burner geometry types, especially the influence of turbulence on the flame. Yasari et al. [62] used RANS simulation to investigate the influence of turbulence on premixed combustion for five configurations, namely, ONERA flames, conical PSI flames, Orleans flames, Bunsen flames and V-shaped flames. Confined turbulent flame was investigated experimentally by [63, 64] in a high-velocity premixed flow. Coriton et al. [60] investigated the

flame in the counterflow experimentally using axisymmetric jets. Can-type combustor is one of the burners used in gas turbine premixed turbulent combustion, as investigated by [65]. Many parameters influence flame stabilization, such as combustor geometry and turbulent flow characteristics. Therefore, the form of geometry should be carefully selected based on the type and purpose of combustion processes.

Therefore, according to previous studies, many parameters affect flame behavior and its stabilization. In addition, many techniques can be used to stabilize flame. In most flame stabilization methods, the geometry of the combustor is distorted. Therefore, a suitable technique that does not change the geometry of the combustor and does not add any complexity should be selected. To circumvent any complexity and difficulty, a smart control that can stabilize a flame without distorting the combustor geometry should be introduced. With this motivation to utilize the boundary condition, turbulence parameters are considered ideal factors for controlling the flame location without distorting the combustor geometry. Given that turbulence intensity and turbulence length scale influence the flame structure and its properties, turbulence flow characteristics could be utilized to control the flame location. Therefore, to study the control of flame location, control methods and strategies should first be understood.

## *1.4 Review of the combustion control*

Using a control strategy in the turbulent combustion system is important because of its role in the performance of the combustion device. Combustion can be controlled by two main methods: active control and passive control [66-69] Passive control is the earliest scheme used in combustion control. Active control suppresses combustion instabilities by controlling the

coupling between the unsteady heat release and the acoustic waves without modifying the combustor geometries.

The classical active controller approach for suppressing combustion instabilities can be generally divided into open-loop control and closed-loop control [69, 70]. Actuators are used in open-loop control systems to disrupt the feedback mechanism that creates an unstable system. The system does not need any feedback in the open loop to create the control signal. Combustion instabilities do not affect the parameters of the open-loop system (Figure **1-2**).

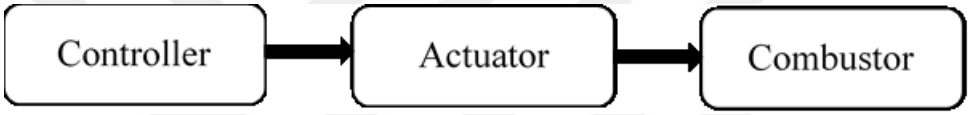


Figure 1-2 The block diagram of the open-loop controller.

The second type of active control is the closed-loop control, which depends on the feedback for measuring heat release (Figure **1-3**).

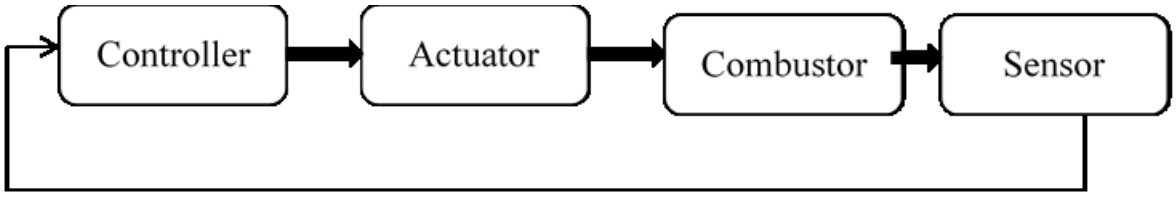


Figure 1-3 The block diagram of the closed-loop controller.

One or more sensors are generally used in the closed-loop control to measure the combustor heat release and/or pressure oscillations. Sensors involve transducers that measure the oscillating pressure, whilst the fluctuating local temperature or moles are measured by single diode-laser sensors [71, 72]. Many active control methods can be used to suppress combustion instabilities; they involve the following [73]:

1) Phase shifts coupled with gain approaches.

2) Model-based approaches.

3) Adaptive observer algorithms.

One of the simplest ways of active control is phase shifting, which is coupled with the gain approach. Essentially, the combustor's dynamic pressure signal is passed through a phase shifter with gain, which is fed back into the combustor through a fuel injector. The added phase shift and gain work to abate the thermo-acoustic instabilities through hardware. This technique is useful due to its ease of implementation and relatively low cost. However, the interactions between turbulence and chemistry play roles in the stabilization of flame and modeling of lifting turbulent flames. The literature on the control of turbulent combustion interaction is reviewed. The control of turbulent premixed flame has been studied by many researchers [74].

Seywertv [75] proposed the active feedback control of combustor dynamics with time delay and noise. They theoretically investigated the longitudinal pressure oscillations in a combustion chamber. They used the low-order model obtained by the systematic reduction from a complete representation. They accommodated the impact of combustion; noise, mean flow and control action by the deriving the equation of a generalized wave, which considers the formulation of the reduced-order model used in their paper. The set of coupled ordinary differential equations from the reduced equations describes the dynamics of the chamber by using spatial averaging. The forms of the equations were suitable for model reduction and for presenting feedback control forms. In addition, they used the same formulation to introduce the active feedback control of the longitudinal instabilities that was rewritten in the state–space form. They broadly used control simulations in their paper to investigate different aspects of the

problem in a unified fashion. The impacts of noise, parameter uncertainties, unmodelled modes and time delay were included. These parameters governed their criterion that ensures the stability of the controlled closed loop. The actual controller used in their study depends on a standard linear quadratic regulator design.

Neumeier et al. [76] experimentally investigated the description of the active instability control in the Jet A-fuelled combustor for a wide range of pressures (up to 11.72 bar). They worked to enhance the understanding of the factors that limit the control performance through experiments. They operated the test rig at the desired level of instability amplitude suppression that increased regularly. They drove the RMS instability amplitude to the desired levels, which were approximately down to 15% of those without control, using a controller. They varied the nonlinear and linear specifications of the self-excited oscillations to perform the experiments under various conditions. They observed that the combustor's nominal dynamics (i.e. without control) influence its response to the over-gaining of the fuel injector control signal (resulting in peak splitting). The influence of the reduced correlation time could also be important.

Banaszuk [77] investigated the control of combustion instability by using an adaptive algorithm that is suitable for reducing acoustic pressure oscillations in gas turbine engines. They presented an adaptive scheme for estimating the optimal phase shift over a high range of operating conditions that distinguish a closed-loop model, with phase-shifting control, of combustion oscillation. This algorithm includes an extended Kalman filter that depends on the frequency tracking observer to find the in-phase part, the quadrature part and the value of the acoustic mode of interest, with the controller phase tuning using extremum seeking. According to the experimental data, the closed-loop model can be distinguished by the phase-shifting control of combustion instability. Stability analysis of the adaptive approach might be performed

depending on the specified model. Finally, they used stable extremum-seeking designs in their experiments.

Tongxun et al. [78] presented a theoretical and experimental study of a pump-style, high-frequency, magnetostrictive fuel actuator. A Terfenol-D rod was used to achieve fuel modulations by pushing the fuel out of a piston-cylinder, and stepper motor was used to control the mean fuel flow rate. They presented the factors and their influence on fuel modulation by developing lower-order models. In the experiments and low-order models, they observed that large fuel modulations could be achieved by short downstream piping, fuel piping with a high diameter, long upstream piping, a bypass fuel passage and a high cylinder-piston system. They found that the air or fuel bubbles within the fuel system could reduce fuel modulations. They also observed that reduced time delay and a short actuating dead region are necessary for the fuel actuator to have rapid dynamics and a low phase. Finally, they made enhancements to the fuel rig test, which proved to be useful for controlling combustion instability.

Bell et al. [79] stabilized the flame location by using a heuristic feedback control algorithm for a turbulent premixed flame in simple geometry. They adjusted and integrated the fuelling rate to control the flame location in the 2D study. They examined the dependence of the local flame speed and flame behavior on flame curvature. They numerically indicated the behavior of the control algorithm for the flames at different equivalence ratios. They studied variation in the speed of propagation using the simulation, which is varied due to flame surface curvature. They observed that the flame is stabilized at statistically stationary conditions using the control algorithm.

Birbaud et al. [80] studied the effect of equivalence ratio nonuniformities on the nonlinear response of V-flames. They numerically studied the steady state of the flame. They concluded that axial velocity perturbations are induced by high levels of modulation. They found that the calculations described in their article can guide the modeling of the interaction between the inhomogeneities of the equivalence ratio and the response of combustion.

Shreekrishna et al. [81] investigated the response of premixed flame to the equivalence ratio. They studied the response of the oscillation heat release of the premixed flame to the perturbation of the equivalence ratio. They found that the dynamics of the heat release, which include the heat of reaction, flame speed and the oscillation of the FAD, can be controlled in three ways. In addition, they indicated the non-quasi-steady-state and flame stretch impact on the dynamics of the flame. They indicated that the equivalence ratio controls the flame response and determined the two main parameters that control the heat release, namely, the flame-kinematic mechanism and the intrinsically nonlinear dependence of the mixture heat of reaction and flame speed on the oscillations of the equivalence ratio. The influence of turbulence on a premixed turbulent flame studied using many methods of modeling for premixed turbulent combustion. For this reason, the review on the flame turbulence model will be explained.

## *1.5 Review on the flame models*

The conventional method for modeling and the simulation of turbulent premixed flame are based on the nature of the combustion process and the mixing method. The reaction occurs in a combustion region called flame sheet, which separates burnt reactants and unburnt combustion regimes. Consequently, the flame front propagates from the burnt reaction side to the unburnt reactant side. Given that the flame sheet separates combustion into burnt and unburnt regions in

the premixed combustion model, the progress of the reaction is the same as the progression of the flame front. That is, the flame front area is estimated at the time of fuel combustion, and the flame propagates from the burnt to the unburnt region. This idea is the basis of flamelet models. Flamelet models are among the methods that introduced to a model of turbulent combustion depending on the division of the combustion into burnt and unburnt regions.

Many studies [82-87] have introduced models of turbulent premixed combustion. Some of these models focus on the influence of turbulence on combustion, whilst the others deal with the modeling of premixed, partially premixed and non-premixed flames (**Figure 1-4**).

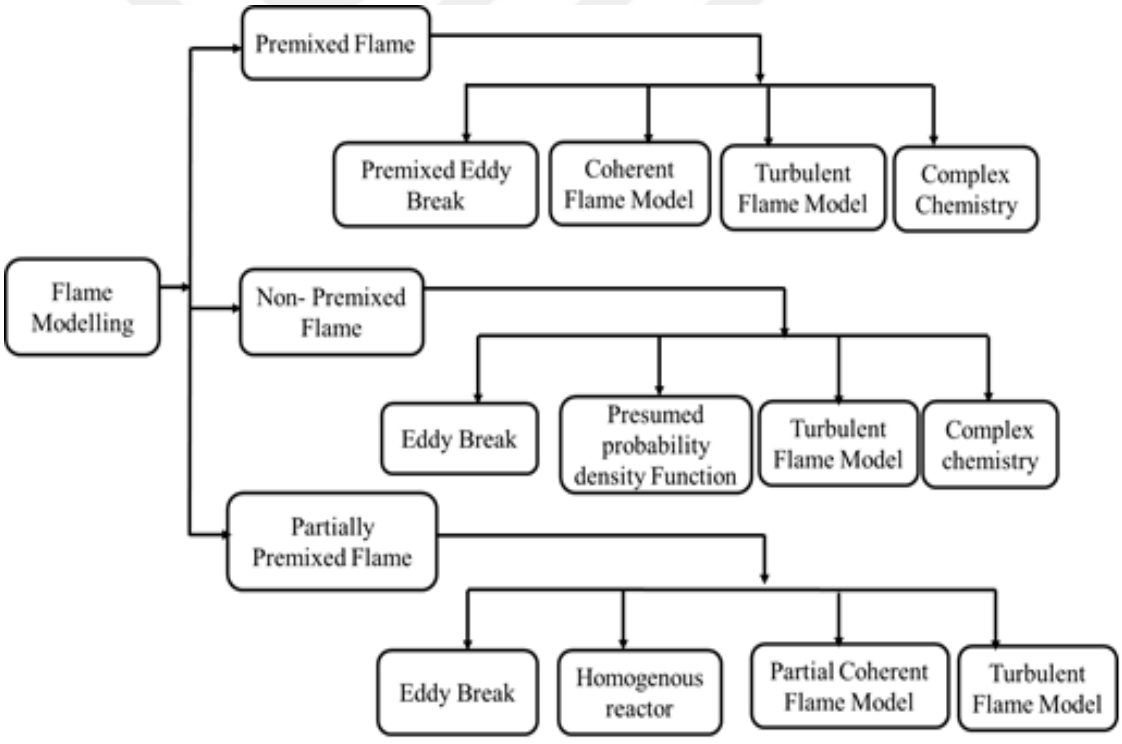


Figure 1-4 The types of the flame modeling scenarios.

In addition, most simplifications of these models are based on the solution of the reaction rate term of the species equation. Most previous studies indicated that the mean challenge in turbulent flame models is source term modeling. These models include the Bray–Moss–Libby

(BML) model, flamelet models, Turbulent flame closure, the eddy-break-up model, the thickened flame approach, the PDF model, flame tracking (G- equation) and the coherent flame model. The common models are discussed briefly.

Flamelet models are earliest modeling methods and are used to model turbulent combustion. Flamelet modeling is based on the mechanisms of flame stretching that is utilized to estimate the effect of turbulence time scales. The literature on flamelet modeling firstly focuses on the method to derive an effective turbulent burning velocity [19]. Bray et al. [88, 89] introduced an alternative modeling method for premixed turbulent combustion, that is, the Bray–Moss–Libby model. The basic formulation of Bray–Moss–Libby depends on the assumption of the average reaction progress variable ($\tilde{c}$) (c = 0 in the unburnt gas and c = 1 in the products) that describes the chemical reaction because the density is variable. This model was basically derived from the premixed turbulent combustion study of Bray and Moss [90]. In addition, they combined physical analysis with the statistical approaches of PDFs. This combination enhanced complex and simple models using probability functions. The reaction rate term of the species equation solves the BML analysis using the following modelling tools:

$$\boldsymbol{S = \rho_u \acute{u}\ k_t \Sigma} \tag{1-1}$$

The above equation indicates that the analysis of the BML model depends on the mean stretch factor ($K_t$), and Σ is the flame surface density. Many studies have dealt with solving the flame stretch and the flame surface density. The flame stretch was defined by Bray [91] as function of the Karlovitz number. Bradley et al. [92] defined flame stretch as a function of the Karlovitz and Lewis numbers. The quantity in the above equation, the flame surface density, wrinkles the flame through turbulence.

Turbulent flame speed closure is another important method for modeling premixed turbulent combustion. Zimont et al [81] proposed a model for premixed turbulent combustion at a high Reynolds number depends on turbulent flame speed. The turbulent flame closure (TFC) model depends on the ideas proposed by Prudnikov [9] and is particularly promising because it has been validated by many groups against the experimental data obtained from different premixed turbulent flames. In addition, they proposed a single transport equation of the progress variable, which considers the basic form of the TFC model, to simulate the average rates of product creation and heat release. The TFC has been used successfully for RANS and LES. For example, Zimont et al. [82], Polifke et al. [93] and Zimont [94] used TFC for gas turbine combustors. In the TFC, the reaction rate term is simplified depending on turbulent flame speed, which is derived as a function of the ratio of the turbulent flame surface area to the laminar flame area. Turbulent burning velocity $S_t$ is the main parameter in the TFC and is defined as a property of the entire flame and commonly as the normal velocity in the normal direction to the flame front. Whilst variable $S_t\ (X)$ is estimated at every position of $x$ in the flame as a function of the local turbulence factors and the physical-chemical characteristics of the air-fuel mixture.

The basic idea of turbulent flame speed is that small-scale turbulent structures intensify the transfer processes inside the flamelets and determine their thickness and propagation velocity, whereas vortices wrinkle the "thickened" flamelets and control the width of the averaged turbulent combustion region for large-scale turbulence.

Zimont and Lipatnikov proposed a relationship between the TFS and turbulence intensity for high turbulence intensity and described it using the following equation:

$$\frac{S_t}{S_l} = A\, Pr^{1/4}\, Re_t^{1/4}\, \left(\frac{\acute{u}}{S_l}\right)^{1/2} \tag{1-2}$$

where Pr is the Prandtl number ($Pr$ = 0.71), and $Re_t = \frac{\acute{u}\,\ell}{\upsilon}$ is the turbulent Reynolds number. $\ell$ is the integral length scale and $u'$ *is* the RMS velocity fluctuation.The constant (A = 0.52) in Equation (1-2) depends on the theoretical and experimental data of Zimont and Lipatnikov [95].

$$\frac{S_t}{S_l} = 1 + 0.62\ Re_t^{1/4}\ \left(\frac{\acute{u}}{S_l}\right)^{1/2} \tag{1-3}$$

Eddy break model (EBU) is one of the simplest and least expensive models that have been used in premixed turbulent combustion. This model was originally introduced by Spalding [96], who proposed that turbulent mixing could control the reaction rates for high turbulent Reynolds number and fast reactions. The EBU model is based on the assumption that the reaction rate is proportional to the intermittency between burnt gases and fuel mixture and inversely proportional to the turbulence time scale. Spalding [96] indicated that only turbulent mixing controls reaction rates. Thus, the chemical kinetic rates can be ignored, and the heat release rate is expressed as

$$S = C_{EBU}\ \frac{\tilde{\rho}}{\tau_{EBU}}\ \widetilde{C''} \tag{1-4}$$

An extension of EBU was proposed by Said and Borghi [97] and has potential applications. Spalding proposed that the reaction zone consists of unburnt and burnt gases that are transported by turbulent eddies and can be solved as

$$\dot{S}_{EBU} = C_{EBU}\,\overline{\rho}\ \frac{\epsilon}{k}\frac{\tilde{Y}_f}{Y^o{}_f}\left(1 - \frac{\tilde{Y}_f}{Y^o{}_f}\right) \tag{1-5}$$

The EBU model was applied to RANS and LES by Möller et al. [98]. The main advantage of this model is simply due to that no additional transport equations are required for solving the function of known quantities.

Kim et al. [99] utilized the EBU model to analyzed and to stabilize the flame in the gas turbine flame holder at different equivalence ratios. They used an additional algebraic equation for the turbulence dissipation rate (TDR) and a transport equation for TKE. They concluded that the stabilization of flame agrees with the experimental data in the stoichiometric condition.

PDF is another method for turbulent flame modeling, especially in non-premixed turbulent flame, which was introduced by Cook and Riley [100]. PDF theory based on the flame front–turbulent flow is described using probability theories and statistical properties, that is, the PDF identifies the point statistics of a random variable. For example, in the PDF methodology, the concentration level of a chemical species within a turbulent flame is considered. In addition, the PDF model depends on knowledge of the statistical properties of the species for the ranges of the progress variable from zero to unburnt and unity for burnt gases. The PDF model has been described using several methods, such as presumed, joint and conditional PDFs. Every PDF method depends on a different methodology, and in the presumed PDF, the shape is assumed by calculating the balance equation of the PDF. In the joint PDF, the transport equation or model is used to solve the probability of a set of variables. The local conditions are the main parameters used in the PDF. Many researchers, such as Pope [101], Givi [102], Möller et al. [98], Cook et al. [103] and Cook and Riley [104], have studied the application and development of PDF methods in turbulent combustion for RANS and LES.

The coherent flame model (CFM) is one of the promising approaches that employ the flame surface density in the transport equation for turbulent premixed combustion. The CFM basically depends on the modified flamelet model introduced by Broadwell [82 & 105]. In the CFM, the flame distribution is described by the FAD, which is defined as the flame area per unit mass. Wrinkling and straining in the flame leads to a change in the flame's area. The flame stretch or the FAD measures the change in the flame. FAD is the main parameter in combustion models that deal with the effect of turbulence on the flame. Flame surface density per unit volume is the simplest definition of the FAD within the turbulent premixed flame and expressed as an algebraic expression. Pope [106] reported that flame surface density can be estimated by solving the transport equation. The FAD in flamelet models can be calculated using two methods. The first method used simple algebraic closure models[107] [82, 107]. The second approach to solving FAD in the coherent flame model is called R-equation [108]. The model of the R-equation is based on the gradient of the progress variable, which is zero for reactants and one for products [89]. In the R-equation model, the equation involves terms of generation and destruction by the flame stretch of the flame surface, transport by mean flow and turbulence and flame propagation. The R-equation model solves transport equations for flame surface density ($\sum$) and the mass fraction of fuel in a premixed flame. Many researchers [82 & 108] have dealt with the R-equation and discussed its numerical solution. The FAD was solved within the frame of RANS and LES by Duclos et al. [109] and Prasad and Gore [110]. Therefore, the CFM depends on solving the source term in the species transport equation in terms of the FAD and the fuel mass fraction [111].

FAD [85] is utilized to study the effect of turbulence on flame behavior, depending on RANS simulations. The flame surface density equation is used in the RANS and LES models of

turbulent premixed combustion. The FAD has been studied in RANS approaches [112, 113] and tested with experiments [108, 114].

Zhang et al. [115] estimated the 3D flame surface density and the global fuel consumption rate using a Bunsen burner. They used five models to estimate FAD and fuel consumption rate. They performed factor fractal analysis on 2D images to estimate flame stretch and integration to evaluate the fuel consumption rate. They observed that the error does not exceed 57%. The first model connected the 2D to the 3D flame surface density with a value cosine of 0.69 in the turbulent Bunsen. Furthermore, they used the isotropic flame front distribution and the direction angle of the front normal distribution in 3D space to build Models 2 and 3. Meanwhile, Models 4 and 5 assume that the normal vector fluctuation intensity of the transverse direction is the same as the x- or y-direction on the plane. They found that all the methods obtained satisfactory results. The global fuel consumption rate was overestimated by approximately 40% by Model 2 under most conditions. Model 3 gave a good estimation. Models 4 and 5 gave the best evaluation of the global fuel consumption rate, with an absolute error within 17% for most turbulence intensities.

Ahmed and Prosser [116] studied the interaction between flame and turbulence in a premixed turbulent flame in the turbulent mixing layer using the Reynolds-averaged Navier–Stokes (RANS) technique. They used an evolution equation for the turbulence–flame interaction ($\Delta c$) to model the scalar dissipation ($c$). They observed that this evolution equation ($\Delta c$) provides a good alternative approach to modeling important physics. They compared the results of the large eddy simulation (LES) and the experiment's data. They concluded that this model provides good approximations of flame locations and average velocities compared with other flame models.

Therefore, the main characteristics that influence the combustion process, especially the turbulent flow characteristics, should be understood for studies that involve turbulent–flame interaction to select the suitable modeling method. Therefore, the CFM is utilized to consider the influence of turbulence on the flame. Details of the CFM and the general simulations are listed in the mathematical and numerical parts.

## *1.6 Review of turbulence models*

In addition to the flame model, the selection of a conventional method for dealing with the turbulence model is also important. Given that the aim of this study is to investigate the effect of turbulence on the flame, a suitable model that deals with turbulence parameters should be selected to manipulate the turbulent flow characteristics.

Previous studies on the turbulence models indicated that many methods deal with the turbulence effect. One of these methods is K-epsilon (K-ε), which involves standard and realizable K-ε, and k–omega is employed to deal with turbulence modeling [117-119]. The K-ε model is simple, computationally inexpensive and based on solving the two-equation RANS. Previous studies indicated that the k-ε model is one of the most popular turbulence models that have been used to provide much identification in terms of economy, robustness and accuracy for the turbulent modeling. The K-ε model includes many method standards and the renormalization group. The standard K-ε turbulence model is a commonly used model for dealing with turbulence combustion interaction. The standard K-ε model was initially introduced to turbulence problems but was limited to problems of certain classes of flows [117, 120]. Wilcox [121] indicated that the standard K-ε model is generally inaccurate for turbulent flow modeling in the presence of flow separation and pressure gradient. The main advantage of the standard K-ε model is its reasonable accuracy and robustness, especially in cases of high Reynolds number.

The standard K-ε model is unsuitable for turbulent flow application, which involves a large pressure gradient, flow separation and a large streamline curvature. In addition, the wall function has limited use because the ε equation involves a term that cannot be evaluated on the wall.

Continuous effort has been exerted to improve the standard model by proposing other models, depending on the realizable K-ε model and the renormalization group (RNG) K-ε model. Yakhot and Orszag [122] developed the standard K-ε model using the RNG theory. They derived the RNG K-ε model, which is mathematically similar to the standard K-ε, except for an additional term that appears in the dissipation transport equation. They modified the $C_{\varepsilon 2}$ expran ession that alters the dissipation term form. They named their new model the RNG model. They summarised the main difference between their newest model (RNG) and the standard K-ε model.

Previous studies indicated that an additional term appears in the K-ε equation in the latest version of the RNG K-ε model. This term is important in the performance of the RNG models because it varies dynamically with the strain rate of the turbulence. Han and Reitz [8] described the background of the RNG model and indicated that compressibility affects dissipation through the velocity dilatation. The effect of velocity dilatation on the dissipation rate is important in small engine applications. However, the RNG model has many features that make it more reliable and accurate for widespread flows than the standard K-ε model. These features include the decrease of dissipation in zones of high strain rates, making the RNG model suitable for non-equilibrium flows. In addition, the influence of swirl on turbulence is considered in the RNG model, which enhances the accuracy for flows. Yakhot and Smith assumed a Cμ constant of 0.0845 in the RNG K-ε model and a turbulence of 0.0845 [123].

Another K-ε model, the k-$\varepsilon$ realizable turbulence model, was proposed by Bardina et al. [119]. This model differs from the K-ε standard in the main modifications that involve formulations for the turbulent viscosity calculation. In addition, the K-ε realisable turbulence model has a different model transport equation for the formulations of dissipation rate viscosity. The realisable K-ε is associated with the eddy viscosity formulation, whereas Cμ is not a constant and is associated with the mean strain rate. The coefficient of the realisable model is represented as a function of the turbulence properties, mean flow and the turbulence properties whilst assumed to be constant in the standard K-ε turbulence model. They tested the constant in an experiment and obtained consistent experimental results. This model is relatively better than the standard K-ε model in terms of accuracy in many applications.

"Realizable" means that the model fulfills the mathematical restriction on the stresses and is reliable in terms of the physics of turbulent flow. Previous studies indicated that the realizable model provides superior performance overall K-ε model versions that involve separation and boundary layers under strong adverse pressure gradients. Therefore, we use the realizable K-ε model in this work [119].

All these formulations and equations are solved with one of the simulation approaches of the simulation of turbulent premixed combustion. The simulations and modeling of turbulent combustion simulations based on the main three types broad which involve Large-Eddy Simulation (LES), direct numerical simulation (DNS), and Reynolds averaged Navier–Stokes (RANS) simulation. The selection of the method suitable depends on the nature and details of the given results and the advantages and disadvantages of each type of these methods. Previous studies indicated that a suitable turbulence model based on the analysis of the turbulence scales should be selected.

Since there are a wide range of the time, length scales and the nonlinearity in the governing equations, the accurate simulation of turbulent premixed flame is difficult. A direct numerical simulation (DNS) is one of the approaches that deal with turbulence–flame interaction a simulation which solves numerically the Navier–Stokes equations without any turbulence model. Therefore, in the DNS, the whole range of temporal and spatial scales of the turbulence are solved from the Kolmogorov microscales up to the large scale. As results, the DNS or the complete solution is prohibitively expensive and is challenging in the turbulent premixed flame. Nevertheless, DNS for the one-step global reaction in simplified geometries is realistic. However, the main challenge in the method of DNS computer power performance in spite of the continuing development in computing power.

The RANS approach is a common method for dealing with turbulence parameters. The RANS approach provides a description of the connection between turbulent fluctuations and the turbulence parameters with respect to the averaged dependent variables. RANS equations are solved with the help of a turbulence model. The RANS is a classical solution, which deals with the problem of a wide range of time and length and scales in premixed turbulent flame by solving the equations for averaged variables. However, there is some disadvantage in the RANs, which associates with predictions of the small-scale fluctuations, which are strongly affected by molecular transport; while the fluctuations of the large-scale are more strongly based on details of boundary conditions and structures of the turbulent flow.

In order to overcome the A weakness and the difficulty in the RANS, the large-eddy simulation (LES) approach proposed by Smagorinsky [124]. The main idea of the LES depends on the resolving the large-scale motions for both time and space and is ignoring the smallest length scales in order to reduce the expensive cost of the computational. In the LES, the small

scales are applied for both perform a temporal and a spatial filtering operation, filtering operation (weighted by *F* of the form. The filtered field, denoted with a bar, is defined as

$$\bar{\boldsymbol{\phi}}\,(\boldsymbol{x},\boldsymbol{t}) = \int \boldsymbol{\phi}\,(\boldsymbol{x}',\boldsymbol{t})\,\boldsymbol{F}\,(\boldsymbol{x}-\boldsymbol{x}');\ \Delta]\,\boldsymbol{dx}' \qquad (1\text{-}6)$$

## *1.7 Motivation*

The main goal of most studies regarding combustion is to decrease the emissions and increase the performance of combustion systems, such as in power plant turbines. Premixed combustion is preferred over diffusion systems for reducing pollution. The main disadvantage of premixed turbulent combustion is that oscillations easily occur. Lean premixed combustion plays a role in reducing NOx emission. In addition, the stability and the location of the flame effect the NOx emission, especially in lean premixed turbulent combustion. Therefore, controlling the flame location within a suitable level is important in most applications of premixed combustion systems.

Controlling the flame location in a combustor without distorting the combustor geometry is a major concern in any combustion system application. This type of flame location control could be achieved by manipulating many parameters, such as the turbulent flow and combustor geometry. Therefore, the characteristics and the behavior of premixed flame and turbulence interaction should be understood, especially the effect of turbulence on flame location. Wrinkling occurs in the flame front when the turbulence scales are larger than the laminar flame thickness. The local laminar flame speed through the flame stretch is affected by the local curvature of the flame front. The irregularly shaped flame front that alters the turbulence properties of the flow for each ahead of and downstream of the flame produces the local velocity field in addition to the impact of turbulence on flame structure [10]. The premixed flame influences the turbulent flow

due to the drop in density (1 to 7) times within the flame. Therefore, the properties of the fluid, such as viscosity and density, change with the change in the heat release of the combustion, and the flame influences the turbulence in turn.

The findings of previous investigations on flame front characteristics, particularly the flame structure, flame shape and flame–flow interaction, revealed a strong relationship between flame and turbulence. Both qualities and quantities are important in describing these interactions, especially for problems ranging from the design of pollutant reduction to performance combustion engines for the prevention of gas explosions. These studies indicated that the properties of turbulence include turbulence intensity, length scale, energy spectrum and Reynolds stress, as well as the turbulent flame structure and the turbulent burning rate. Many studies [19, 23, 19, 32, 28, 29] considered different levels of turbulence intensities and turbulence length scales in turbulent premixed flame. They revealed that the turbulence length scale and turbulence intensity affect the shape and motion of the front. Furthermore, the flame is highly sensitive to wrinkle at high turbulence intensities due to the changing turbulence and turbulence dominates the process, and the flame is less sensitive to wrinkling at low turbulence intensities. Strategy for control the flame location by manipulate the local properties of combustion and the turbulence levels of the flow could be proposed.

## *1.8 Methodology*

The conclusions from previous studies associated with the turbulent–combustion interaction indicated that turbulence has a significant effect on the flame, and the flame has an influence on the flow. Therefore, the turbulent combustion interaction divided into two: that which involves the impacts of turbulence on the flame front and the effects of the flame front on the flow [3]. The interaction between turbulence and combustion could also be utilized to

stabilize the flame. Despite the continuous efforts focused on the effect of turbulence intensities and turbulence length scales on the flame shape and flame structures, the influence of turbulence on flame location still requires extensive investigation. The turbulence effect on the flame location in premixed turbulent combustion and a suitable model for studying the impact of turbulence on combustion should be determined. The study on the effect of turbulence on flame location depends on the suitable selection of flame model and combustor geometry. Therefore, the influence of turbulence on flame location should be considered in an extensive investigation of a simple combustor in which the sole effect of turbulence on flame can be tested. In this study, the diffuser form is selected because the flow slows down along the flow direction, and thus, the flame is expected to propagate towards the inlet when the flame speed increases. In this manner, the effect of turbulence can be observed without changing the thermal power. Furthermore, a V-type object is placed in the diffuser to prevent any flow separation that could occur in the combustor.

The selection of a suitable method to model the turbulent flame is based on many rules. First, it considers the object requirement of the study to control the various parameters. Second, a set of problem variables are defined with the new transport equations, which can be added depending on the directly rewritten new variables as functions of the already known variables using empirical and theoretical formulations. Given that this study is about flame–turbulence reactions and due to the strong interaction between flame reactions and turbulent flow, the efficient numerical model calculation of turbulent premixed flames is not straightforward. However, many numerical approaches to computational fluid dynamics exist and are used to simulate turbulent premixed flames, such as the RANS equation, the unsteady RANS equation (URANS), LES) hybrid RANS/LES and DNS. The RANS approach is the cheapest among the

simulation approaches. The RANS formulation is a classical method of solving the equations of turbulent flow, and it is coupled with the reacting flow that involves a wide range of time and length scale in terms of the averaged variables. In turbulent flow problems, RANS simulation could be attributed to steady RANS modeling or unsteady URANS. In addition, RANS could be applied to both non-reacting and reacting turbulent flows. The RANS approach deals with the balance equation of Favre average density. Therefore, the URANS model is used in this work because it is the cheapest. The main properties of the flow can be described by solving the partial differential equations for mass, momentum and turbulence (the K-ε model) for the non-reacting flows, whereas additional equations for the chemical species and energy are essential for reacting flows.

A suitable flame model should be selected to study the effect of turbulence intensity and length scale on the flame front. Many flame models have been used to deal with flame turbulence interaction, such as the eddy break model, FAD, flame speed closure and LESs. FAD is one of the main quantities in turbulent premixed combustion and plays a role in the interaction between combustion and turbulence. Understanding the FAD of a turbulent flame is important in turbulent combustion research and combustion control. The CFM plays a role in the study of the effect of turbulence on combustion. Marble and Broadwell [85] initially introduced the CFM based on the flamelet model. Turbulence generates wrinkling in the flame. This wrinkling increases the area of the flame. Therefore, the FAD is used to represent the turbulence in the CFM. This study investigates the effect of the turbulence on the flame, and thus, the CFM and the *K*-ε model are used. The combined turbulence intensity and length scale parameters within the CFM is utilized to develop models for simulating the effect of turbulence on flame location.

## *1.9 Novel aspects*

Strategy to control the flame location in the diffuser is crucial in keeping the flame at a desirable level while avoiding blow off. A smart approach to controlling flame at a certain location within desirable levels can be achieved by varying turbulent flow characteristics. The current work objectives first depend on previous observations of turbulence impact on the flame. Then, the best type of combustor geometry that is suitable for studying the flame location in the premixed turbulent flame is selected. This study investigates the control of a flame location in a diffuser combustor by actively changing turbulent flow characteristics at the inlet without distorting the combustor geometry and without changing the mixture velocity, i.e., the thermal power.

## *1.10 Research objectives*

Turbulent flow characteristics influence flame behavior and the design of combustion systems. Flame behavior is based on the characteristics of the turbulent flow. The primary aim of this work is to introduce a method for controlling the flame location using the turbulent flow characteristics. Turbulence intensity and length scale are among the main parameters of turbulent flow. Therefore, the secondary purpose of this work is to study the response of the flame location of premixed turbulent flame to varying turbulence intensities and turbulence length scales. A diffuser combustor is used in this study to investigate the response of the flame location to various turbulence intensities and turbulence length scales without changing the velocity of the mixture, i.e. the thermal power.

## *1.11 Structure of the thesis*

The primary aim of this research is to introduce strategies for controlling the flame location based on flow characteristic parameters, such as turbulence intensity, turbulence length scale and turbulent Reynolds number. The secondary aim of this work is to investigate a flame location that has been exposed to a wide range of turbulence intensities and turbulence length scales in the diffuser combustor.

This thesis is organized as follows.

**Chapter 1** presents the background and reviews of previous studies on turbulence–combustion interaction and control of combustion. Several studies on the effect of turbulence on flame have been conducted by many researchers. These studies introduced many premixed turbulent combustion models. A review of flame models, including EBU, CFM and TFC, is presented. Given that this work studies turbulence, turbulence models are also discussed. In addition, reviews on flame stabilization and configuration, which are related to the control of the flame location, are presented. At the end of this chapter, the motivation and objectives of the study are presented.

In **Chapter 2**, the modeling of the flame–turbulence that is based on the fundamentals of the premixed turbulent flame is discussed. The fundamentals of turbulence, the premixed flame, the main parameters and the governing equation in the premixed turbulent combustion are presented. Then, descriptions of the flame modeling strategy, the RANS equation, the Favre averaging method of the flame models, the CFM and the FAD are presented.

In **Chapter 3**, a numerical simulation, test cases and the combustor geometry are presented. Given that a diffuser combustor is used to investigate the response of flame location to

various turbulence intensities and turbulence length scales, the geometries of the diffuser with and without a conical insert are introduced. The detail of the mesh applied to the geometry is introduced in this chapter. The flowchart of the physical model is presented, including the CFM, K-ε, RANS, 3D premixed reacting flow and turbulent flow. Simulations are applied to two cases, namely, the steady and implicit unsteady states. STAR CCM+ is used to test all simulation models. Two main properties of combustion, namely, turbulence intensity and turbulence length scale, are used to study the impact of turbulence on flame location. Ranges of the turbulence length scales and turbulence intensities are used to study the behavior of flame location. Then, the control algorithm methodology is discussed based on the turbulent flow characteristics.

In **Chapter 4**, the obtained results and the discussions on the response of flame location to various turbulence intensities and turbulence length scales are firstly presented for the steady state. In practice, temperature contour and FAD are used to study the effect of turbulence intensities and turbulence length scales. TKE indicates the behavior of the flame with the change in turbulence intensity and turbulence length scale. The obtained results are validated with those of previous studies.

In **Chapter 5**, the unsteady-state results are discussed. Turbulence intensity and turbulence length scale are utilized to study the influence of turbulence on flame location. Temperature and FAD represent the flame location. Flow separation within the diffuser, which influences the flame location, is observed. Therefore, the flow structure is discussed in terms of flow separation.

In **Chapter 6**, the results of the unsteady state, using a conical insert, are introduced. Given that flow separation is observed within the diffuser combustor, with a conical insert at the

middle of the diffuser to eliminate it, the results of the flame location under the effect of the various turbulence intensities and turbulence length scales are first discussed. Then, the similarity and dissimilarity between the behaviors of the flame location for both diffusers (with and without using conical insert) are discussed. The behavior of the dynamic pressure and mean velocity are used to explain the behavior of the flame location under simultaneous effects of turbulence and flow separation. These results are then validated by the results of previous studies.

In **Chapter 7,** the results of the control of the flame location are presented. The methodology is presented briefly. Then, smart control of the flame location using macro Java is presented. In **Chapter 8**, the overall conclusions of the investigations are provided.

Finally, the Appendix contains the algorithm of the control program.

# CHAPTER II

# 2 MATHEMATICAL MODEL

## 2.1 *Fundamentals of turbulent premixed flame*

### 2.1.1 Introduction

In the first part of this chapter, the physical phenomena and simplification, fundamentals of turbulent combustion are explained. They involve many basic parameters and concepts, such as turbulence, laminar flame speed, length scale, flame thickness, dimensionless numbers and regimes of the turbulent premixed flame. The basic aspects of turbulence and the method of turbulence modeling are discussed in the next section. The RANS and Favre average are discussed and explained. Then, this chapter presents the combustion model;ing and focuses on the information related to the turbulent flow characteristics. The CFM and K-epsilon are discussed. The final part of the chapter focuses on the FAD, which is the main parameter that characterizes the relationship between turbulence and flame.

### 2.1.2 Physical phenomenon and simplification

Combustion systems are important in many engineering applications, such as gas turbines, internal combustion engines, furnaces, and power station combustors. In these systems, combustion, heat transfer, chemical reaction, turbulent flow, and radiative heat transfer interact (Figure **2-1**).

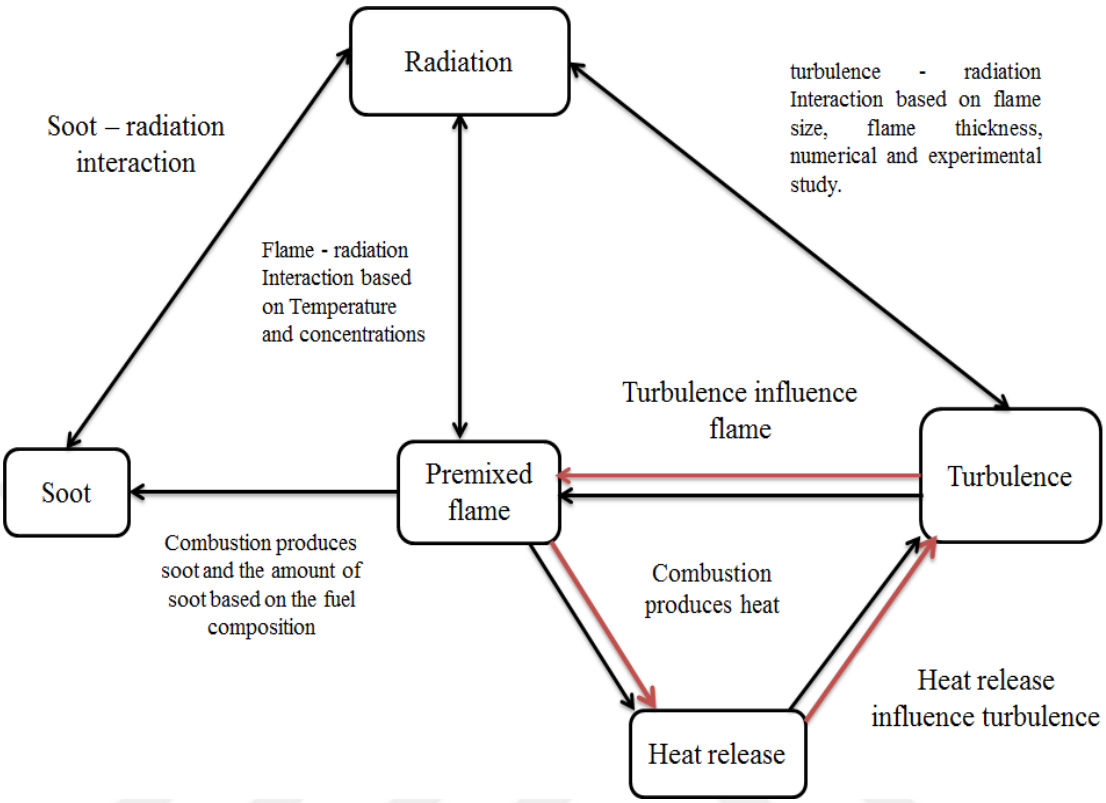


Figure 2-1 Radiation–turbulence interaction and soot in the combustion process.

Predicting the combustion process output, such as the temperature, flame shape, and emission of the combustion, is essential for enhancing the performance and reducing the emission of these combustion systems [125]. Therefore, considering the characteristics that influence combustion analysis is essential to obtaining and avoiding errors in the target output results for any combustion process. The output types of the flame shapes are based on many parameters, such as the flow type, boundary condition, and the mixing method. Flow is turbulent in most combustion systems. Thus, understanding the basis of premixed turbulent combustion is important in predicting a suitable approach for the numerical modeling of turbulent combustion.

Reacting flow, turbulence, and thermal radiation are challenging and are the main factors that affect turbulent combustion. In turbulent reacting flows, these phenomena are coupled in

highly nonlinear methods, thus leading to interaction between these phenomena. Flow is turbulent in most combustion systems. That is, turbulence influences flame and heat releases, which in turn influence flow. In combustion processes, heat is transferred by heat transfer, conduction, convection, and radiation. The main part of the heat, which is due to the temperature increase during the combustion process, is transferred to the surroundings by radiative heat transfer [126]. Radiative heat transfers to media by particle absorption and scattering and gas emission. Radiative fluxes and properties are based on concentration, temperature, and fields. Fluctuations are affected by the temperature and concentrations in turbulent combustion processes. The spectral radiative absorption coefficient of a mixture, which is identified by high fluctuations, is also a function of the concentration and temperature of the mixtures. Fluctuations in the radiation field interact with those of the flow field, thereby causing the so-called turbulent–radiation interactions. However, the overall radiation values are mostly described in terms of the total amount of heat loss from the flame and normalized as a radiation fraction [126].

Turbulence–radiation interactions occur in nonreactive and reactive flows. The nonreactive hot gases of radiatively participating species comprise nearly water vapor and carbon dioxide, which may exist in the exhaust gases of combustors. The turbulence–radiation interactions in nonreactive turbulent flows are usually small and negligible because scalar fluctuations in nonreactive turbulent flows are nearly smaller than those occurring in reactive flows. Mazumder and Modest [127] introduced a study that supported this belief and found that the role of turbulence–radiation interactions is based on how the concentration fluctuations of carbon dioxide and water vapor relate to temperature fluctuations. The authors concluded that the increase in radiative transfer, which is less than 1%, is indeed negligible, considering the turbulence radiation interaction effect.

Recently, the effect of radiation in reactive turbulent flow has either been ignored or treated using simplistic models. In previous studies, concentrations and temperatures were taken as input data, which are mostly calculated on the basis of experimental or artificial data. These studies indicated that radiation is affected by turbulence in the same manner as convection. In turn, the influence of radiation on turbulence levels is generally small and has received minimal attention. Early results found that turbulence leads to an increase in the transmissivity of a gas column [128,129]. These results have been validated by experimental data. Fischer et al. [130] introduced stochastic simulations to indicate the intensities of leaving for an ethanol pool fire. They found that the mean radiation intensities increased with the turbulence considered in [131,132]. The net radiative heat increased with the flame thickness [133]. Li and Modest [133] indicated that as the flame became optically thicker, the actual values of radiative heat loss, thereby ignoring turbulence–radiation interaction. The turbulence–radiation interaction has been investigated by many studies. All studies showed that turbulence leads to an increase in the intensities of mean spectral radiation and is based on the nature of the mixture, which ranges from small in carbon monoxide/air flames [132] to moderate in methane/air flames and to high in hydrogen/air flames [134]. Meanwhile, Coelho [135] exhaustively investigated these studies.

Li and Modest [133] [132] introduced a model to consider the effect of radiation in turbulent combustion. They investigated the turbulence–radiation interaction in reactive flows and considered three different scenarios. In the first consideration, radiation was completely neglected. In the second and third scenarios, the effect of radiation was considered in the study of the flame but turbulence and radiation were considered and ignored, respectively. Temperature decreased in the scenarios that considered the radiation from high temperature. This phenomenon depends on the temperature and thickness of the flame. The authors found that the flame peak

temperatures decreased as a result of considering radiation–turbulence at 18 K. They also found that fractions of radiation for scenarios without and with turbulence–radiation reaction were 3.1%, and 4.6%, respectively, and 5.1% for an experimental case. Coelho et al. [136] and Coelho [137] introduced a numerical investigation for the turbulence–radiation interaction numerical model, which was validated for the experiment. For comparison, they proposed many scenarios without radiation effect and scenarios with radiation–turbulence interaction. They reported temperature decrease due to radiation, which had a radiation–turbulence interaction similar to that reported by Li and Modest. In addition, they indicated that the fractions of radiation with turbulence–radiation interaction were 5.3%. However, studies on the effect of radiation on small laboratory flames, such as Flame D, showed low radiation. Thus, the influence of radiation on the flame is limited. Zheng et al. [138,139] recently introduced extensive radiative measurements on six workshop flames. They computed the spectral radiation intensities using the mean property approach and validated the results with experimental data. They found that the influence of Reynolds number on radiation intensities is weak and the influence of turbulence–radiation is not remarkable; furthermore, the fractions of radiation were $\leq 1$. They also concluded that laboratory flames tend to be small and thus loses only small amounts of heat. Therefore, the value of reduced laboratory flames is mostly small. Consequently, the influence of radiation is generally neglected in the numerical simulations of such flames. .

Wang et al. [140] also investigated the influence of radiation on the turbulent kinetic energy of scaled flames. They found that radiation causes a decrease in the turbulent kinetic energy by approximately 5%, whereas the influence of turbulence–radiation interaction is indeed negligible. In addition, turbulence is reduced because temperature fluctuations are small. In most modeling studies on the radiation effect, a particle-based photon Monte Carlo method was used.

Modest and coworkers [133] used the probability density function approach to deal with turbulence–radiation interaction flame modeling.

Most combustion processes produce pollutant emissions and soot [141]. The soot formed during combustion is in the fuel-rich region, where oxidizer concentration is low. Soot is mostly carbon, and other components such as hydrogen are usually present in small amounts [142]. Soot particles form and grow in the region between two flames because of coagulation and surface reactions. Many studies have dealt with soot formation, but the review of Haynes and Wagner [143] is still the best source for describing the phenomenon. Small hydrocarbons are initially generated as hydrocarbon pyrolyze. The formation of the first aromatic species from these aliphatic hydrocarbons is the initial step in soot production. Large polyaromatic hydrocarbons are formed from the aromatic species, which grow due to the addition of small alkyl species and other aromatics. The continued growth of large polyaromatic hydrocarbons results in the production of soot particles. Soot is the result of the incomplete combustion of hydrocarbons in the formation of condensed carbon particles and is created in flame regions, where oxygen is not enough to complete the fuel reaction. Therefore, soot is difficult to avoid under fuel-rich conditions. In most combustion systems, soot forms in temperatures that range from 1000 °C to 2500 °C. The amount of soot formed is small compared with that of carbon present in the consumed fuel. Previous studies on soot indicated that soot does not form for C/O = 1 or less than unity but is usually close to C/O = 0.5. The soot process is classified into four major sub-processes [142-145], namely, surface reaction of particles, coagulation, formation conglomeration of polycyclic aromatic hydrocarbons, and particle oxidation. The formation of particle-like structures by coagulation of polycyclic aromatic hydrocarbons is known as soot particle inception or nucleation. Soot particle inception considers the link between soot particle

dynamics and the chemistry of combustion, which controls the number of soot particles that emerges from flames. Considering the influence of soot in combustion simulations requires the use of detailed mechanisms that represent chemical reactions.

Previous studies have explored the influence of mixture composition and temperature on soot formation on the basis of the changing compositional components of fresh mixtures for carbon oxygen ratio and the magnitude of temperature changes in laminar premixed flames. The results indicated that an increase in C/O ratio increases the soot volume fraction. When the C/O ratio is constant, a temperature exists characteristic for the ratio of C/O whereas soot volume fraction exhibits a maximum value [146]. Furthermore, soot volume fraction strongly decreases under high and low temperatures [147]. The influence of C/O ratio on soot distribution and the high-molecular-weight species condensed along rich, premixed C2H4/O2 combustion have been investigated. The results indicated that with an increase in C/O ratio, the depletion of total aromatic carbon, which corresponds with soot formation, increases and is attributed more to the participation of these species to soot inception than to their oxidation. The balance of oxidation and carbon controls and influences the number of particles formed. Soot oxidation changes solid soot particles into gas-phase species. Molecular oxygen with OH radial and surface reactions causes CO and $CO_2$ formation. However, the factors that control soot can be recognized by the accurate prediction of oxidation and soot formation, thereby reducing cost and time consumed in designing practical systems. Moreover, soot influences the radiation transfer in combustion processes, especially in furnaces [148]. Thermal radiation increases for the sooting flame and considers the majority of flame radiation. Researchers have found that spectral gas radiation emission decreases for lightly sooting fuels and observed that the soot amount present in non-premixed system is higher than that in premixed systems because oxide and carbon are not

distributed. Therefore, previous studies focused on the effects of soot and radiation on non-premixed flames.

Modeling of processes that include complex interactions between turbulence with soot and particle dynamics is complicated. Detailed kinetics are mostly used in modeling detailed soot models [149]. Empirical soot models were used for most studies that dealt with soot effect [150]. Brookes et al. [151] used an extended flamelet and conditional moment closure approach to model the soot formation in air/methane. In most studies on soot, detailed chemical kinetics was used to describe the evolution of soot. So far, soot predictions have agreed well with experimental results. In addition, the model cannot be used for complicated geometries. Premixed combustion systems are preferred over non-premixed systems due to their superiority in reducing pollutants and soot [3].

The selection of a suitable method for modeling turbulent flame is based on the nature of the combustion process. Given that this study is about flame–turbulence reactions and due to the strong interaction between flame reactions and turbulent flow, a suitable flame model should be selected to investigate the effect of turbulence on flame. Many flame models have been used to deal with flame–turbulence interaction, such as the eddy break model, FAD, and flame speed. FAD is a quantity in turbulent premixed combustion and plays a role in combustion–turbulence interaction. Understanding the FAD of a turbulent flame is important in turbulent–combustion research and combustion control. Turbulence generates wrinkling in the flame, thus increasing the flame area. The per unit volume of this area is referred to the FAD. initially introduced CFM based on an FAD, which is used to represent the turbulence in the CFM. This study investigates the effect of turbulence on flame. Thus, the CFM and the $K$-ε models are used. In the coherent flame model, the mean species concentrations are obtained as functions of the mean fuel mass

fraction and a one-step global reaction scheme, which is internally calculated on the basis of the unburnt gas composition.

The boundary condition of the system also influences the output prediction of the combustion process, such as the temperatures, flame shapes, and combustion emissions. Therefore, selecting the suitable condition is essential to ensure optimum results. The environmental boundary, especially temperature and pressure, is a parameter that influences combustion. The boundary conditions of the walls influence the combustion process because of the heat that transfers from the combustion toward the wall. Therefore, adiabatic wall conditions have been used to neglect the heat losses to the walls. In this manner, the behavior of the flame location under sole turbulence effect at the same boundary conditions can be compared without including the influence of heat losses. Given that this study deals with the influence of turbulence on sole flame location, the wall is assumed to be adiabatic to examine the sole effect of the turbulence on the flame.

Simplifications of physical phenomena in our case, which deal with the effect of turbulence on the flame location, have been made on the basis of findings of previous studies. Past works on the turbulence– radiation–flame interaction indicated that turbulence influenced radiation, thus rendering the effect of radiation on turbulence negligible. Conclusions from previous studies have shown that the radiation is less than 5% and 3% for the experimental and numerical data, respectively. In addition, the influence of radiation leads to a small decrease in temperature, especially for laboratory flames. The effect of radiation has also been ignored in numerical simulation studies. Thus, the influence of radiation is ignored because this study is a numerical investigation and is about the effect of turbulence on flame. References [133] used the probability density function approach to deal with turbulence–radiation interaction flame

modeling. Turbulence parameters cannot manipulate the without use suitable method because the current study is about the influence of the turbulence on flame location.

Conclusions from previous studies on soot formation have suggested that soot occurs due to incomplete hydrocarbon combustion, increases with rich fuel, and decreases for level values with the C/O values. Soot formation occurs when C/O $\geq$ 1 in the fuel-rich side due to the low concentration of oxidizer species. Soot is important in non-premixed systems, where incomplete combustion occurs in the flame region due to the nonmixing between the oxide and the carbon. The effect of soot is ignored because the study focuses on lean, premixed turbulent combustion and the C/O ratio is 0.58, which is less than 1. This study focuses on the influence of turbulence on flame location. Therefore, a flame model that deals with the control of turbulence parameters should be selected. Combustion simulations that deal with soot require the representation of chemical reactions by detailed mechanisms. Thus, the effect of soot is ignored. A coherent flame model is used to deal with the effect of turbulence on flame location. The multistep reaction is used in the detail chemistry model, which uses models that deal with soot and chemistry effect. The coherent flame model is based on step reaction instead of the multi-step reaction.

### 2.1.3 Turbulence

Turbulence occurs daily in many applications, such as the water flowing from waterfalls, a mixture of flow in a swirl and smoke from chimneys. Turbulence also occurs around objects, such as cars, trains, and airplanes. The generation or avoidance of turbulence plays a role in engineering systems. Therefore, extensive research has been conducted on turbulence in engineering applications and technology.

Turbulence is generally a feature of fluid flow. In the turbulent flow, fluctuations occur in the quantities of fluid motion, such as velocity and pressure components with the time and location. In addition, the stretching of the vortex in the turbulence flow causes velocity fluctuations to spread to all wavelengths between the minimum estimated by the viscous forces and the maximum estimated by the boundary conditions of the flow. Turbulence has been defined by many researchers [16]. The turbulent flow represents the characterization of fluid motion that is distinguished by random and chaotic turbulence. The quantities of the fluid motion indicate the random variation with space and time called turbulent flow. Therefore, the quantities and fluctuation could be averagely discerned. Turbulence, which occurs due to the fluctuation from large down to the smallest eddies and leads to random flow, has a wide range of length scales. These scales of fluctuations interact dynamically in a complex way. Previous studies indicated that turbulence enhances the mixing and increases the transport and spread of fluctuations. These studies also indicated that in turbulence, kinetic energy is transformed into heat, which is called dissipation.

This work focuses on the turbulent flame. Thus, the fundamentals of turbulence are addressed with basic phenomena related to turbulent flame. The randomness and unsteadiness of the turbulent flow, size and eddies vary. Turbulence deals with the averaged and fluctuation velocity and pressure fields. The characteristics of turbulence could be calculated by using different methods. Previous studies found that the measurement of velocity with space and time approximately results in the curve shown in Figure **2-2**.

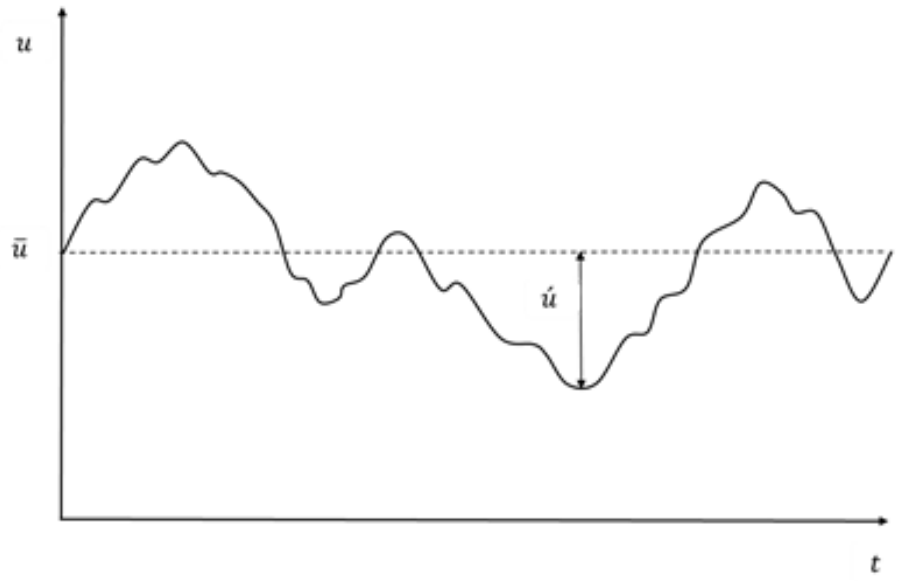


Figure 2-2 Instantaneous velocity via time.

As shown in **Figure 2-2**, instantaneous velocity is decomposed into mean quantities average velocity component and the fluctuating component of the velocity, which is called Reynolds decomposition. Therefore, instantaneous velocity follows **.**

$$u = \overline{\boldsymbol{U}} + u' \qquad (2\text{-}1)$$

### 2.1.4 Turbulence scales

In turbulent premixed combustion, a reaction supplies the chemical time and a timescale. In the case of a propagating flame, the combustion reactions introduce velocity, flame thickness , and flame velocity. Before dealing with the turbulent flame interaction, the time and length scale in the turbulent premixed flame should be discussed. The time required to transform all reactants entering the reaction zone into products could be measured by these chemical times and a

timescale. However, the diffusion process considers the link between the chemical time scale and the velocity scale. Therefore, the length and timescale are important in combustion studies.

These scales are utilized to introduce different regimes in premixed turbulent combustion, which are expressed in terms of the premixed turbulent diagrams [20]. The difference between several length scales is one of the characteristic features of turbulent combustion regimes.

An idea with regard to energy cascade was introduced at the beginning of the last century [152]. The author indicated that kinetic energy is dissipated when it enters the largest scales of motion and is converted to a small scale because of the action of viscous processes. The rate of TKE that produces and converts the large length scale into a small scale is called the dissipation rate or is roughly equal to fluctuation energy dissipation. He also calculated the dissipation of TKE at the large-scale dynamics of turbulence. However, in the turbulent combustion process, small eddies are created due to the break-up of large eddies. These small eddies continue to break up until they disappear due to viscous forces.

The rate of production (or dissipation) of fluctuation energy is expressed as

$$\varepsilon = \frac{k^{3/2}}{\ell} \tag{2-2}$$

Previous studies also indicated that the TDR could control the turbulence for the ranges of eddies within the small and large scale of energy content. The small scale is expressed in terms of the rate of energy dissipation and fluid viscosity and is called the Kolmogorov microscale [153]. The small scale can be calculated using the dissipation rate ($\varepsilon$) and the kinematic viscosity ($v$).

$$\eta_k = \left(\frac{{v_t}^3}{\varepsilon}\right)^{1/4} \quad (2\text{-}3)$$

$$\eta_k = \left(\frac{v_t}{\varepsilon}\right)^{1/2} \quad (2\text{-}4)$$

$$u'_i = (v_t\, \varepsilon)^{1/4} \quad (2\text{-}5)$$

The integral time scale ($\tau_t$), which is associated with large eddies, is defined as follows:

$$\tau_t = \frac{\ell}{\acute{u}_t} \quad (2\text{-}6)$$

$$\ell = C_D \frac{(\acute{u}_t)^3}{\epsilon} \quad (2\text{-}7)$$

### 2.1.5 Taylor scale Reynolds number

Taylor-scale Reynolds number $R_\lambda$ is one of the common quantity that used in the turbulent flow characterization. The active grid turbulence generated by Makita [154] which also developed and extended to generate the turbulent flow up Taylor microscale. Makita and Warhaft [155] introduced their study for the range of the velocity ($50 \leq Re_\lambda \leq 700$) using activethe grid. They indicated that there is relatiaonship between the $R_\lambda$ and velocity. They observed that the turbulence is weak for the $Re_\lambda \leq 100$. Whilst the region for $Re_\lambda \geq 700$, the turbulence is strong. The $R_\lambda$ depend on fluctuation velocity and the Taylor microscale. In addition, the Taylor scale Reynolds number is related to the turbulent Reynold number. Since the turbulent Reynold number is defined based on the fluctuation velocity and turbulent length scale as follows

$$Re_L = \frac{\acute{u}\,\ell}{v} \quad (2\text{-}8)$$

In addition, the Taylor-scale Reynolds number as follows

$$Re_\lambda = \frac{\lambda_r \acute{u}}{\upsilon} \tag{2-9}$$

The Taylor-scale Reynolds number relates to the turbulent Reynold number based on the relationship between the Taylor scale and the length scale. As result, the Taylor microscale falls between small-scale eddies and the large-scale eddies. Therefore, it is crucial to define the relationship between the Kolmogorov and Taylor scales

$$\boldsymbol{\lambda_r}/_{\boldsymbol{\ell}} = \sqrt{\mathbf{10}}^{\,-1/2}\sqrt{\boldsymbol{Re_L}} \tag{2-10}$$

The Reynolds number based on the Taylor microscale is related to the Reynold number as follows.

$$\boldsymbol{Re_\lambda} = \sqrt{\frac{\mathbf{20}}{\mathbf{3}}\boldsymbol{Re_L}} \tag{2-11}$$

### 2.1.6 Flame thickness

Flame thickness, $\ell_f$, is the main quantity in laminar premixed flames. It is important in the modeling of premixed turbulent flame. In addition, this quantity is crucial in the regimes of the premixed turbulent combustion because it is strongly associated with the length scale. Laminar flame thickness is mostly used in premixed turbulent flame models to categorize the turbulence scale [156]. Multiple definitions for flame thickness have been proposed by researchers based on the flame model, such as Poinsot and Veynante [22]. Gottgens et al. [102, 157] presented a correlation for the scaling laws that involve the relationship of the thickness of the laminar premixed flame with the length scale:

$$\boldsymbol{\ell_f} = \frac{\boldsymbol{\upsilon_t}}{\boldsymbol{\rho_u\ C_p\ S_L}} \tag{2-12}$$

$S_L$ is the laminar flame speed that is used as a reference speed in most combustion studies [16]. In the regimes of the turbulent premixed flame, the Schmidt number assumes unity [18-20], which leads to the equality of the diffusion coefficient with the dynamic viscosity, and the flame thickness is defined as follows:

$$\ell_f = \frac{D_t}{S_L} \tag{2-13}$$

### 2.1.7 Laminar flame speed

Laminar flame speed is the main property of combustion. Therefore, the laminar flame should be studied to understand turbulent flame. Firstly, the flame should be defined to understand laminar flame speed. Flame is simply defined as the self-sustaining propagation of a localized combustion area at subsonic speed. Laminar flame speed is the property of a combustible fuel mixture that is traveling as a wave at subsonic speed. Laminar premixed flames have many applications, such as Bunsen burners, gas ranges and heating appliances. Numerous studies [158, 159] indicated that flame speed is a function of temperature at atmospheric pressure and fuel mixtures. Therefore, laminar flame speed is a physicochemical constant for a given fuel mixture

Generally, laminar burning velocity describes the gaseous flow at the flame. Laminar flame speed is defined based on the theory that divides the flame into the preheat region (or region of conduction) (zone 1) and the reaction region (zone 2) as shown in Figure **2-3**. Laminar flame speed is defined by Glassman [160] as the thickness of the burning zone, δ.

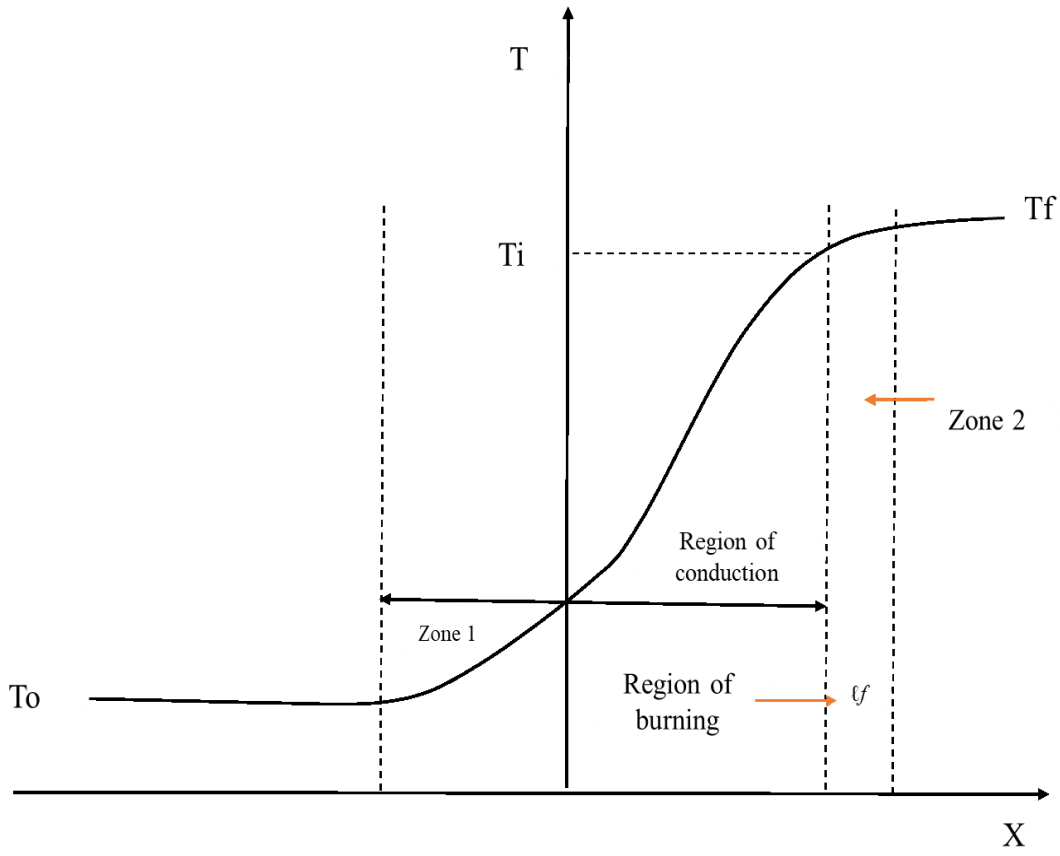


Figure 2-3 The temperature in Laminar flame speed.

Laminar flame speed is an important quantity in the modeling of turbulent combustion. The correlation for laminar flame speed has been introduced by many researchers. For instance, Metghalchi [161] proposed the correlation for laminar flame speed with respect to the pressure and temperature of unburnt gases as follows:

$$S_L = S_{L0}\left(\frac{T_u}{T_o}\right)^{\alpha}\left(\frac{P_u}{P_o}\right)^{\beta} \tag{2-14}$$

Another correlation for laminar flame speed was proposed by Gulder [21] and is calculated as follows:

$$S_L = Z\,W\,\phi^{\eta}\,exp[-\xi(\phi - 1.075)^2]\left(\frac{T_u}{T_o}\right)^{\psi}\left(\frac{P_u}{P_o}\right)^{\Lambda} \tag{2-15}$$

where $Z = 1$, $W = 0.446$, $\eta = 0.12$, $\xi = 4.95$, $\psi = 1.77$ and $\Lambda = -0.2$.

## 2.2 *Modeling strategies*

### 2.2.1 Introduction

Turbulent combustion processes are governed by basic transport equations, which include continuity, momentum, energy and species equations. The problems of the turbulent combustion system are simplified and modeled by deriving and solving the governing equations. The mean properties of the flow can be achieved by solving the partial differential equations for mass, momentum and turbulence *(*K-$\varepsilon$ model) for the non-reacting flows. For the reacting flows, additional equations for the chemical species and energy are essential [162]. Turbulent combustion modeling requires the species equation aside from the other governing equations.

The governing equations of the flow are introduced to prepare the model for simulations. The details of the modeling of turbulent premixed flame are presented in the next sections. The RANS with Favre average is explained.

### 2.2.2 Conservation governing equations

The parameters of and the main equations in the turbulent premixed flame should be understood before modeling the classical approach of the flame model. The description of turbulent combustion depends on the main governing equations. These equations include the following:

1. Conservation of mass (continuity equation).
2. Conservation of momentum (for each independent spatial direction).
3. Conservation of energy.

4. Conservation of species.

These conservation equations can be derived and simplified starting from the mass balance over an infinitesimal differential fluid element. Firstly, the mass conservation equation of each species can be derived in a multicomponent mixture, and the same procedure is applied to derive the form momentum, species and energy equations (Figure **2-4**) [10, 16, 125].

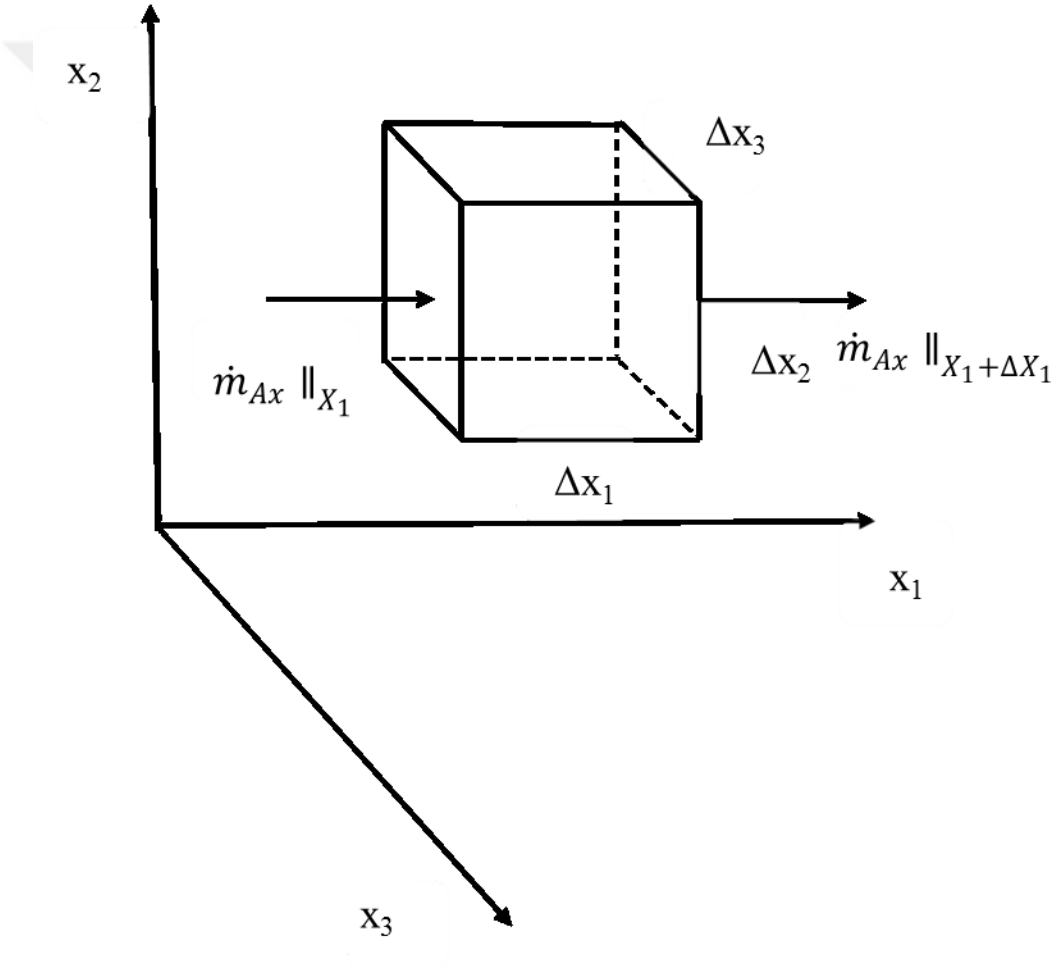


Figure 2-4 Fixed infinitesimal control volume $\Delta x_1\ \Delta x_2\ \Delta x_3$ through which a fluid is flowing.

The rate of accumulation of the mass of species A within the CV is

$$\boldsymbol{\partial \rho_A / \partial t}\ \Delta \boldsymbol{x_1 \Delta x_2 \Delta x_3} \tag{2-16}$$

The rate of the mass of species that enters the CV can be written as follows:

$$\dot{\boldsymbol{m}}_{\boldsymbol{Ax}} \|_{X_1}\ \Delta \boldsymbol{x_2}\ \Delta \boldsymbol{x_3} \tag{2-17}$$

whereas the rate of the mass of species exiting the CV is equal to

$$\dot{\boldsymbol{m}}_{\boldsymbol{Ax}} \|_{X_1+\Delta X_1}\ \Delta \boldsymbol{x_2 \Delta x_3} = \dot{\boldsymbol{m}}_{\boldsymbol{AX_1}} \|_{X_1}\ \Delta \boldsymbol{x_2 \Delta x_3} + \frac{\partial \dot{\boldsymbol{m}}_{\boldsymbol{AX_1}}}{\Delta \boldsymbol{x_1}}\ \Delta \boldsymbol{x_2 \Delta x_3} \tag{2-18}$$

The rate of the production of species A by chemical reactions inside the CV is expressed as follows:

$$\dot{\boldsymbol{m}}_{\boldsymbol{Ax}} \|_{X_1}\ \Delta \boldsymbol{x_2 \Delta x_3} \tag{2-19}$$

The following is obtained by adding the rate of the mass of species' input and output terms in the $x_2$ and $x_3$ directions and dividing them by $\Delta x_1 \Delta x_2 \Delta x_3$:

$$\frac{\partial \boldsymbol{\rho_A}}{\partial \boldsymbol{t}} + \left(\frac{\partial \dot{\boldsymbol{m}}_{\boldsymbol{Ax_1}}}{\partial \boldsymbol{x_1}} + \frac{\partial \dot{\boldsymbol{m}}_{\boldsymbol{Ax_2}}}{\partial \boldsymbol{x_2}} + \frac{\partial \dot{\boldsymbol{m}}_{\boldsymbol{Ax_3}}}{\partial \boldsymbol{x_3}}\right) = \boldsymbol{S_A} \tag{2-20}$$

Equation (26) can be rewritten in tensor form as

$$\frac{\partial \boldsymbol{\rho_A}}{\partial \boldsymbol{t}} + \frac{\partial (\boldsymbol{\rho\, u_A})}{\partial\, \boldsymbol{x_i}} = \boldsymbol{S_A} \tag{2-21}$$

Similarly, the mass conservation equation of species B can be written as follows:

$$\frac{\partial \boldsymbol{\rho_B}}{\partial \boldsymbol{t}} + \frac{\partial (\boldsymbol{\rho\, u_B})}{\partial\, \boldsymbol{x_i}} = \boldsymbol{S_B} \tag{2-22}$$

where the first term on the left hand of the equation is the rate of the gain of the mass of species (k) per unit volume, and the second term on the equation is the net rate of the mass flow of the species out by diffusion and the bulk flow per unit volume. The term on the right-hand equation is the net rate of the mass production of species (k) per unit volume.

The following result is obtained by adding the mass conservation equation of species A and B is Continuity equation of the mixture. :

$$\frac{\partial \rho}{\partial t} + \frac{\partial(\rho u_i)}{\partial x_i} = 0 \quad (2\text{-}23)$$

The group of species (reactants) is converted into another group of species (products) in the combustion process because the mass is not created or destroyed in the combustion.

The momentum equation is derived in the same procedure as the quantity equation

$$\frac{\partial \rho}{\partial t}(\rho u_i) + \frac{\partial}{\partial x_i}(\rho u_i u_j) = -\frac{\partial p}{\partial x_i} + \frac{\partial \tau_{ij}}{\partial x_j} \quad (2\text{-}24)$$

The energy equation is derived as follows:

$$\frac{\partial}{\partial t}(\rho h) + \frac{\partial}{\partial x_i}(\rho h_i) = -\frac{\partial \rho h u_i}{\partial x_i} - \frac{\partial}{\partial x_j}\left(\rho D_t \frac{\partial h}{\partial x_j}\right) \quad (2\text{-}25)$$

$$\frac{\partial}{\partial t}(\overline{\rho}\tilde{c}) + \frac{\partial}{\partial x_j}(\overline{\rho}\tilde{u}_j\tilde{c}) = \frac{\partial}{\partial x_j}\left(\overline{\rho}\frac{\nu_t}{S_C}\frac{\partial \tilde{c}}{\partial x_j}\right) + \overline{S_f} \quad (2\text{-}26)$$

## 2.3 *Reynold - averaged Navier - Stokes equations*

Computational fluid dynamics deal with information on the averaged quantities of flow, such as mean velocities, mean pressures and mean stresses. Given that this study investigates the influence of turbulence on the flame, turbulent fluctuations should be resolved. Many approaches can be used to deal with the effects of turbulence on flame [163]. The RANS approach is one of these approaches. It depends on the ensemble averaging of the instantaneous transport equations for mass, momentum and energy for the non-reacting turbulent flow and reactive scalars for the turbulent combustion problems [117, 164]. Therefore, RANS approaches are used in this study to solve the equation set for the steady and unsteady state cases. An additional term appears with

the introduction of the averaged governing equations because of the nonlinearity of the original equations. The complexity of these unclosed terms is one of the critical problems of the reaction source terms in the species equations that must be modeled. However, in the procedure of RANS in the turbulent flow, a time average is created over a time period ($\tau$) that is longer than the largest time scale in terms of variable $\phi$(x, $t$).

$$\bar{\boldsymbol{\phi}}\,(\boldsymbol{x}) = \frac{\mathbf{1}}{\boldsymbol{\tau}}\int_{\mathbf{0}}^{\boldsymbol{\tau}} \boldsymbol{\phi}\,(\boldsymbol{x},\boldsymbol{t})\boldsymbol{dt} \tag{2-27}$$

The change in length and time scale is considered because this study deals with turbulent combustion. Firstly, the URANS equations are derived based on the main properties of turbulent flow, including velocity, pressure, density and fuel mass fraction. According to the RANS, these properties are decomposed [117] into average and fluctuation [121, 164] as follows:

$$\boldsymbol{\phi} = \bar{\boldsymbol{\phi}} + \acute{\boldsymbol{\phi}} \tag{2-28}$$

where $\bar{\phi}$ is the mean and $\phi'$ the fluctuation. The instantaneous properties of turbulent flow can be represented according to the RANS as follows:

$$\boldsymbol{u} = \bar{\boldsymbol{u}} + \boldsymbol{u}^{\boldsymbol{i}} \tag{2-29}$$

$$\boldsymbol{p} = \bar{\boldsymbol{p}} + \boldsymbol{p}' \tag{2-30}$$

$$\boldsymbol{\rho} = \bar{\boldsymbol{\rho}} + \boldsymbol{\rho}' \tag{2-31}$$

$$\boldsymbol{h} = \bar{\boldsymbol{h}} + \boldsymbol{h}' \tag{2-32}$$

$$\boldsymbol{Y_i} = \bar{\boldsymbol{Y}}_{\boldsymbol{\iota}} + \acute{\mathbf{Y}}_{\boldsymbol{i}} \tag{2-33}$$

When this so-called Reynolds averaging introduces compressible Navier–Stokes equations, correlations that involve density fluctuations appear. The main problem in modeling

turbulent combustion is that the combustion process introduces a high variation in density with respect to the position. The correlations between the variation in density and the fluctuations of other properties are expressed using the Favre property [122, 164]. The Favre average is formed to simulate combustion [33] as follows:

$$\widetilde{\boldsymbol{\phi}} = \frac{\overline{\rho\boldsymbol{\phi}}}{\bar{\rho}} \tag{2-34}$$

where $\bar{\rho}$ is the Reynolds average of using Favre averaging [85] on the property of the Favre that reads

$$\boldsymbol{\phi} = \widetilde{\boldsymbol{\phi}} + \boldsymbol{\phi}'' \tag{2-35}$$

where $\phi''$ is the fluctuation with respect to the Favre-averaged mean value. However, the averaged quantities and fluctuations in terms of Favre [17, 108, 164] have rules that can be set as follows:

Depending on the definition of the Favre-averaged rule, the value of the Reynolds average of a Reynolds fluctuation is zero.

$$\overline{\boldsymbol{\phi}'} \equiv \mathbf{0} \tag{2-36}$$

The quantity of the Reynolds average is equal to the Reynolds average of a Reynolds-averaged quantity.

$$\overline{(\bar{\boldsymbol{\phi}})} = \bar{\boldsymbol{\phi}} \tag{2-37}$$

The product of the two Reynolds-averaged quantities equals the product of the Reynolds average of a product of two quantities as follows

$$\overline{(\bar{\boldsymbol{\phi}}\boldsymbol{\Omega})} = \bar{\boldsymbol{\phi}}\,\bar{\boldsymbol{\Omega}} \tag{2-38}$$

The quantity of Favre average equals the Reynolds average of a Favre-averaged quantity

$$\overline{\widetilde{\boldsymbol{\phi}}} = \widetilde{\boldsymbol{\phi}} \tag{2-39}$$

Because of

$$\widetilde{\boldsymbol{\phi}} = \overline{\left(\frac{\overline{\rho\,\phi}}{\rho}\right)} \tag{2-40}$$

The spatial differentiation of Reynolds averaging is as follows:

$$\overline{\left(\frac{\partial \boldsymbol{\phi}}{\partial \boldsymbol{x_j}}\right)} = \frac{\partial \bar{\boldsymbol{\phi}}}{\partial \boldsymbol{x_j}} \tag{2-41}$$

The quantity of Reynolds averaging equals approximately the temporal differentiation.

$$\overline{\left(\frac{\partial \boldsymbol{\phi}}{\partial \boldsymbol{t}}\right)} \approx \frac{\partial \bar{\boldsymbol{\phi}}}{\partial \boldsymbol{t}} \tag{2-42}$$

The rules of the Favre average are applied to the governing conservation equation. Therefore, the continuity equation is recalled first 2-23.

$$\frac{\partial \boldsymbol{\rho}}{\partial \boldsymbol{t}} + \frac{\partial(\boldsymbol{\rho}\,\boldsymbol{u_i})}{\partial\,\boldsymbol{x_i}} = \mathbf{0} \tag{2-43}$$

With the substitution of $\bar{u}_i$ and $\bar{\rho}$, the equation of Reynolds average becomes

$$\frac{\partial \bar{\boldsymbol{\rho}}}{\partial \boldsymbol{t}} + \frac{\partial(\bar{\boldsymbol{\rho}}\,\bar{\boldsymbol{u}}_{\boldsymbol{i}})}{\partial\,\boldsymbol{x_i}} + \frac{\partial(\overline{\boldsymbol{\rho' u'_i}})}{\partial\,\boldsymbol{x_i}} = \mathbf{0} \tag{2-44}$$

The term ($\frac{\partial(\overline{\rho' u'_i})}{\partial\,x_i}$) in Equation 2-44 is eliminated in the reaction process according to the averaged rule. Therefore, the continuity equation of the Reynolds average for a constant density is as follows:

$$\frac{\partial \bar{\boldsymbol{\rho}}}{\partial \boldsymbol{t}} + \frac{\partial(\boldsymbol{\rho}\,\bar{\boldsymbol{u}}_{\boldsymbol{i}})}{\partial\,\boldsymbol{x_i}} = \mathbf{0} \tag{2-45}$$

In the current turbulent combustion process, the density-weighted mean velocity is represented in Favre averaging as follows:

$$\widetilde{\boldsymbol{u}} = \frac{\overline{\boldsymbol{\rho}\,\boldsymbol{u}}}{\bar{\boldsymbol{\rho}}} \tag{2-46}$$

Therefore, instantaneous velocity $u$ can be expressed as

$$\boldsymbol{u = \tilde{u} + u'' = \frac{\overline{\rho u}}{\bar{\rho}} + u''} \quad (2\text{-}47)$$

In the second term of the continuity equation, the Favre average product ( $\rho u_i$) is required. It can be introduced by multiplying Equation 2- 47 by $\rho$ . Thus, we obtain

$$\boldsymbol{\rho u = \rho(\tilde{u} + u'')} \quad (2\text{-}48)$$

By time-averaging Equation 2-48, one can obtain

$$\boldsymbol{\overline{\rho u} = \bar{\rho}\tilde{u} + \overline{\rho u''})} \quad (2\text{-}49)$$

According to the definition of Favre averaging, $\overline{\rho u''}) = 0$. Therefore, the Favre average of the mass conservation equation can be written as

$$\boldsymbol{\frac{\partial \bar{\rho}}{\partial t} + \frac{\partial(\bar{\rho}\,\tilde{u}_i)}{\partial x_i} = 0} \quad (2\text{-}50)$$

The original continuity equation, the Reynolds-averaged continuity equation and the Favre equation 2-50, have the same terms and similar except that the mean velocity, mean density and density-weighted Favre-averaged velocity for the various equations, respectively. Therefore, the RANS formulation is used in the combustion simulations that are similar to the Favre-averaged equations to deal with the fluctuations of density and velocity. The momentum equation is expressed as follows:

$$\boldsymbol{\frac{\partial \rho}{\partial t}(\rho u_i) + \frac{\partial}{\partial x_i}\left(\rho\, u_i u_j\right) = -\frac{\partial p}{\partial x_i} + \frac{\partial \tau_{ij}}{\partial x_j} \quad i = \{1, 2, 3\}} \quad (2\text{-}51)$$

The momentum equation after substituting the RANS and the Favre average in the equation can be written as

$$\boldsymbol{\frac{\partial}{\partial t}(\overline{\rho \tilde{u}_i}) + \frac{\partial}{\partial x_j}\left(\overline{\rho \tilde{u}_i \tilde{u}_j}\right) = -\frac{\partial \bar{P}}{\partial x_i} + \frac{\partial}{\partial x_j}\left(\tilde{\tau}_{ij} + \bar{\tau}_{tij}\right)} \quad (2\text{-}52)$$

The same procedure is applied to the energy equation, which expresses the energy equation in the form of a Favre average as follows:

$$\frac{\partial}{\partial t}\left(\overline{\rho}\widetilde{h}\right)+\frac{\partial}{\partial x_i}\left(\overline{\rho}\widetilde{u}_i\widetilde{h}\right)=-\frac{\partial\overline{\rho}\,\widetilde{u_i''h''}}{\partial x_i}-\frac{\partial}{\partial x_j}\overline{\left(\rho D_t\frac{\partial h}{\partial x_j}\right)} \tag{2-53}$$

The mass-weighted Favre mean transport equations of the species equation can be written as follows:

$$\frac{\partial}{\partial t}\left(\overline{\rho}\widetilde{c}\right)+\frac{\partial}{\partial x_j}\left(\overline{\rho}\widetilde{u}_j\widetilde{c}\right)=\frac{\partial}{\partial x_j}\left(\overline{\rho}\frac{\nu_t}{S_C}\frac{\partial\widetilde{c}}{\partial x_j}\right)+\overline{S_f} \tag{2-54}$$

## 2.4 *Flame model*

The CFM is used in this study for the modeling and simulation of turbulent premixed flame. The CFM includes FAD, which is one of the key parameters in premixed turbulent flame and deals with the problem of turbulence–flame interaction. With FAD [14, 110, 115, 165] the impacts of turbulence on flame can be studied by solving the source term in the species equation in terms of the FAD.

For reacting flows, the transport equations of the chemical species and energy are used to describe the main reactive and thermal processes. In this study, the K-ε model is selected to deal with turbulent flow. The K-ε model can calculate turbulence length scales and turbulence intensities by using the TKE and TDR. These formulations and equations are solved using the RANS method, which is among the numerical techniques for the simulation of turbulent premixed combustion [23, 62, and 164]. Favre averaging is used to solve the equations in this model because of the variation in density during combustion.

Therefore, the governing equations of continuity, momentum, energy and species are formulated in terms of the Favre-averaging density of [23, 166, and 167] as follows:

Continuity equation

$$\frac{\partial \bar{\rho}}{\partial t} + \frac{\partial(\bar{\rho}\,\tilde{u}_i)}{\partial x_i} = 0 \tag{2-55}$$

Momentum equation

$$\frac{\partial}{\partial t}(\bar{\rho}\widetilde{u_i}) + \frac{\partial}{\partial x_j}\left(\bar{\rho}\widetilde{u_i}\widetilde{u_j}\right) = -\frac{\partial \bar{P}}{\partial x_i} + \frac{\partial}{\partial x_j}\left(\tilde{\tau}_{ij} + \bar{\tau}_{tij}\right) \tag{2-56}$$

Energy equation

$$\frac{\partial}{\partial t}\left(\bar{\rho}\tilde{h}\right) + \frac{\partial}{\partial x_i}\left(\bar{\rho}\tilde{u}_i\tilde{h}\right) = -\frac{\partial \bar{\rho}\,\widetilde{u_i''h''}}{\partial x_i} - \frac{\partial}{\partial x_j}\overline{\left(\rho D_t \frac{\partial h}{\partial x_j}\right)} \tag{2-57}$$

In the coherent flame model, the fuel mass fraction and the FAD are solved using the source term of the species equation [168 & 169]. The transport equation of species is thus formulated in terms of the an-normalized reaction progress as follows:

$$\frac{\partial}{\partial t}(\bar{\rho}\tilde{c}) + \frac{\partial}{\partial x_j}\left(\bar{\rho}\tilde{u}_j\tilde{c}\right) = \frac{\partial}{\partial x_j}\left(\bar{\rho}\frac{\nu_t}{S_C}\frac{\partial \check{c}}{\partial x_j}\right) + \overline{S_f} \tag{2-58}$$

where $\tilde{c}$ is the un-normalised reaction progress and is defined as

$$C = Y_{ft} + Y_{res} - Y_f \tag{2-59}$$

The fuel mass fraction is calculated in terms of the progress reaction variable (b), which is equal to zero for unburnt gases and unity for burnt gases.

$$b = \frac{c - Y_{res}}{Y_{ft} - Y_{res}} \tag{2-60}$$

The second term on the right side of Eq. 2-58 is the source term in terms of the fuel mass fraction ($S_f$).

$$S_f = -(\rho_u S_L \Sigma)(Y_{ft} - Y_{res}) \tag{2-61}$$

The laminar flame speed is calculated based on the correlation of Gulder [21] as follows:

$$S_L = Z\,W\,\phi^{\eta}\,exp[-\xi(\phi - 1.075)^2]\left(\frac{T_u}{T_o}\right)^{\psi}\left(\frac{P_u}{P_o}\right)^{\Lambda} \tag{2-62}$$

where $Z = 1$, $W = 0.446$, $\eta = 0.12$, $\xi = 4.95$, $\psi = 1.77$ and $\Lambda = -0.2$.

In the coherent flame model, FAD ($\sigma$) is defined as the flame area per unit mass. According to [168], the transport equation of species in terms of the FAD is as follows:

$$\frac{\partial}{\partial t}(\overline{\rho}\tilde{\sigma}) + \frac{\partial}{\partial x_j}\left(\overline{\rho}\tilde{u}_j\tilde{\sigma}\right) = \frac{\partial}{\partial x_j}\left(\overline{\rho}\frac{\nu_t}{S_C}\frac{\partial\tilde{\sigma}}{\partial\tilde{x}_j}\right) + \overline{S}_{\Sigma} \tag{2-63}$$

where the source term is represented in terms of the FAD per unit volume ($\sum$) and is equal to

$$S_{\Sigma} = \alpha K_t\,\Sigma - \beta\frac{\rho_u Y_{ft} S_L\left(1 + a\sqrt{k}/S_L\right)}{\rho\,Y_f}\Sigma^2 \tag{2-64}$$

Equation (66) indicates that the flame stretch is a function of the K-ε model, that is, the turbulence intensity and the turbulence length scale. For the FAD, the turbulence effect is represented in terms of the flame stretch, which is a function of the K-ε model (i.e. turbulence length scale and turbulence intensity). Therefore, flame stretch ($K_t$) in Equation 2-64 is calculated as

$$\Gamma_K = \frac{K_t}{\varepsilon/k} = f\left(\frac{u'}{S_L}, \frac{\ell}{\ell_f}\right) \tag{2-65}$$

$\Gamma_K$ is defined as

$$\Gamma_K = \Gamma_p - B\,\Gamma_q \tag{2-66}$$

where $\Gamma_p$ and $\Gamma_q$ are the flame production and quench due to the stretch, respectively. The fluctuation velocity ($u'$) is calculated [170] using the K-ε model as

$$\boldsymbol{u'} = \sqrt{\frac{2}{3}\,\boldsymbol{k}} \tag{2-67}$$

The turbulence length scale ($\ell$) is also calculated using the K-ε model by employing TKE and TDR.

$$\boldsymbol{\ell} = \frac{\boldsymbol{k}^{3/2}}{\boldsymbol{\varepsilon}} \tag{2-68}$$

# CHAPTER III

# 3 COMBUSTOR DESIGN AND NUMERICAL SIMULATIONS

## *3.1 Introduction*

Computational fluid dynamics and heat transfer approaches are used to model combustion processes. Through CFD, combustion systems have been enhanced, and with CFD the progress in the design of the combustion system could be made [171]. Most turbulent combustion problems involve the strong interaction between turbulence and flame. Therefore, the analytical calculation of turbulent combustion is not as straightforward as the laminar calculations. Numerical simulations are widely used for complex processes, such as turbulent combustion processes, instead of analytical calculation. Numerical simulations of turbulent combustion problems are based on the solution of the main governing equations with multiple input parameters and boundary and initial conditions. In addition, numerical simulations are generally used to solve the models of processes, such as the flame and turbulence models. In the last chapter, the main differential equations of the premixed turbulent flame and the described methods of flame and turbulence are presented. These models must be solved using one of the computer code packages. In this study, STAR-CCM + is utilized to solve these equations. This chapter focuses on the numerical simulations applied to the models using STAR-CCM+. In addition, the mesh and all essential physical processes, which include solving the coherent flame model, turbulent model, implicit unsteady compressible flow, premixed reacting flow, multicomponent gases and 3D, are introduced. Both steady and unsteady flows are implemented in STAR-CCM. In the second part, the algorithm of the control of flame location using the NetBeans program is discussed. The combustor geometry is described in this chapter.

## *3.2 Combustor design and numerical simulations*

Fuel and air are assumed to be premixed upstream of the diffuser combustor with an actual stoichiometric air-fuel ratio ($\lambda$) of 1.7, and the mass percentages of the gas components of fuel are 3.81% $C_3H_8$, 23.55% $O_2$ and 72.63% $N_2$. The initial and inlet boundary conditions of the mixture temperature are 300 K, whilst the pressure is set as the ambient pressure of one bar. The atmospheric pressure is assumed in the surrounding outlet conditions of the diffuser. The fuel mixture is propane–air. At the inlet, fresh mixtures are injected at a fixed velocity of 0.3 m/s and a temperature of 300 K into the diffuser burner with an inner diameter of 10 cm and an outlet diameter of 20 cm.

At the outlet of the combustor, flue gases flow away through the combustor with the pressure-outlet boundaries. The length of the diffuser is 95.3 cm, the downstream diffuser outlet is constant with a length of 40 cm and the angle of the half expansion of the diffuser is 3° (Figure **3-1**).

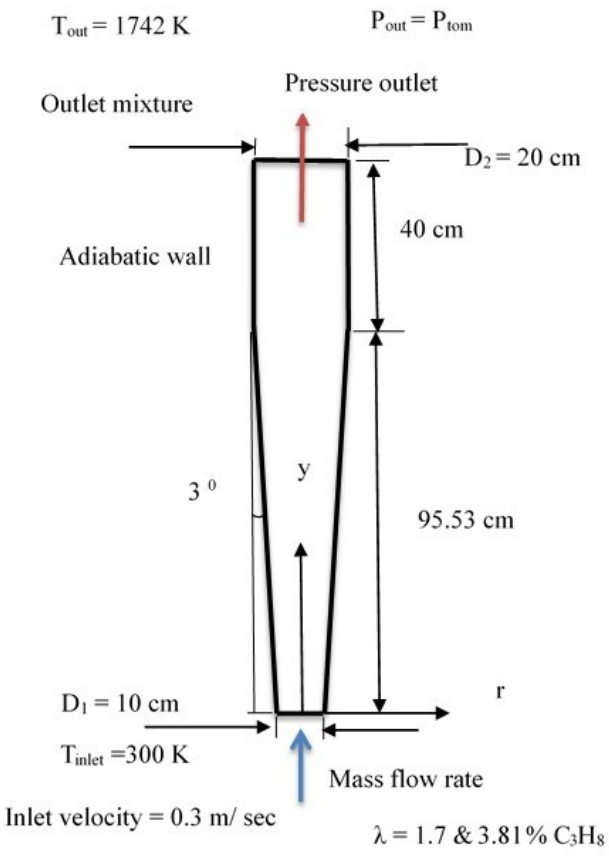


Figure 3-1 Geometry of the diffuser combustor and boundary conditions.

The outcomes of a CFD are dependent on the mesh quality. Therefore, we should ensure that the mesh is of high quality before proceeding to the physical process. The mesh structure should be good to anticipate strong gradients of the variables. The appropriate number and type of mesh are necessary to ensure the accuracy of the solution. The mesh size and the percentage of open area are selected based on the diameters and lengths of the diffuser. Polyhedral meshes are selected to build the core mesh of the diffuser geometry because they provide a balanced solution for mesh generation problems and are more efficient and easier to use than tetrahedral meshes. The prism layer mesh is also used to deal with the core volume mesh for generating orthogonal prismatic cells next to boundaries or wall surfaces. A prism mesh was selected in this

study because it provides an accurate solution, especially near the wall of the combustor, and is crucial to enhancing the accuracy of the solution (Figure **3-2**).

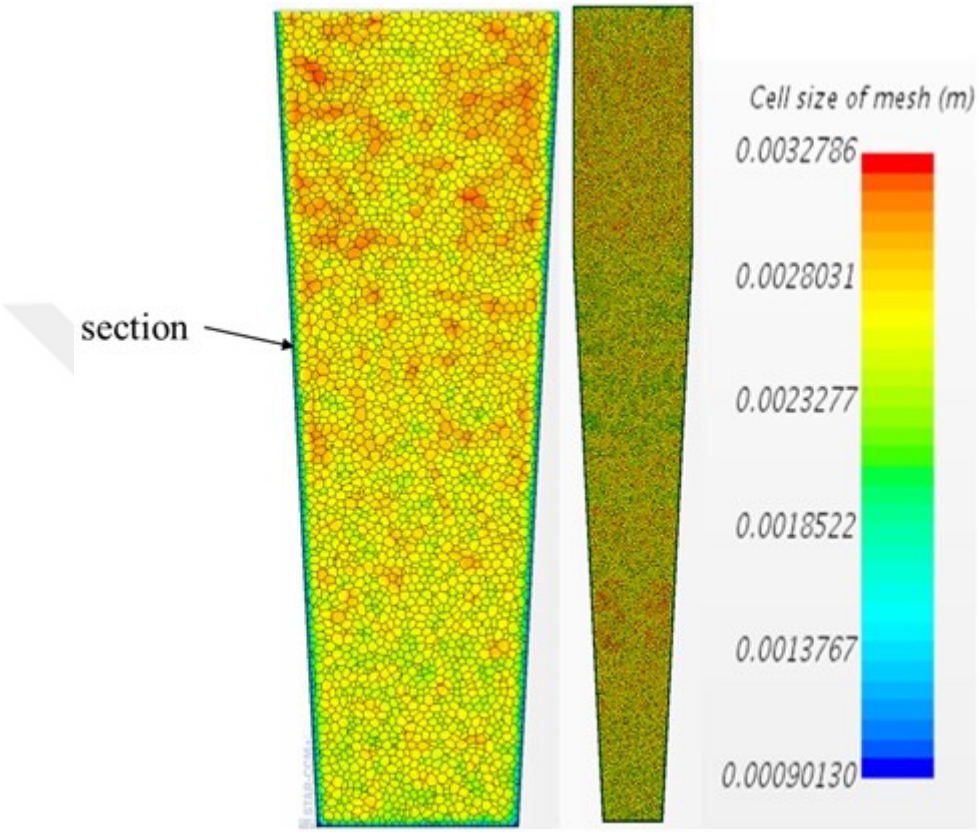


Figure 3-2 Number of cells of the mesh for 5% turbulence intensity and 1 cm turbulence length scale for the diffuser without conical insert.

Mesh independence is tested for the ranges of mesh size to indicate the accuracy of the obtained results. The number of mesh cells is 551,381. Figure **3-3** shows the flame location via the number of mesh cells for 5% turbulence intensity and 1 cm turbulence length scale. For a low number of mesh cells, a small deviation of 2 mm is detected in the flame location from those of the other cases. Then, the flame location is fixed with an increase in the number of mesh cells. No change in flame location is observed with the increase in the number of meshes.

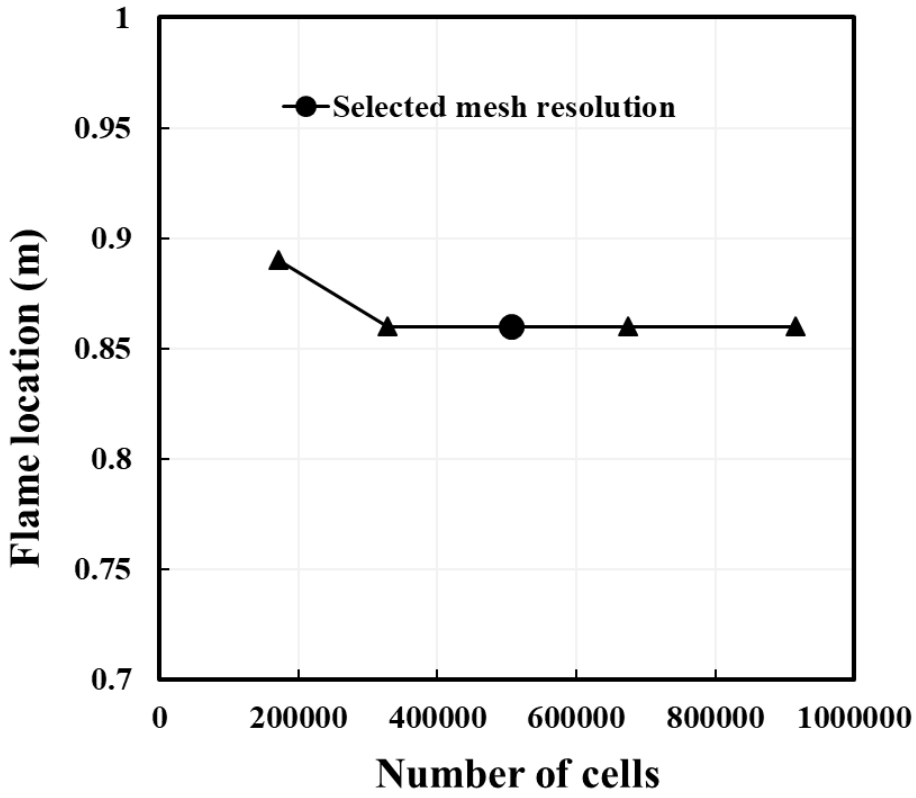


Figure 3-3 Flame location with the number of mesh cells for TI = 5% and $\ell$ = 1 cm.

Given the flow separation that appears near the wall of the diffuser in the unsteady-state conditions, a conical insert is applied to this diffuser to eliminate the flow separation that could occur behind the flame front, which occurs in the diffuser without a conical insert [172]. The diffuser introduced by Nazzal and Ertunc [172] has the same geometric specification as the diffuser in the current, except the current diffuser has no conical insert in the middle (Figure **3-4**). The conical insert is placed at the centre of the diffuser with a diameter and length of 10 and 40 cm, respectively. Thus, all simulations of the unsteady state are repeated with a conical insert.

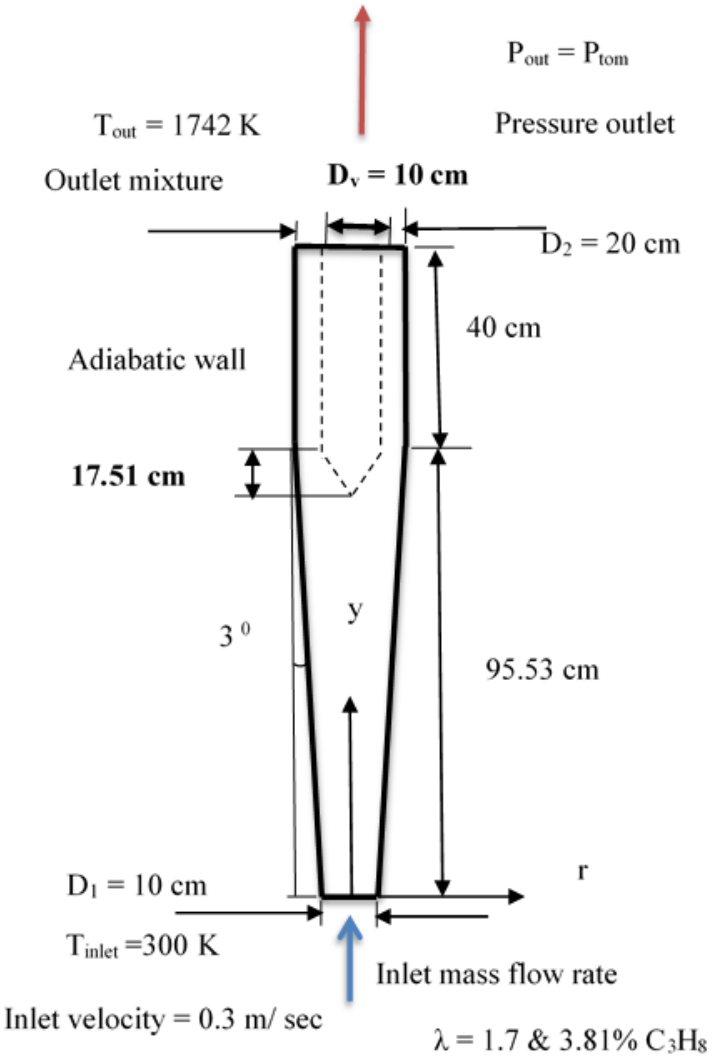


Figure 3-4 Geometry of the diffuser combustor with conical insert and boundary conditions.

The second diffuser used in this study has a conical insert. The same mesh conditions as the first diffuser (without a conical insert) are applied to this diffuser. The minimum cell size of the mesh is 0.11636 mm as shown in Figure **3-5**.

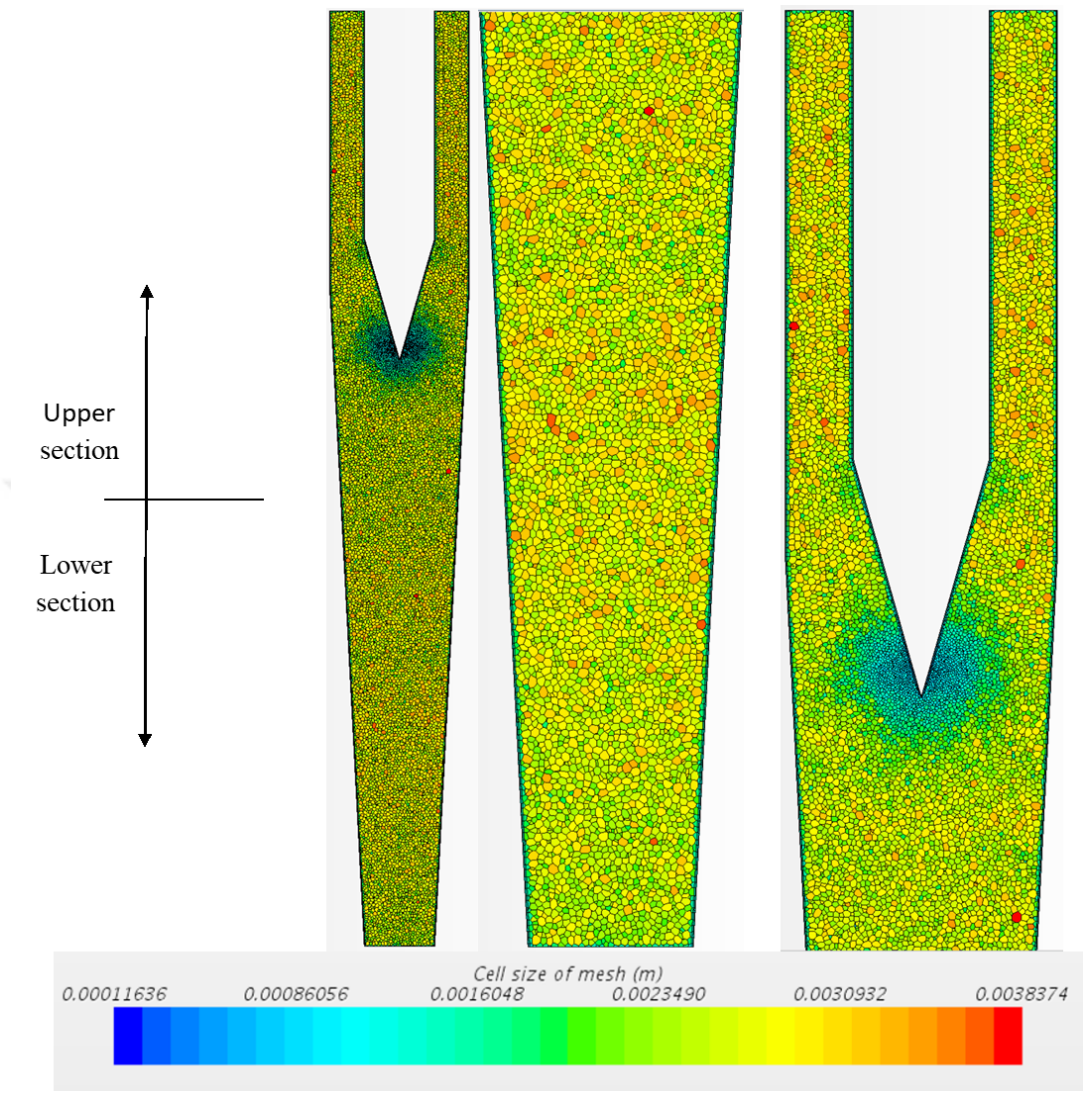


Figure 3-5 the cross-section of the generated mesh and the upper and lower sections of the mesh diffuser with conical insert to clearly indicate the section of the mesh diffuser. The number of mesh cells is 506,387.

Mesh independence is also performed with large ranges of mesh size to assess the accuracy of the simulation results. Figure **3-6** shows the flame location via the number of mesh cells for 5% turbulence intensity and 1 cm turbulence length scale. For a low number of mesh

cells, a small deviation of 2 mm is detected in the flame location from those of the other cases. Then, the flame location is fixed with an increase in the number of mesh cells.

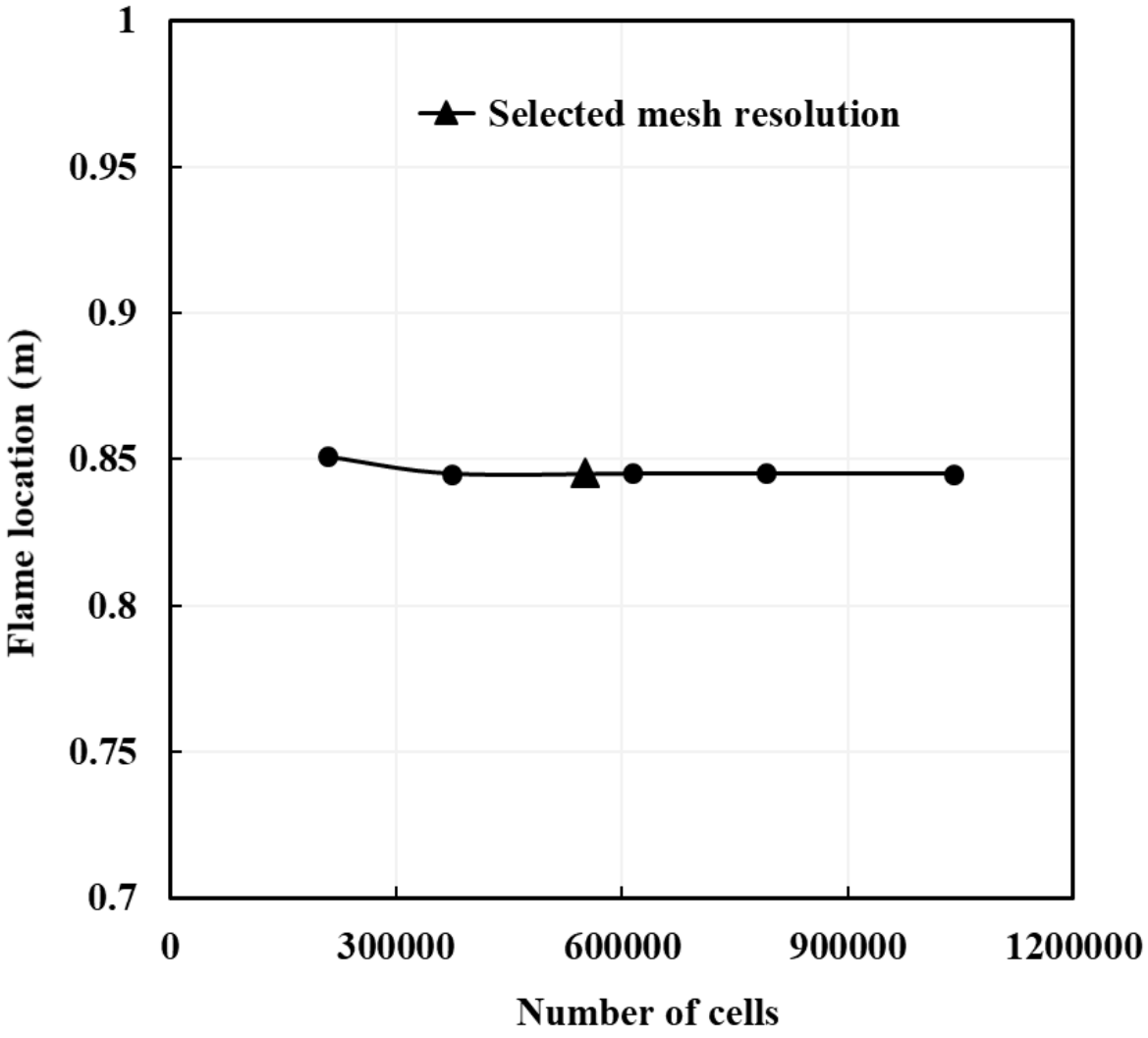


Figure 3-6 Flame location with the number of mesh cells for TI = 5% and $\ell$ = 1 cm for steady state conditions.

All numerical and physical simulations are applied to the diffuser after completing the mesh. The tree of the simulation chart is presented in Table 3-1:

Table 3-1 The physical simulations of the test, which is applied to the diffuser combustor.

| |
|---|
| Coherent flame model |
| Three-dimensional |
| Realisable K-ε model |
| Premixed flame |
| Turbulence |
| Reacting flow |
| Steady and unsteady implicit |
| One-step global reaction |

$$\mathbf{C_3H_8 + 5O_2 \longrightarrow 4H_2O + 3CO_2} \quad (3\text{-}1)$$

Firstly, simulations are conducted using the steady-state conditions. The boundary conditions imposed on the simulation model are ambient pressure and a temperature of 300 K at the inlet. The wall condition is assumed adiabatic. The output temperature is set to the temperature of a fully burnt gas, which is 1742 K. The conditions considered include the turbulence intensities at the inlet of the combustor from the low level (TI = 5%) to the high level (TI = 35%). The turbulence length scales ($\ell$) are set to 1 cm to 10 cm, as shown in

Table 3-2 Test cases at various turbulence intensities and length scales in the inlet of the combustor**.** The turbulence intensity and turbulence length scale are changed at the inlet of the combustor for all test cases as shown in

Table 3-2 Test cases at various turbulence intensities and length scales in the inlet of the combustor.

| Test cases | ℓ | TI | TI | TI | TI | TI | TI |
|---|---|---|---|---|---|---|---|
| **1** | 1 cm | 5 % | 10 % | 15 % | 20% | 25 % | 30% |
| **2** | 5 cm | 5 % | 10 % | 15 % | 20% | 25 % | 30% |
| **3** | 10 cm | 5 % | 10 % | 15 % | 20% | 25 % | 30% |

Secondly, the simulations are repeated for the unsteady-state conditions at the same conditions and physical process. Furthermore, to prevent numerical divergence, the simulation is based on the steady-state condition at TI = 5% and ℓ = 1 cm. Then, this test simulation is considered the initial condition for all the cases of unsteady-state simulations. In the unsteady-state simulation, the inlet conditions of the turbulence are changed stepwise to the required levels of turbulence length scale and turbulence intensity. In addition, the simulations are conducted for a sufficiently long time to allow the stabilization of the flame location with the updated value of the turbulence length scale and turbulence intensity. Given that the Taylor-scale Reynolds number is related to TKE and TDR, they cannot be changed independently of each other. Consequently, TKE and turbulent dissipation are varied to achieve the required level of Taylor-scale Reynolds number ($Re_\lambda$). Thus, the Taylor-scale Reynolds number ($Re_\lambda$) is varied in a wide range at the inlet of the combustor as shown in Table 3-3.

Table 3-3 Test cases at various turbulence intensities and length scales in the inlet of the combustor.

| Test cases | ℓ | 1 cm | 5 cm | 10 cm |
|---|---|---|---|---|
| 1 | TI | 5% | 5% | 5% |
| | $Re_{\lambda i}$ | 38.81 | 65.7 | 75.05 |
| 2 | TI | 10% | 10% | 10% |
| | $Re_{\lambda i}$ | 45.43 | 69.37 | 98.14 |
| 3 | TI | 15% | 15% | 15% |
| | $Re_{\lambda i}$ | 51.51 | 84.94 | 120.14 |
| 4 | TI | 20% | 20% | 20% |
| | $Re_{\lambda i}$ | 59.4 | 98.07 | 139 |
| 5 | TI | 25% | 25% | 25% |
| | $Re_{\lambda i}$ | 66 | 109.6 | 155 |
| 6 | TI | 30% | 30% | 30% |
| | $Re_{\lambda i}$ | 72.50 | 120.07 | 169.16 |

# CHAPTER IV

# 4 STEADY SIMULATIONS OF FLAME IN DIFFUSER COMBUSTOR

## 4.1 *Introduction*

In this Chapter, the results of the steady-state condition are discussed. In the first section of the Chapter, the map of the flame within the Borgi diagram is presented to understand the behavior of flame location with the change in the turbulence intensity and turbulence length scale. In the second section of this chapter, the effect of the turbulence on flame location is presented in terms of temperature distribution. The third part discusses the behavior of the TKE along the axis of the diffuser combustor. In the final section, the behavior of the FAD for various turbulence intensities and turbulence length scales is introduced.

## 4.2 *Effect of turbulence on the flame location*

Understanding how the flame responds and manifests within the regime of the turbulent premixed flame is essential in analyzing the combustion–turbulence interaction at different turbulence intensities and turbulence length scales. This regime [18-20] is based on velocity and turbulence scale ratios and divided into many zones depending on the dimensionless numbers, as shown in Figure 14. Changing the level of turbulence leads to a change in the location within the regimes of the premixed turbulent combustion, which leads to different physical processes. Figure 4-1indicates the locations of the flame for all of the test cases. The locations of the flame are within the wrinkled and corrugated flamelet regimes.

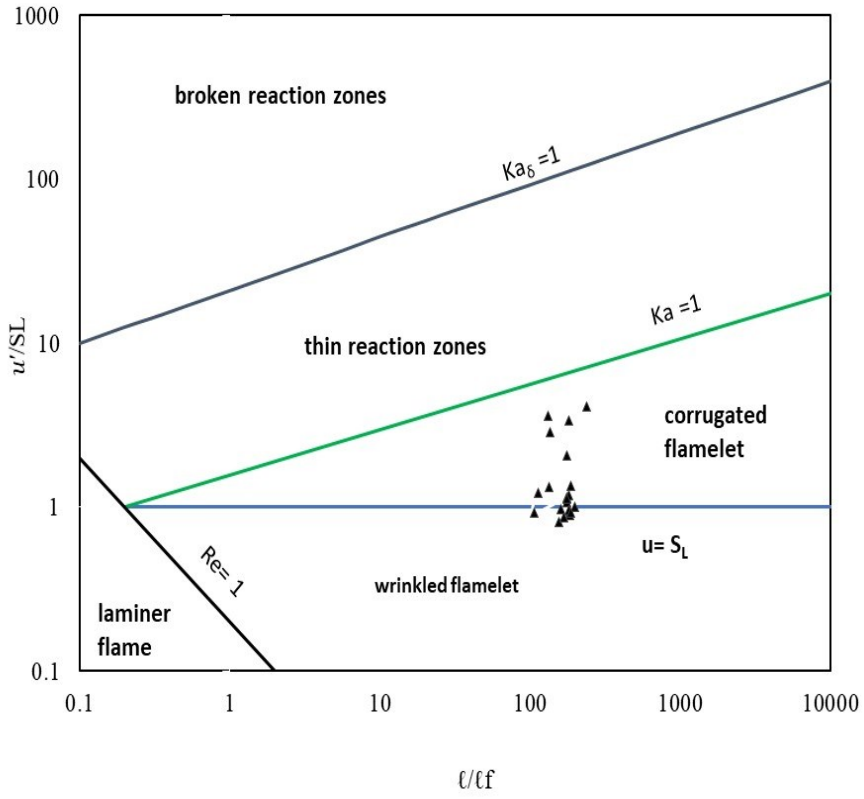


Figure 4-1 Locations of the flames in the turbulent combustion regime.

Temperature and flame area density are the main parameters used to determine the location of the flame front. Flame area density and temperature are represented as a function of turbulence intensity and turbulence length scale. A line probe, which is set along the axial centerline of the diffuser, is used to obtain the main properties, such as temperature, TKE, and flame area density. Figure **4-2** presents a comparison of temperature contours at various turbulence intensities and turbulence length scales. Figure **4-3** illustrates flame location as a function of turbulence intensity and turbulence length scale. Flame location is extracted from a stationary temperature field of 1,400 K for all cases. Figures 4-2 & 4-3 16 show that the flame front location generally moves toward the inlet of the diffuser with the increase in turbulence intensity for 5 and 10 cm turbulence length scales. However, this behavior depends on the values

of turbulence intensities. First, the flame location moves toward the inlet of the diffuser combustor with an increase in turbulence intensity from 5% to 10%. Second, the flame stabilizes at turbulence intensities of 10% and 15% before decreasing with an increase in turbulence intensity to 20%, 25%, 30%, and 35%.

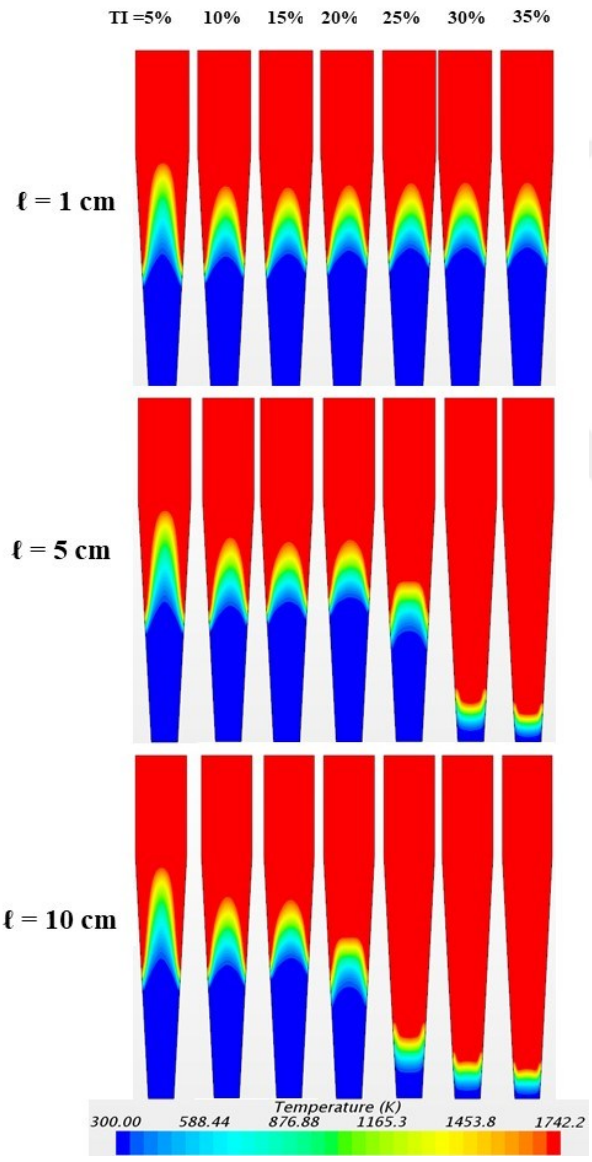


Figure 4-2 Temperature contours with various turbulence intensities and turbulence length scales at the inlet of the diffuser.

The behavior of the flame location for the 1 cm turbulence length scale is also observed. First, the flame location moves toward the inlet of the diffuser combustor with an increase in turbulence intensities from 5% to 10%. Second, the flame location stabilizes with a further increase in the turbulence intensity, as illustrated in Figure **4-3**.

The effect of turbulence intensity on the movements of the flame location at the inlet is more visible with the 5 and 10 cm turbulence length scales (high turbulence Reynolds number) and 30% and 35% turbulence intensities compared with a low turbulence intensity and small turbulence length scale. The results generally show that the flame location is dependent on turbulence intensity and turbulence length scale.

Similar effects of turbulence on flames have been observed by many researchers. For example, Yuan et al [29] analyzed the effects of turbulence on the flame front by changing turbulence intensity within 1% to 50% and found that hydrodynamic instability dominates the growth of flame cells at low turbulence intensities of 1% to 5%. Meanwhile, turbulence wrinkles the flame front and dominates the process at a high turbulence intensity of 50%. Therefore, we set the range of turbulence intensity to within 5% to 35%, and the results indicate the expected effect of turbulence on the flame, that is, the turbulent flame speed increases with turbulence and moves toward the inlet of combustor.

In addition to the change in the flame location, the flame shape changes with an increase in turbulence intensity (greater than 25%) and turbulence length scales (5 and 10 cm). The flame shape can be convex or concave. Many types of flame shapes exist depending on the shape factor, which is based on the flame position and axis planes Chakraborty and Cant [173], Zhang and Rutland [27]. and Kerl et al [44] presented three flame shapes (i.e., hyperbolic, parabolic,

and elliptic) in a diffuser combustor with an annular swirling flow at its inlet. Given that their work is the most similar to the present work, the flame shapes obtained in the present work can be considered realistic.

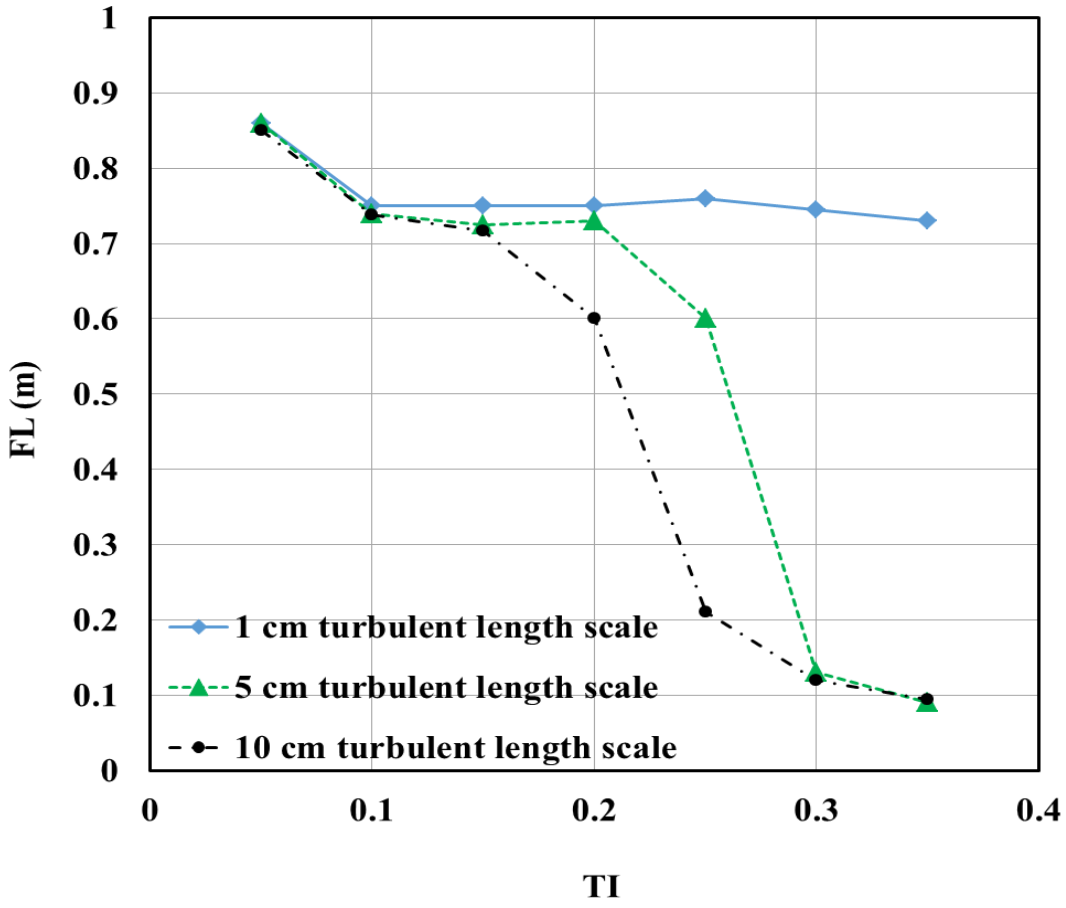


Figure 4-3 Flame location on the axial centerline of the diffuser combustor with various turbulence intensities and turbulence length scales.

## 4.3 *Turbulent kinetic energy*

The behavior of TKE is crucial in revealing the characteristics of turbulence–combustion interactions. Therefore, TKE is plotted together with turbulence intensities and turbulent length scales in the same graph. A physical explanation for flame location behavior with the change in turbulence intensity and turbulence length scale due to the variation in TKE with changing TI and $\ell$ is also provided.

Turbulence intensity and turbulence length scale are functions of TKE, as illustrated in Equations 2-67 & 2-68. Therefore, considering TKE is essential in understanding the effect of turbulence on flame location. The TKE along the axial centerline of the diffuser combustor is measured using a line probe.

Figures 4-4, 4-5 & 4-6 show the variation in the TKE along the centerline of the diffuser combustor with turbulence intensity and turbulence length scales of 1, 5, and 10 cm, respectively. TKE initially decays and then increases in the flame region and further downstream. The increase in TKE occurs within the region of combustion, starting with a flame temperature of $T$ = 1,400 K. At a constant turbulence length scale (Equation 2-68), increasing the turbulence intensity means an increase in the turbulence dissipation rate ($\varepsilon$). In addition, the decay rate of TKE downstream of the inlet is larger than that of high turbulence intensity.

Figure **4-4** also shows that the TKE for 5% turbulence intensity is less than that for 10% turbulence intensity. The development of all the other TKE cases is similar for other values of turbulence intensities. This behavior is similar to that of the flame shown in Figure **4-3**. The flame moves toward the inlet of the diffuser with an increase in the turbulence intensity from 5% to 10%. Subsequently, the flame location stabilizes with an increase in the turbulence intensity.

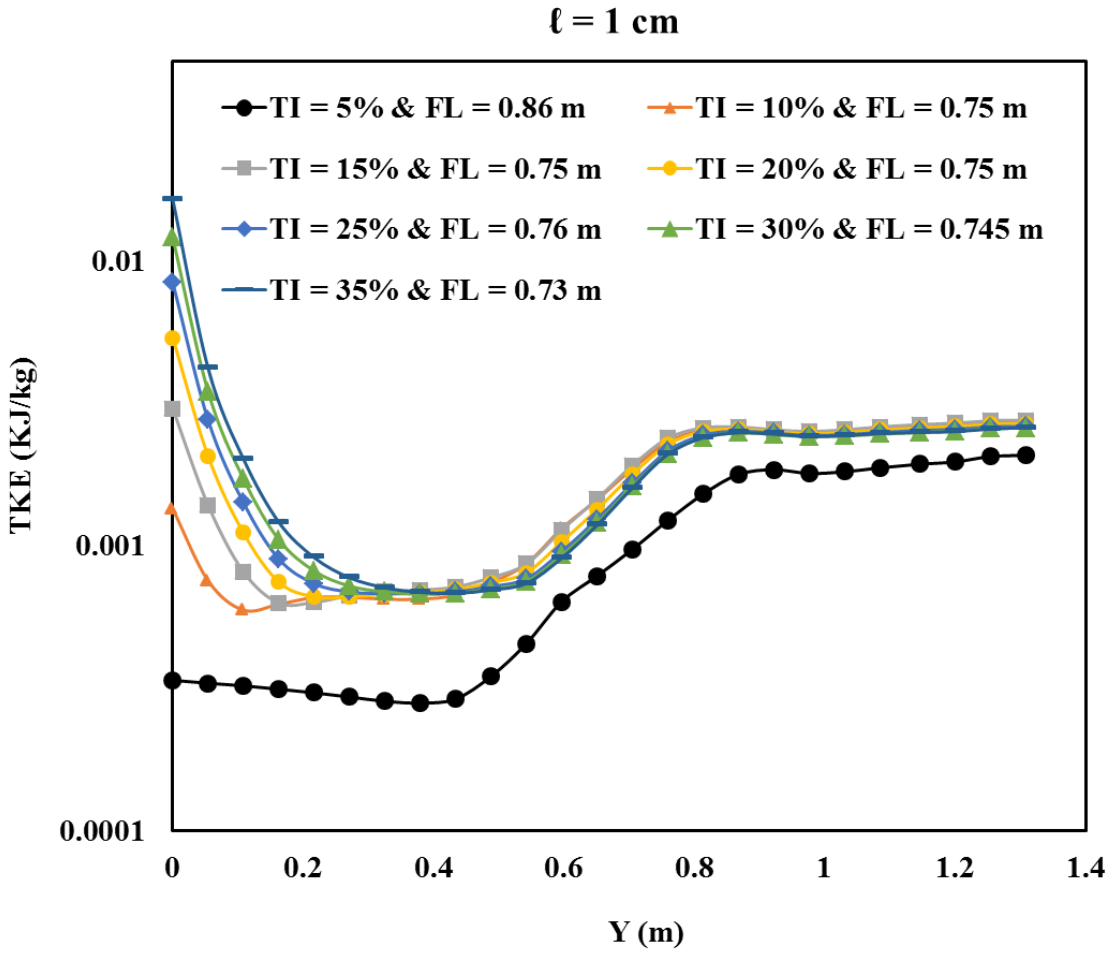


Figure 4-4 TKE along the axial centerline of the diffuser combustor at various turbulence intensities and at 1 cm turbulence length scale.

Figure **4-5** shows TKE with turbulence intensity for the 5 cm turbulence length scale. Two sharp TKE peaks are observed with the increase in turbulence intensity to 30% and 35%. No significant differences are observed at turbulence intensities of 10% and 15% in the flame regions. Hence, the flame location for low turbulence intensity is stabilized, and the flame location sharply moves to the inlet of the diffuser combustor at turbulence intensities of 30% and 35%, as illustrated in Figure **4-2**.

Figure **4-5** shows that the curve of TKE for turbulence intensity = 0.25 is less than the curve of TKE for turbulence intensity = 0.1, 0.15, and 0.2 after $y$ = 0.8 m. In addition, the curve of turbulence intensity = 0.35 is less than the curve of turbulence intensity = 0.3 after $y$ = 0.8 m. This behavior is related to the drop in the flame location and the deceleration of the flow in the diffuser. More specifically, when the flame pulled towards the inlet the flow with increased TKE in the wake the of the flame is exposed to the deceleration of the mean flow. The deceleration of the mean flow augments the decay of the TKE. Therefore, depending on the flame location in the diffuser, cases with higher TKE at the inlet might have lower TKE at far downstream locations.

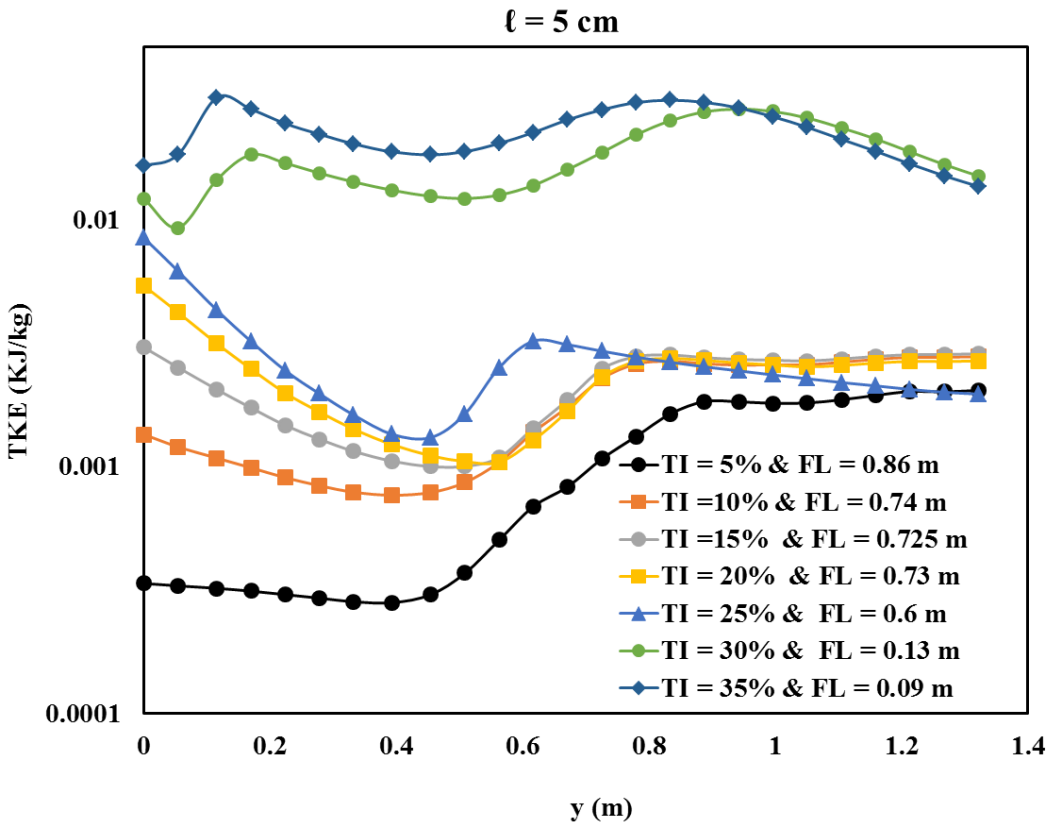


Figure 4-5 TKE in the axial centerline of the diffuser at various turbulence intensities and at 5 cm turbulence length scale.

Figure 4-6 shows the TKE for various turbulence intensities and for the turbulence length scale of 10 cm. Three sharp TKE peaks are observed with the increase in turbulence intensity to 25%, 30%, and 35%. No significant differences are observed at turbulence intensities of 10%, 15%, and 20% in the flame regions. Hence, the flame location for a low turbulence intensity is stabilized, and the flame location sharply moves to the inlet of the diffuser combustor at turbulence intensities of 25%, 30%, and 35%, as illustrated in Figure **4-2**.

Figure **4-6** shows that the curve of TKE at turbulence intensity = 0.2 is less than the curve of TKE at turbulence intensity = 0.1 and 0.15 after $y$ = 0.8 m. In addition, the curve of turbulence intensity = 0.3 is less than the curve of turbulence intensity = 0.25 after $y$ = 0.9 m. This behavior is related to the drop in the flame location and the deceleration of the flow in the diffuser. More specifically, when the flame pulled towards the inlet the flow with increased TKE in the wake the of the flame is exposed to the deceleration of the mean flow. The deceleration of the mean flow augments the decay of the TKE. Therefore, depending on the flame location in the diffuser, cases with higher TKE at the inlet might have lower TKE at far downstream locations.

However, important observations can be formulated for TKE with varying turbulence intensities and turbulence length scales. The flame location moves toward the inlet of the combustor with a concurrent increase in turbulence intensity and TKE. In addition, the highest value of TKE is observed at the lowest value of the flame location. This behavior is due to the increase in TKE, which increases the value of $S_{\sum}$ in Equation 2-64. Thus, the combustion zone becomes narrow, and the flame is pushed toward the inlet of the combustor.

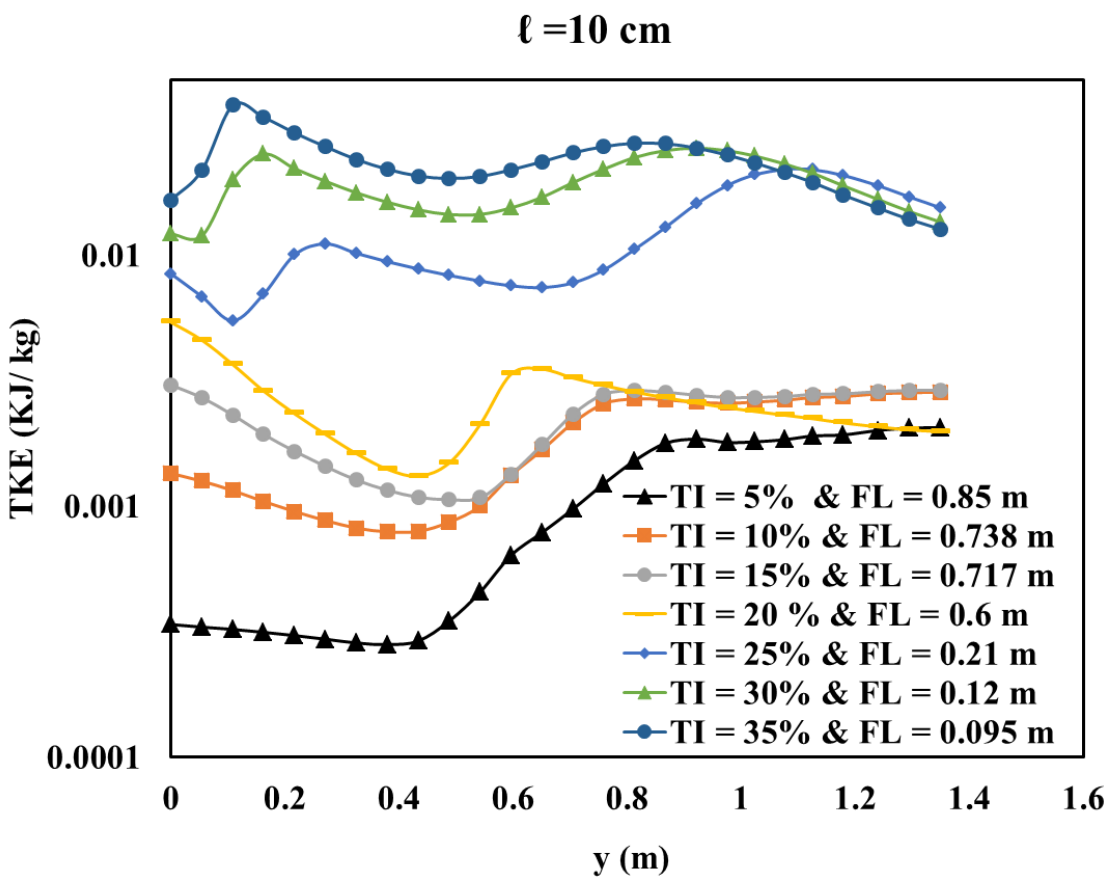


Figure 4-6 Variation in TKE along the axial centerline of the diffuser combustor at various turbulence intensities for the 10 cm turbulence length scale.

## 4.4 *Flame area density*

Flame area density is also used to indicate the flame response in this study. Figures 20 and 21 shows the maximum and integrated flame area (IFA) density with respect to turbulence intensities and turbulence length scales, respectively. The maximum flame area density remains constant with the increase in turbulence intensity for a low turbulence length scale ($\ell$ = 1 cm) (Figure **4-7**). Meanwhile, for $\ell$ = 5 and 10 cm, the maximum flame area density remains constant with the increase in turbulence intensity until it reaches 20% and then increases with the increase

in turbulence intensity to 25% and 30% before becoming constant again. [9], who examined the flame area density in a premixed turbulent flame at various levels of turbulence intensity in a Bunsen burner and concluded that the maximum flame surface density varies with turbulence intensity but show no systematic correlation with it, as it is the case in the present investigations. The integrated flame area has almost the same values, as illustrated in Figure **4-8**.

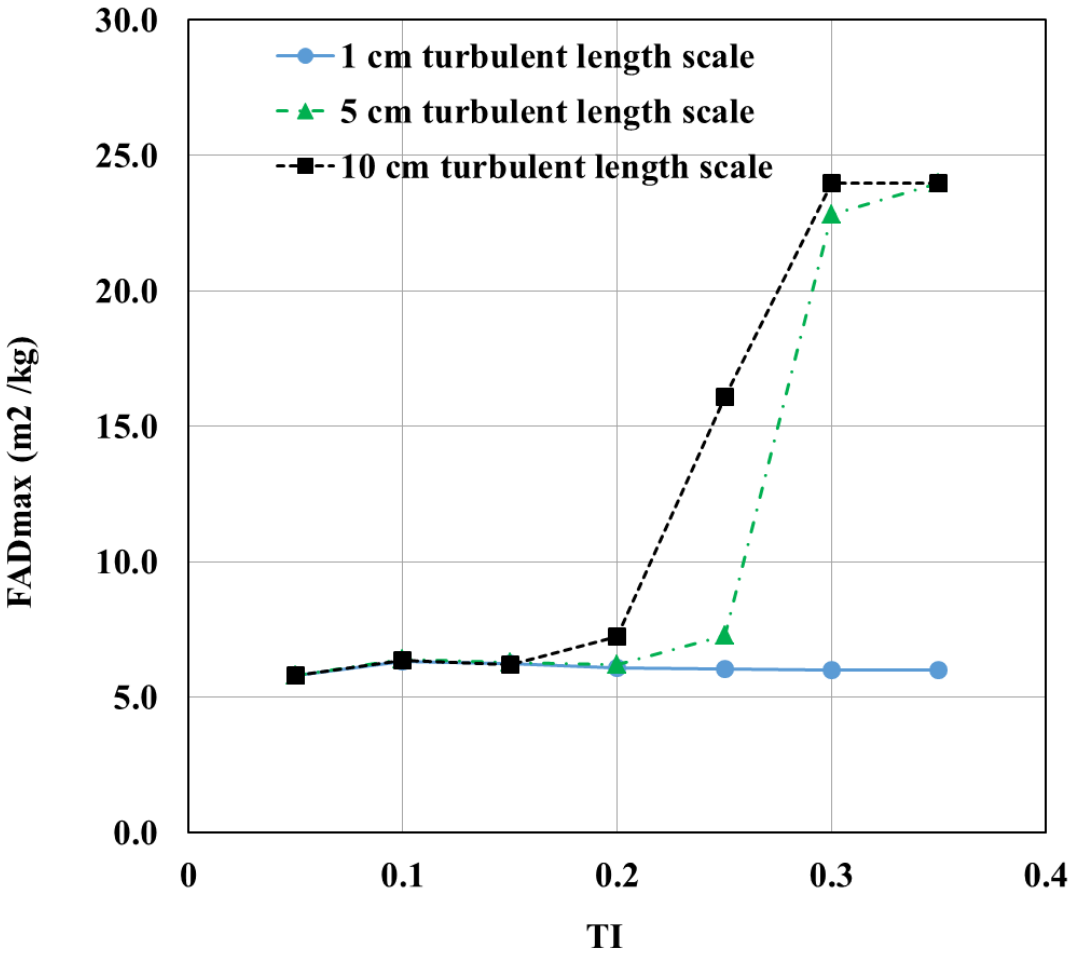


Figure 4-7 Maximum flame area density $FAD_{max}$ along the axial centerline of the diffuser with various turbulence intensities and length scales values.

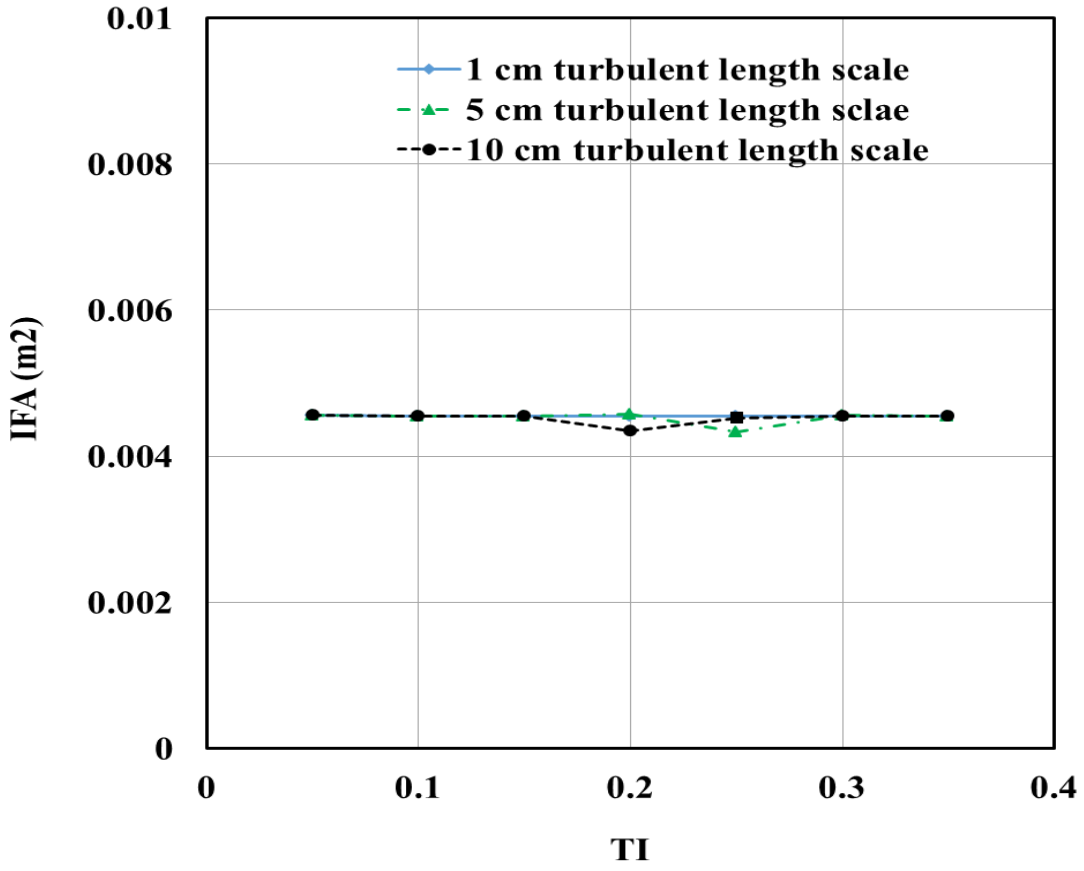


Figure 4-8 Integrated flame area over the diffuser for various turbulence intensities and length scales values.

# CHAPTER V

# 5 UNSTEADY STATE SIMULATIONS OF FLAME IN DIFFUSER COMBUSTOR

## *5.1 Introduction*

The results of the unsteady-state condition simulations are presented and discussed in this Chapter. Simulations are performed under the steady-state condition in the last Chapter. Therefore, the steady-state conditions at TI = 5% and $\ell$ = 1 cm are taken as the initial conditions for the unsteady-state simulations. The inlet turbulence conditions in the unsteady-state simulations are changed stepwise to the required levels of turbulence intensity and turbulence length scale. In particular, the map of the flame within the Borgi diagram is introduced to understand the behavior of the flame location with the change in turbulence intensity and turbulence length scale. The behavior of the flame location exposed to various turbulence intensities and turbulence length scales is discussed in the flame location section. The second part of this chapter presents the effect of the secondary flow within the diffuser, and the third part presents the behavior of the TKE along the axis of the diffuser combustor. In the final section, the behavior of the FAD at various turbulence intensities and turbulence length scales is discussed.

Flame behavior should be indicated within the regime map of the premixed turbulent combustion to understand the influences of turbulence intensity and length scale on flame location. [18-20] depended on velocity and turbulence scale ratios to establish the regimes of premixed turbulent combustion. Therefore, a change in turbulence intensity level and length scale causes a change in the type of combustion zone within the regimes of the premixed

turbulent combustion as a result of the change in the physical process. The value of the laminar flame speed was constant for all test cases ($S_L$= 0.14 m /s), while the fluctuation velocity varies with a change in the turbulence intensity. The fluctuation velocity increases with an increase in the turbulence intensity as shown in

Table **5-1**, which indicate the values of the fluctuation velocities for the various turbulence intensities and at 5 cm length scale. In addition, the flame thickness was 0.0005421 m at the temperature 1400 K.

Table 5-1 The values of fluctuation velocities for different turbulence intensities and 5 cm length scale.

| TI [ - ] | 5 % | 10 % | 15 % | 20 % | 25 % | 30 % | 35 % |
|---|---|---|---|---|---|---|---|
| u [m /s] | 0.116 | 0.144 | 0.157 | 0.197 | 0.247 | 0.252 | 0.258 |

Figure **5-1** which represents the flame locations on the Borghi diagram for all the test cases, shows that the flames in the test cases are wrinkled and of corrugated flamelet types. The temperature field is used to measure flame location, which is assumed to be at 1400 K at the centerline of the combustor for all cases. Line probe is used along the axial direction of the diffuser combustor to measure the characteristics of the mixture combustion, such as instantaneous velocity, temperature, and flame area density. The results are discussed in three sections.

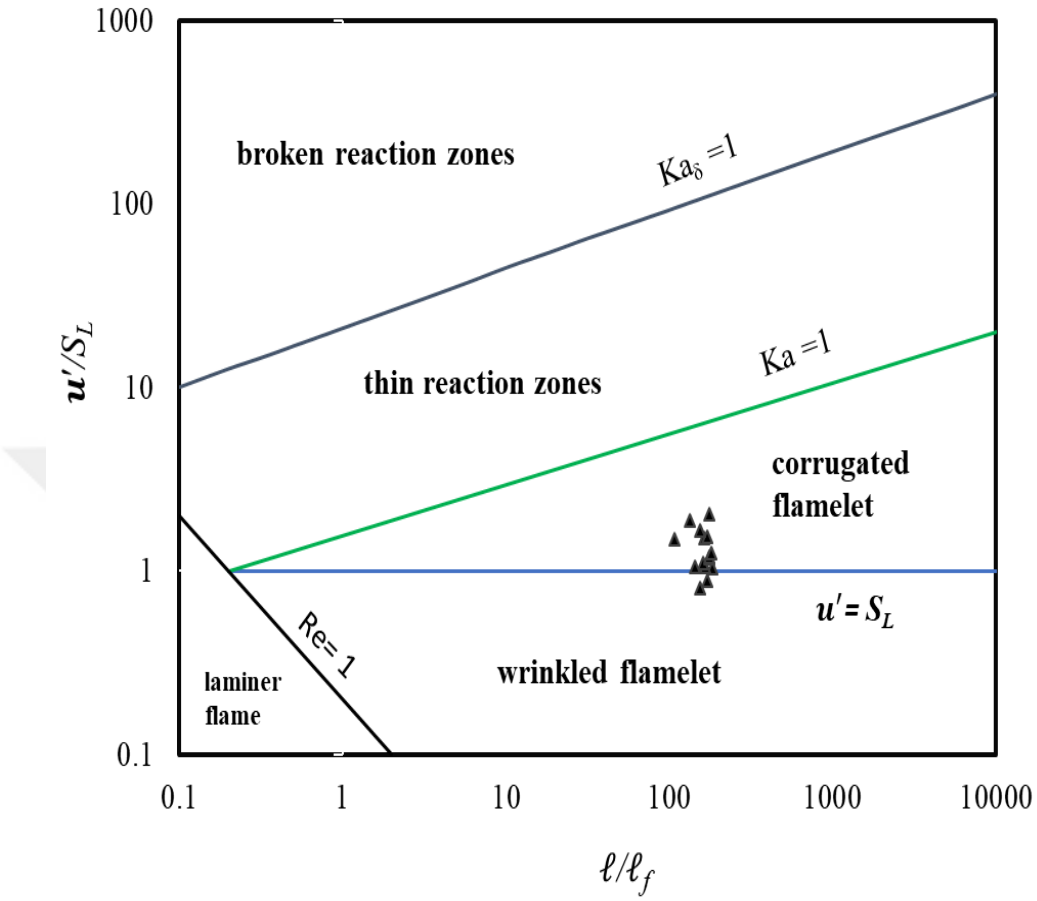


Figure 5-1 Flame locations on the premixed turbulent combustion regime (Borghi diagram) for all cases.

The effects of turbulence intensity and length scale on flame location are explained in the first section, the effect of the secondary flow on flame location is discussed in the second section, and the flame area density and the flame shape are explained in the third section.

## *5.1 The Effect of turbulence on the flame location*

All temperature profiles are plotted together for the difference in turbulence intensities and length scales to indicate the influences of turbulence intensity and length scale on flame location. Figure **5-2** compares temperature contours over various turbulence intensities and

length scales, and Figure **5-3** illustrates the flame location in the axial direction respect to the diffuser length as a function of turbulence intensity and length scale.

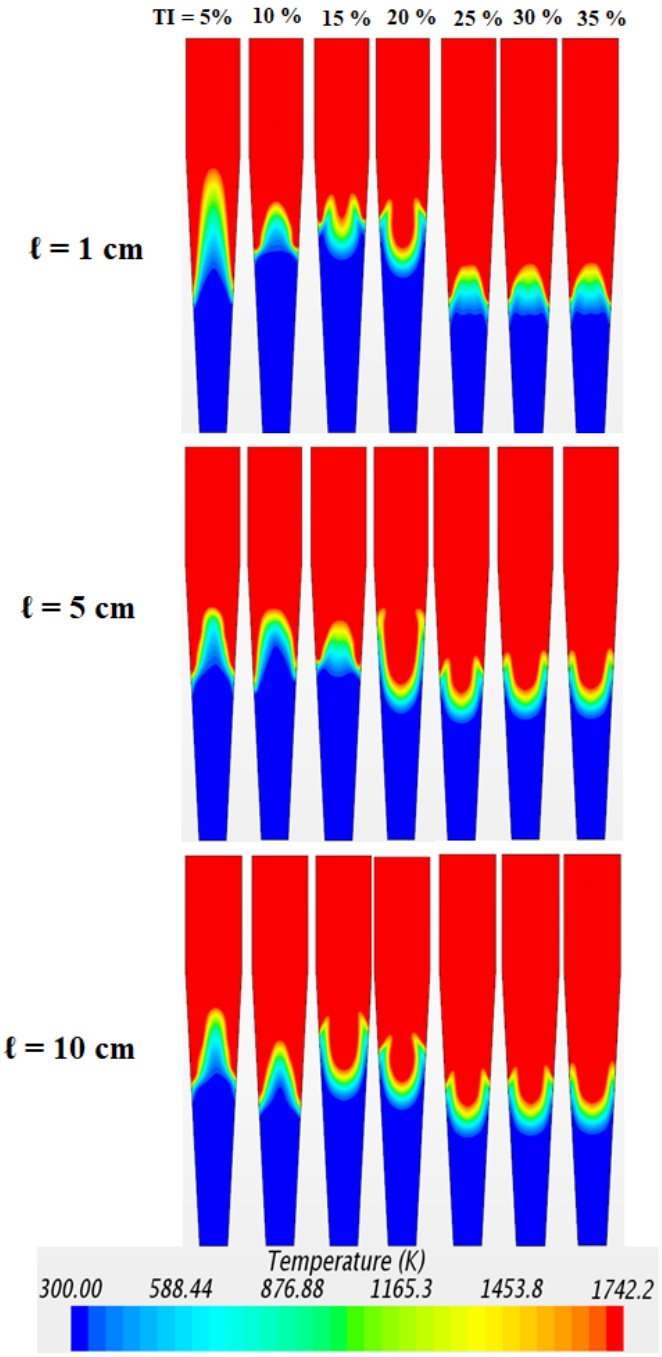


Figure 5-2 Contours of temperature at different TI and $\ell$.

These figures show that flame location depends on turbulence intensity and length scale, with the flame front location generally moving toward the diffuser inlet gradually with increases in the two factors. The impact of turbulence intensity on flame location is more visible than that of turbulence length scale. Flame location is stabilized with an increase in TI of 25% to 35%. Nevertheless, an increase in turbulence length scale at a constant TI generally causes a decrease in flame location. For $\ell = 5$ cm, it can be seen that the same the flame location almost as either $\ell = 1$ cm or $\ell = 10$ cm cases. The obtained results show that flame location depends on turbulence intensity and length scale. In addition to the change in flame location, the flame shape may change when the turbulence intensity and length scale are varied.

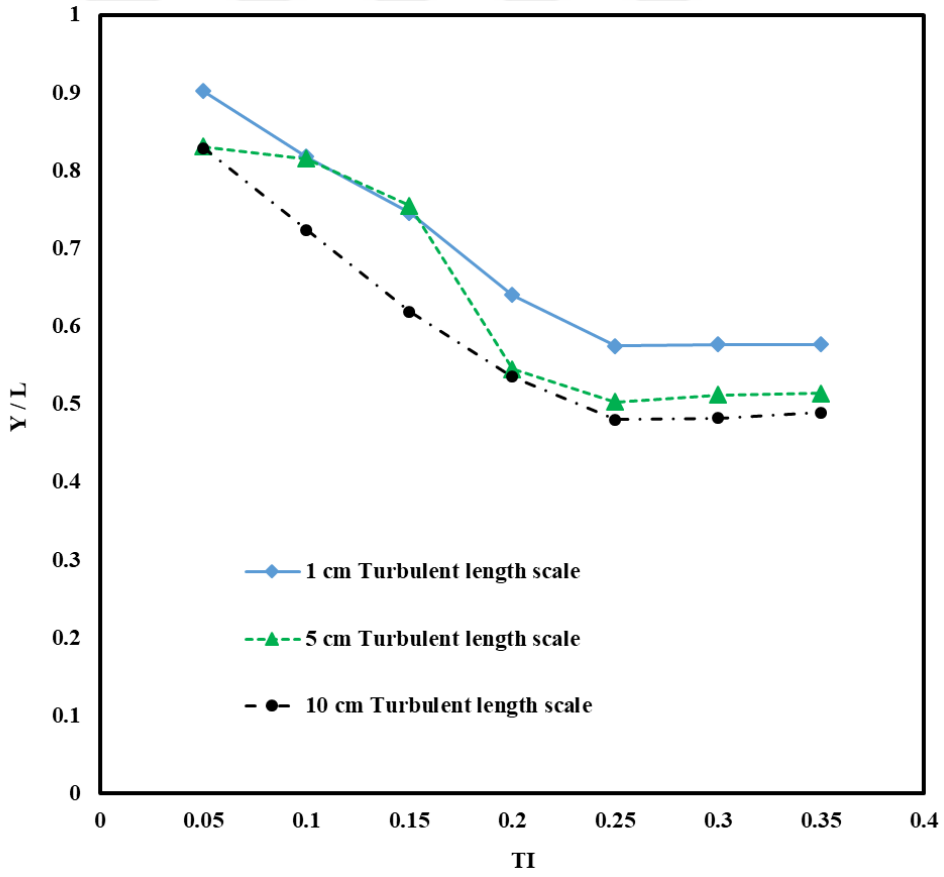


Figure 5-3 Flame location normalized with the length of the diffuser at different TI and ℓ.

Similar effects of turbulence on flame have been indicated by many researchers. For example, Yuan et al [29]studied the influences of turbulence on the flame front by changing turbulence intensity within 1% to 50% and found that hydrodynamic instability dominates the growth of flame cells at low turbulence intensities of 1% to 5%. Meanwhile, turbulence wrinkles the flame front and dominates the process at a high turbulence intensity of 50%. Therefore, we select the range of turbulence intensity within 5% to 35%, and the results indicate the expected effect of turbulence on the flame, i.e. the turbulent flame speed increases with turbulence and it moves toward the inlet.

## *5.2 The effect of secondary flow structures*

Most turbulence intensities and length scales give reasonable predictions for the behavior of flame location, but the flow separation that occurs within the diffuser combustor has an effect on this behavior as well. Line integral convolution is used to illustrate the imaging vector fields, which were proposed by [174] to understand the flow separation. Figure **5-4** shows the effects of flow separation and turbulence intensity on flame location for all cases. Flow separation occurs at the diffuser wall behind the flame front and causes an increase in the velocity at the combustor center.

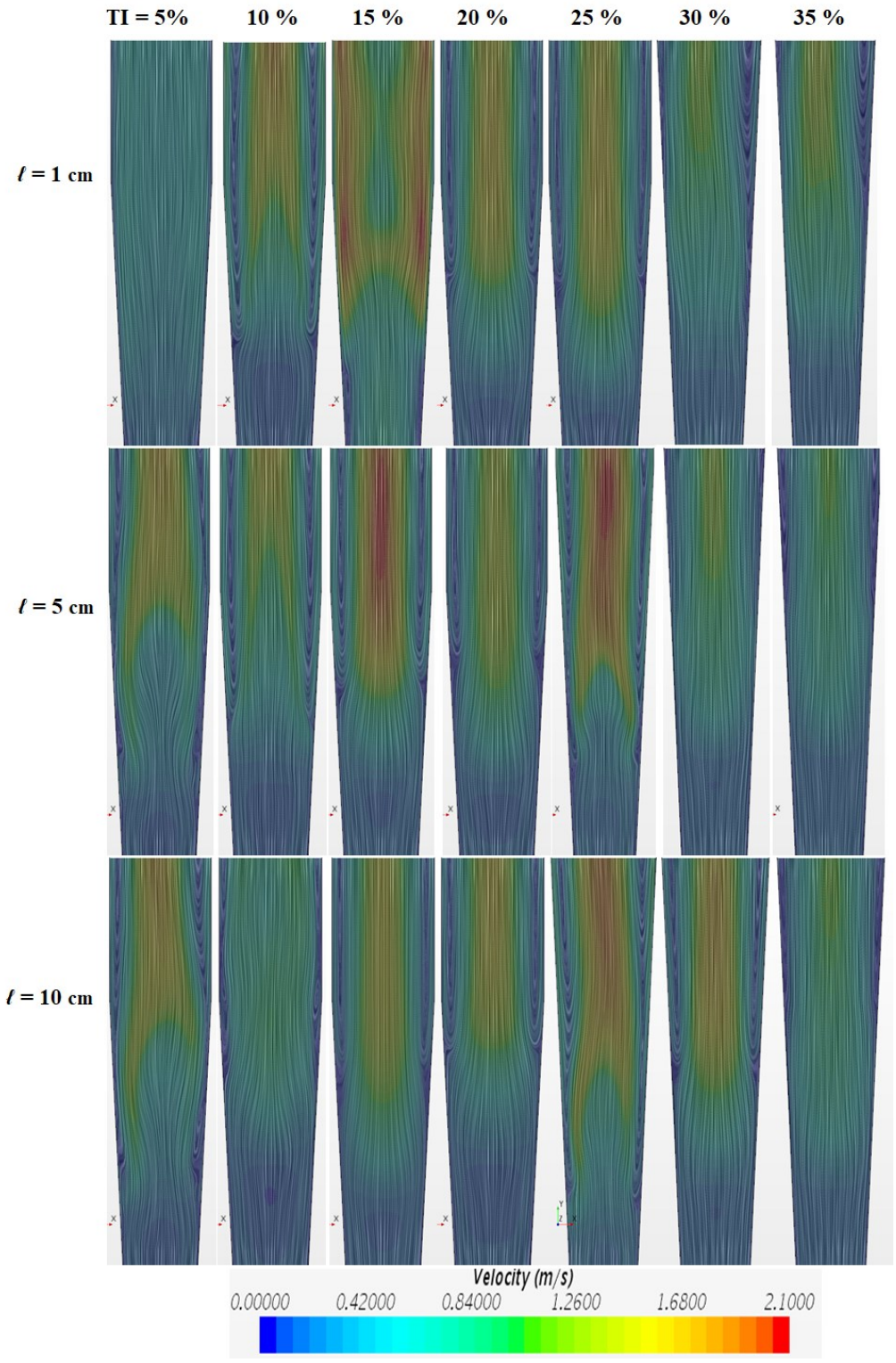


Figure 5-4 Contours of the line integral convolution (flow streamline).

This flow separation is influenced by the increases in turbulence intensity and length scale. As flow separation occurs, the axial mean flow rises and pushes the flame away from the inlet. Consequently, flame location is influenced by the flow separation, which generally occurs downstream in the flame zones for most of the cases.

The turbulent kinetic energy along the central axis of the diffuser combustor is measured using a line probe. **Figure 5-5** illustrates the profiles of the turbulent kinetic energy with different turbulence intensities and length scales of 10 cm, in the diffuser. These profiles show the turbulent kinetic energy before combustion (cold zone) and after combustion (reacting zone). The turbulent kinetic energy changes with the increase in TI at the inlet and $\ell$ for all cases, as illustrated in Figure 6. In all cases, the TKE initially decays from turbulence dynamics as expected, and then rises suddenly within the flame region. The increase of the TKE that occurs within the region of the combustion starts at T = 1400 K. The TKE is based on the dissipation rate (ε) according to Eq. 2-68. Thus, an increasing TI means an increase in ε with a constant turbulent length scale. Therefore, the decay rate of the TKE downstream of the inlet is high when turbulence intensity is high.

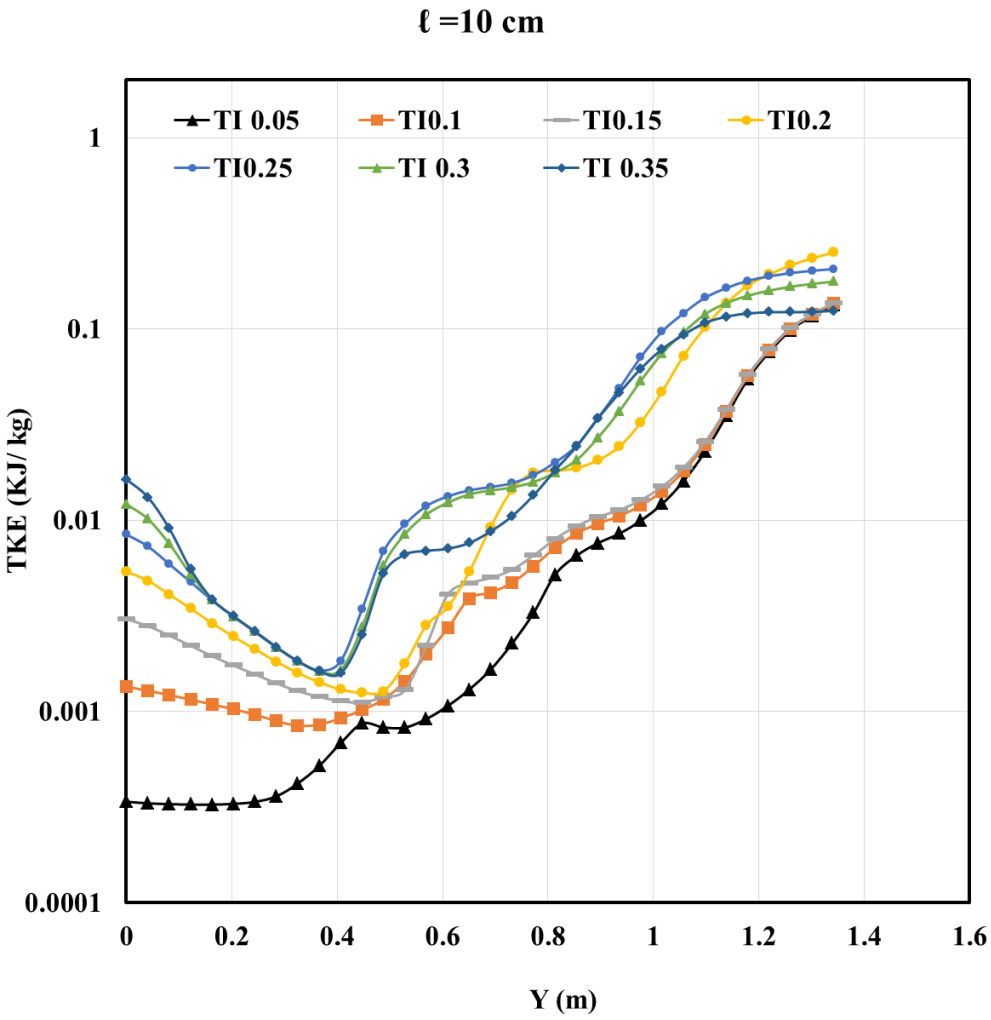


**Figure 5-5** Turbulent kinetic energy along the axial direction of the diffuser combustor with various turbulence intensities and at 10-cm turbulent length scale.

## *5.3 Flame area density*

Figure **5-6** shows the flame area density for various turbulence intensities and length scales. The shape of the value of the flame area density varies with the increases in turbulence intensity and length scale. The flame shape can be convex or concave. Many types of flame shapes exist depending on the shape factor, which is based on the flame position and axis planes

[144, 151].

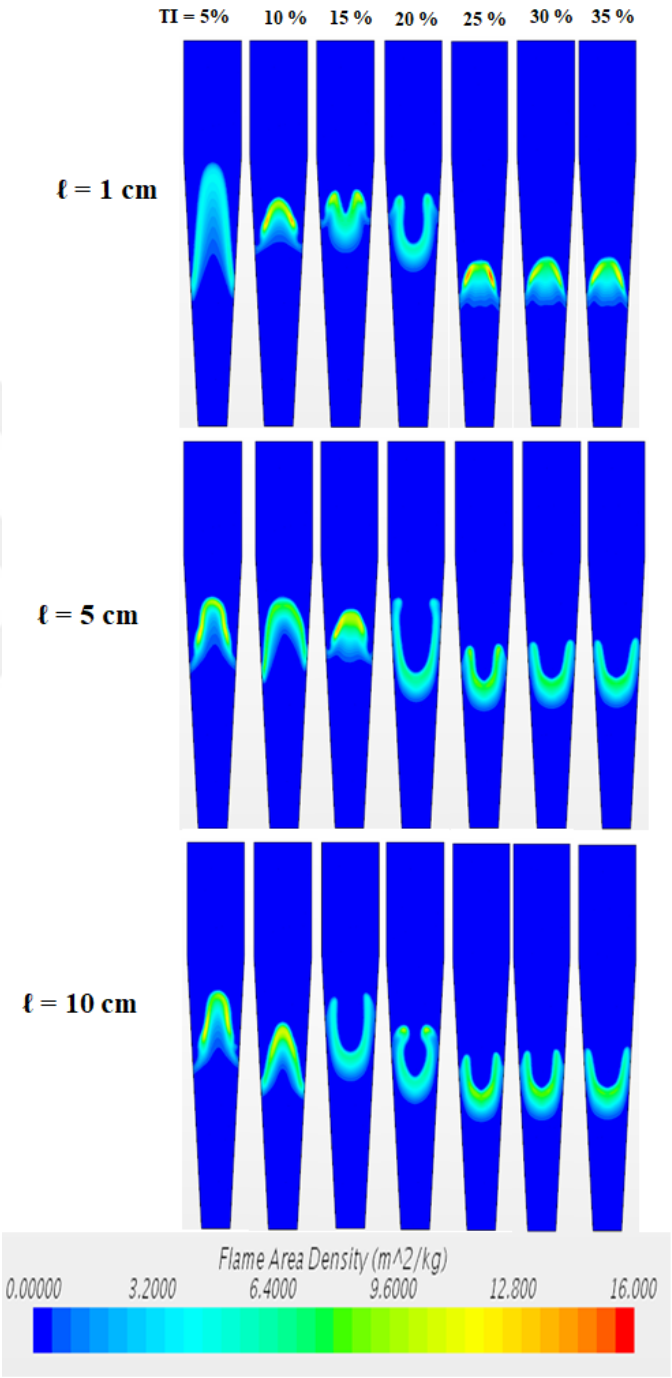


Figure 5-6 Profile of the flame area density for various TI and $\ell$.

Kerl et al [44] presented three flame shapes (hyperbolic, parabolic and elliptic) in a diffuser combustor with an annular swirling flow at its inlet. As this work is the most similar study to the present work, the flame shapes obtained here can be accepted to be realistic. [25] indicated that front shape and motion can be controlled by a flame stretch. In addition, it can be seen from the Figure **5-6** the maximum flame area density does not change with the increase in turbulence intensity. This result is consistent with those found by [31], who studied the flame area density in a premixed turbulent flame at a vast level of turbulence intensity in a Bunsen burner and concluded that the maximum flame surface density does not vary with turbulence intensity.

# CHAPTER VI

# 6 UNSTEADY SIMULATIONS OF FLAME IN DIFFUSER COMBUSTOR WITH A CONICAL INSERT

## *6.1 Introduction*

In this Chapter, we present the results of the influence of turbulence intensities, length scale and Taylor-scale Reynolds number on flame location in the diffuser. The results of the diffuser with and without conical insert is compared in this section. In particular, the mean quantities, such as temperature contours and flame area density, as well as the turbulent quantities, such as the turbulent kinetic energy and Taylor-scale Reynolds number are utilized to determine the effect of turbulence on the flame. Flame refers to the location at which temperature is 1400 K and is used to compare different flame cases. A line probe is set along the axial centerline of the diffuser to measure flame location. It is compared the results of the flow structure of diffuser with conical insert respect to the results of the diffuser without the conical insert.

In order to indicate the impact of the turbulence intensity and turbulent length scale on the flame location, it is crucial to reveal the location of the flame within the regimes of the premixed turbulent combustion. These regimes were initially introduced by many studies [18 - 20]. These regimes are divided into many regimes based on the dimensionless numbers and according to the velocities ratios and length scale ratios. It is seen from Figure 6-1; all the locations of the flame are of the corrugated and wrinkled types.

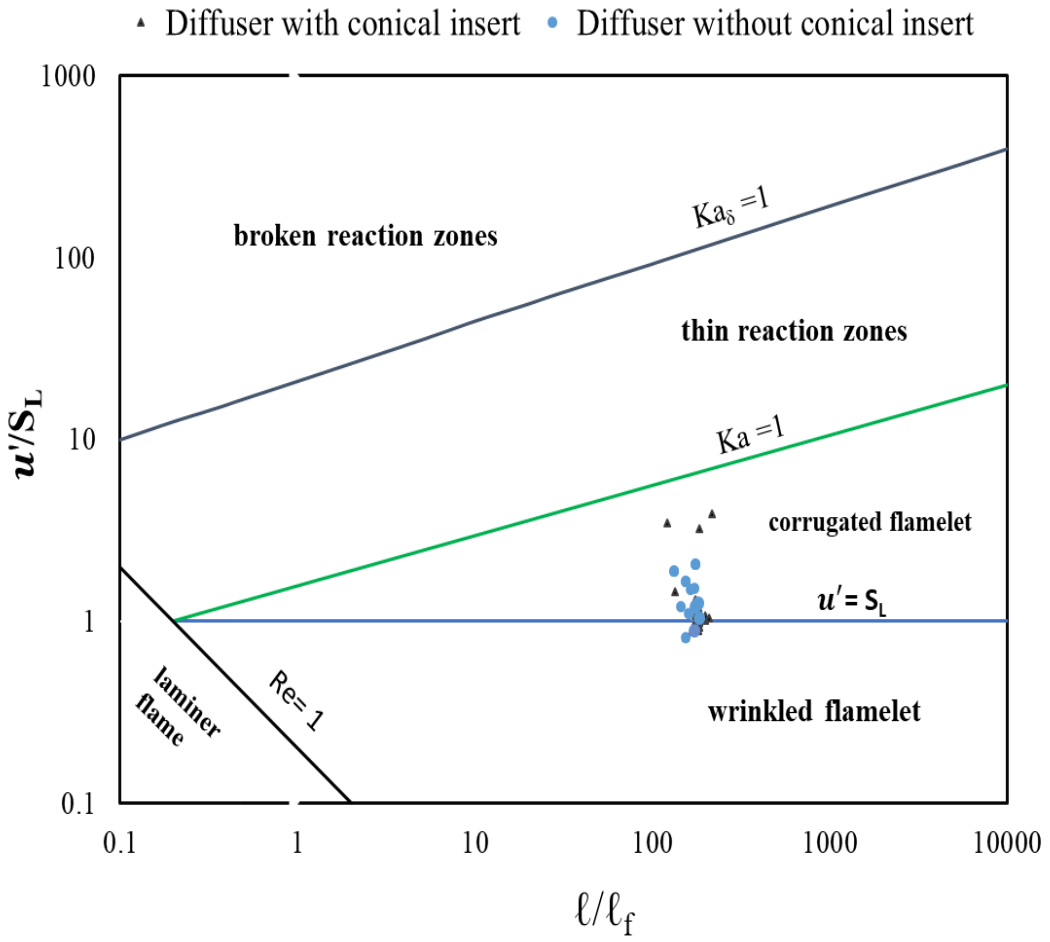


**Figure 6-1** the location of the flame within the regimes of the turbulent premixed combustion.

## *6.2 The Effect of turbulence on the flame location*

The effect of turbulent flows on flame location behavior is studied in terms of temperature contours. The temperature contours within the diffuser combustor are portrayed for various turbulent. Temperature contours are utilized to measure the flame location with the help of a line probe, which is set along the axial centerline of the combustor-diffuser.

Figures 6-2 & 6-3 show the contours and behavior of the temperature distribution with various turbulence intensities and turbulent length scales in the diffuser (with conical insert) and diffuser respectively. The figures show that flame location and shape are influenced by turbulence intensity and length scales for both cases. The flame location generally moves toward the inlet of the combustor with the increase in turbulence intensity for both diffusers (diffusers with and without using conical insert). The main difference between the two cases (diffusers with and without using conical insert) is the flame location behavior. The flame location moves at the inlet of the combustor for the current diffuser, whereas the flame location decreases to the middle of the cylindrical diffuser (without conical insert) with the increase in turbulence intensity (TI = 30%) and turbulent length scale ($\ell$ = 10 cm). The flame topology also changes with the increase in turbulence intensity and turbulent length scale. The flame topology changes at 25% turbulence intensity for 5 cm and 10 cm length scales as shown in Figures 29 and 30. Similar flame shape behavior is observed by Kerl et al [44], whose found three flame shapes (parabolic, hyperbolic and elliptic) in the diffuser combustor for the annual swirl.

Figure **6-3** shows the behavior of flame location for diffuser combustor (with a conical insert) compare with a diffuser (without conical insert) at different turbulence length scales and turbulent intensities. A similarity exists between the flame location behavior for both diffusers (with and without conical insert) at the low turbulent intensities (5%, 10%, and 15%); the flame is less sensitive to the increase in turbulence intensities and remains constant with increase in the turbulence intensities. The major differences between two cases of diffusers are observed at high turbulence intensities and turbulent length scale. When TI > 25%, the flame location moves to the inlet of the diffuser with use conical insert, whereas the flame location for diffuser without conical insert moves to the middle of the combustor at 25% TI. In order to understand this

difference in behavior of the flame location for both cases of the diffusers (with and without conical insert), the flow structure and turbulent kinetic energy will be discussed in the following sections.

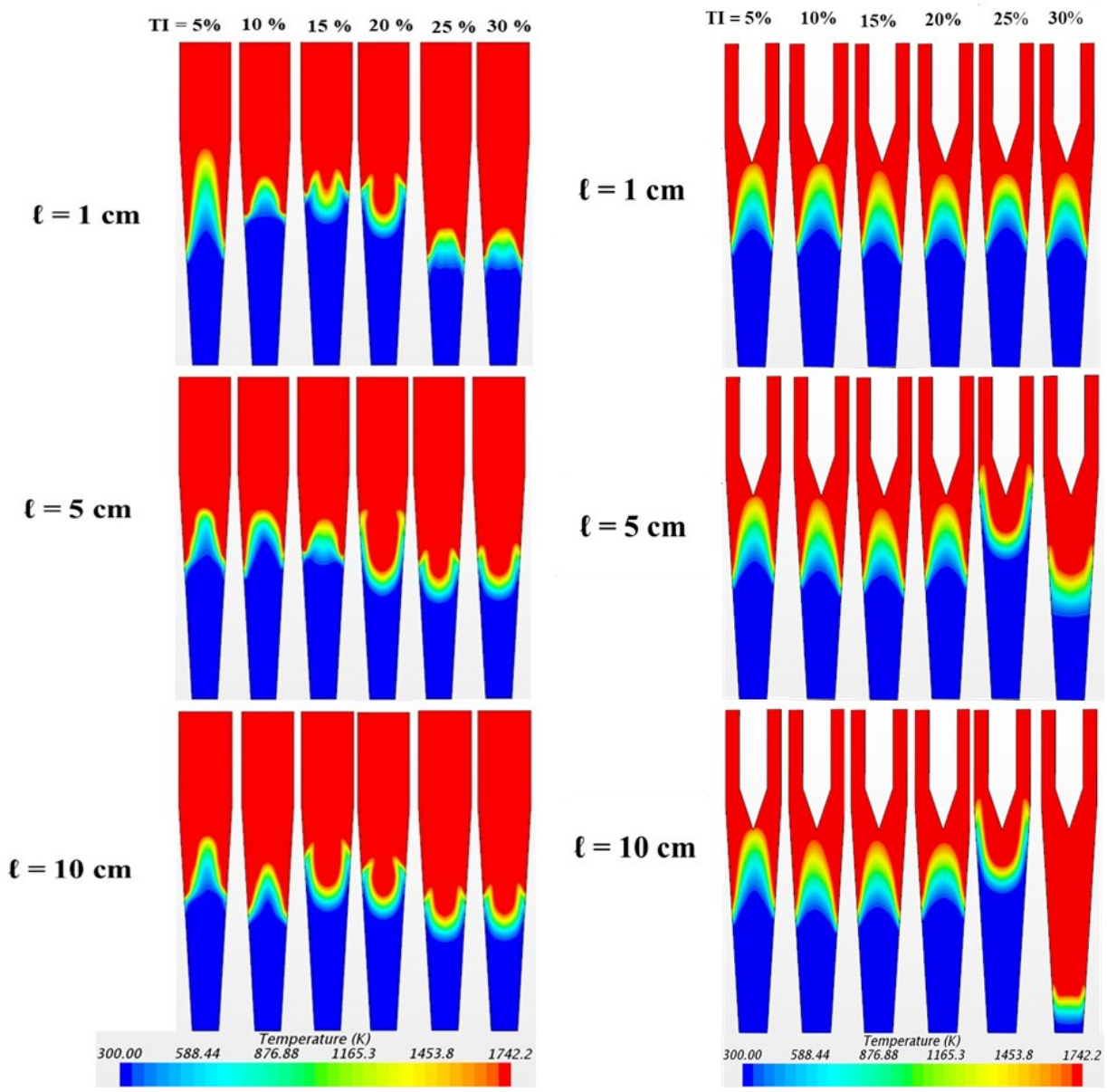


Figure 6-2 Temperature contours with various turbulence intensities and turbulent length scale on the diffuser without conical insert (left picture) and diffuser with conical insert (right picture) respectively.

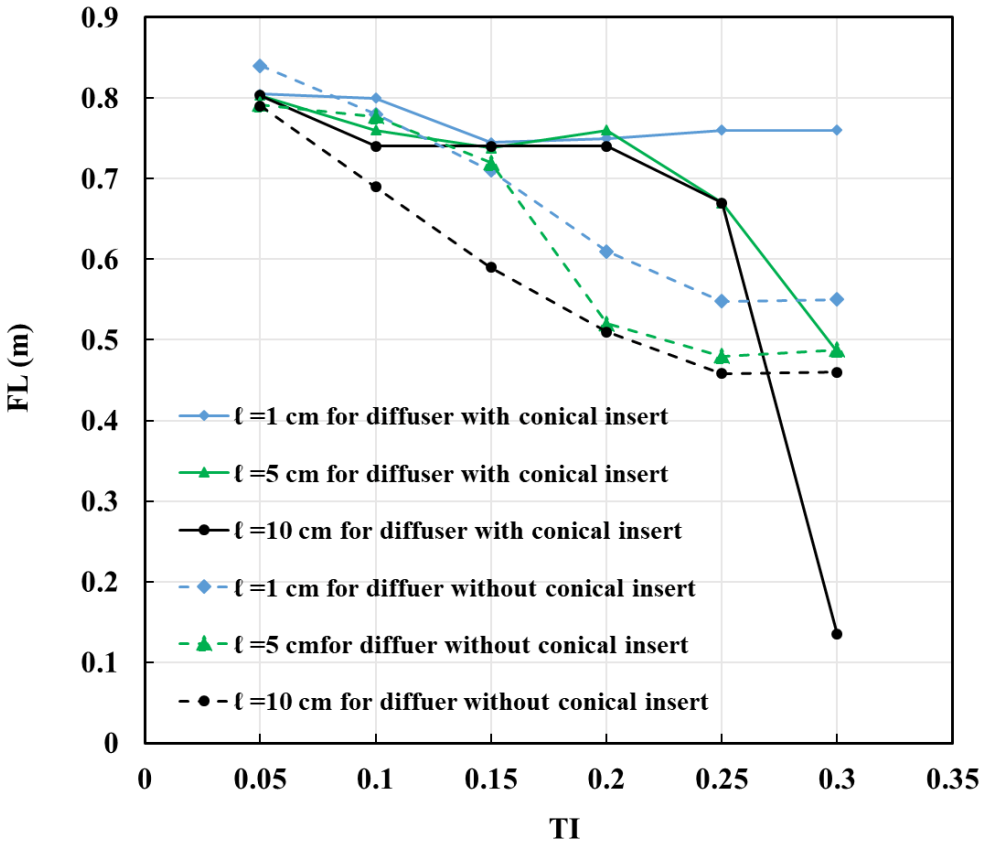


Figure 6-3 Flame location with various turbulence intensities and turbulent length scales for both diffusers (with and without conical insert).

Many researchers have introduced similar behavior of the flame under turbulence effect. For instance, Clavin and Joulin [25] indicated that the motion and shape of the flame could be controlled by the flame stretch under a large-scale and high-intensity turbulent. Yuan and Law [29] also examined the effect of the turbulence on the flame by changing turbulence intensity within 1% to 50%. They indicated that the flame highly wrinkled by turbulence for the high turbulence intensity (5% to 50%), consequently dominate the process of the turbulence and flame interaction. While for the low turbulence intensities level (1% to 5%), the flame was less sensitive to the turbulence and hydrodynamic instability dominates the growth of flame. For this

reason, the ranges of the turbulence intensities were selected within 5% to 30%, and the outcomes show the expected influence of turbulence intensity and length scale on the flame location, i.e. the turbulent flame speed increases with increase in the turbulence intensity and length scale.

## *6.3 The effect of secondary flow structures*

Flow separation observed behind the flame front in the diffuser without using a conical insert [172]. This flow separation effects on the flame location and prevent the sole effect of turbulence on flame location. In addition, this flow separation changes with a change in the turbulence intensity and turbulent length scale but not all cases. Therefore, a conical object is placed inside the diffuser. The conical object pushes the flow toward the wall, thus, the flow separation is eliminated.

In order to understand the flow structure for both cases of the diffusers (with and without conical insert), the flow fields within the diffusers for two cases (20% TI & $\ell$ = 10-cm) and (30% TI and $\ell$ = 10-cm) are indicated as shown in Figure **6-3**. The line integral convolutions proposed by Cabral and Leedom[174] has been used to illustrate vector fields to understand the flow structures. Figure **6-4** shows the flow separation at the wall of the diffuser without conical insert behind the flame, which causes an increase in the velocity at the center. This increase in the velocity, which occurs in the combustion region, causes to occur deaccelerating in the velocity before the combustion region. For the case of the high turbulence intensity (30% TI and $\ell$ = 10-cm), flow separation, which occurs nearly at the wall of the diffuse and causes to push the flame away from the inlet. While with using the conical insert for 30% TI and $\ell$ = 10-cm, flow separation is eliminated, and the flame drops toward the inlet of the diffuser with the conical

insert. As results, the flow separation causes the difference between the behavior flame locations in diffusers (with and without conical insert).

For the moderate turbulence intensity (20% TI & ℓ = 10-cm), the flow separation pushes the flame towards the middle of the diffuser without using a conical insert. In addition, flow separation is eliminated by using the conical insert, which pushes the flow toward the wall. The flame location moves towards the outlet of the diffuser. Hence, the conical object plays a key role in suppressing the flow separation that occurs near the wall of the cylindrical diffuser without the conical insert, consequently, the flame location behavior changes with using the conical insert.

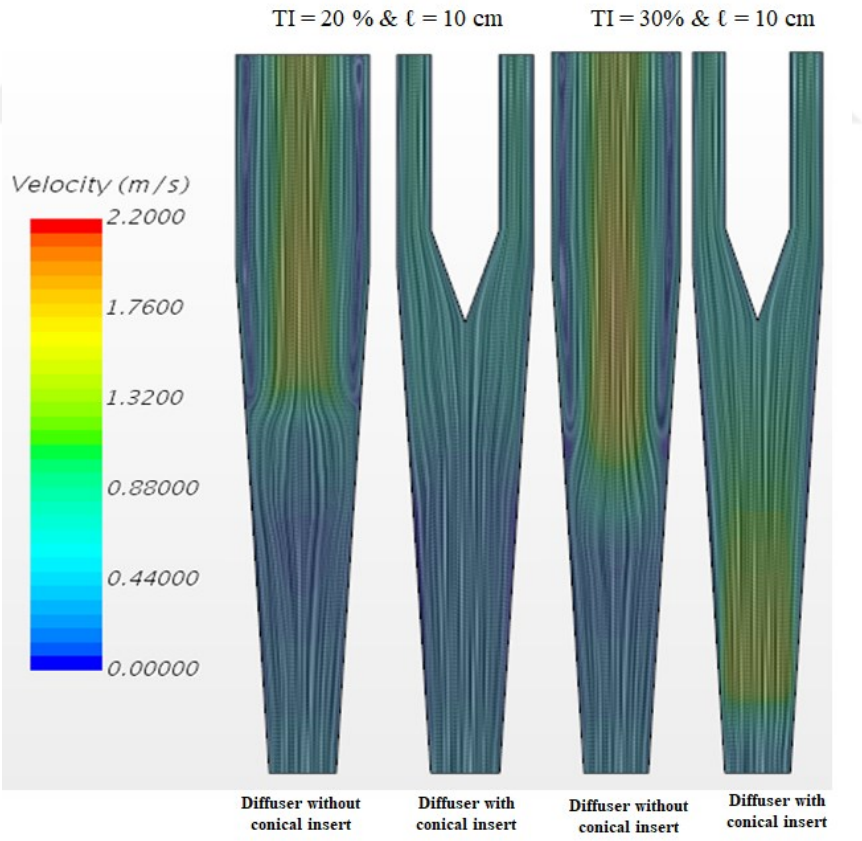

Figure 6-4 Contours of the line integral convolution (flow streamline) for the two cases (TI = 20 and ℓ = 10) and (30% and ℓ = 10) for the diffuser with conical insert and the diffuser without the conical insert.

This behavior of the flame location for the case of (20% TI & ℓ = 10-cm) attributes to the behavior of others parameters the turbulent kinetic energy, dynamic pressure and the mean velocity besides of the flow separation. For this reason, the turbulent kinetic energy, dynamic pressure and mean velocity along the axis of the diffusers (with and without conical insert) is utilized for cases (30% TI and ℓ = 10-cm) and (20% TI & ℓ = 10-cm) in order to understand simultaneously the effect of the flow separation and the turbulence on the flame location. As can be seen in Figure **6-3**, increasing turbulence intensity causes the flame to moves towards the inlet in both diffusers. This can recognize clearly when temperatures profile along the centerline of the diffuser are explained (Figure **6-5**) for ℓ =10 and TI =20% & TI=30%.

However, there are two distinct tends for both diffusers, consider TI = 20% and ℓ = 10, the flame is located at a higher level in the diffuser with conical insert than that in the diffuser without the conical insert. A contrary state occurs when TI is set to 30%. This intriguing trend needs to be explained.

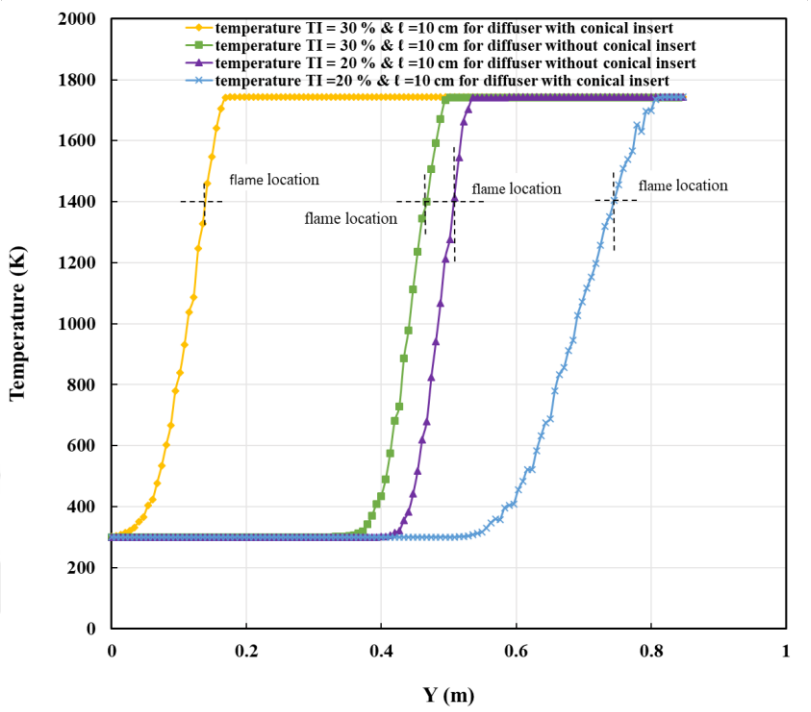


Figure 6-5 Temperature along the axial centerline for both diffusers (with and without conical insert) for (TI = 20% & ℓ= 10 cm) and (TI =30% & ℓ= 10 cm).

As can be seen in the flow field, there is a flow separation within a diffuser without conical insert (Figure **6-4**). This flow separation causes extra deceleration of the velocity upstream of the flame, i.e. between the flame and the inlet as shown in Figure **6-6**. This is deceleration is partially due to the stagnation due to the vena contraction effect in the diffuser, as might also happen without combustion. However, when the static pressure field is examined Figure **6-7**, it can be recognized that the static pressure rises in the diffuser without conical insert around the flame location. This rise creates a strong adverse pressure gradient, which reflects itself as the large deceleration of the flow velocity. As the local speed drops, flame penetrates towards the inlet more than that compared to the causes without conical insert, i.e. causes without flow separation at TI = 20% & ℓ = 10 cm.

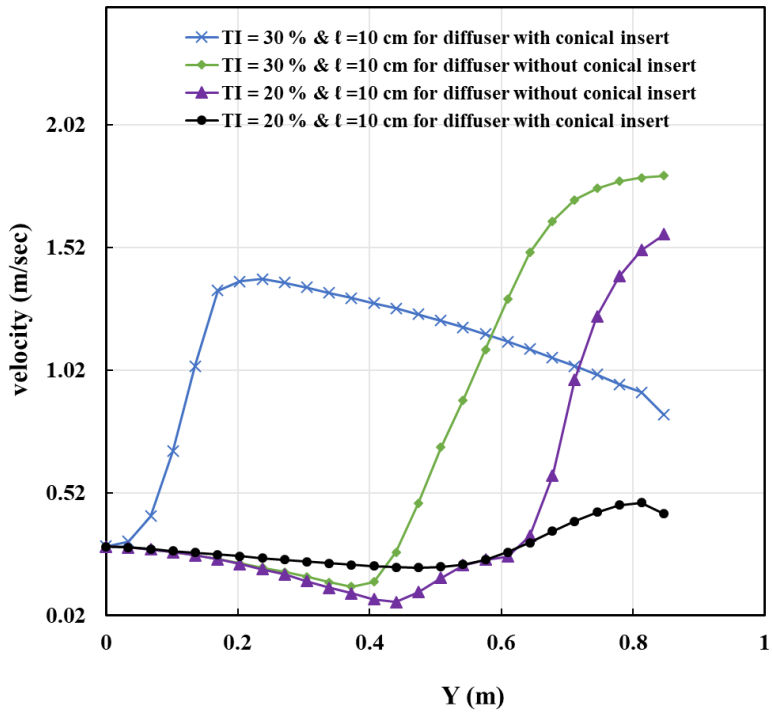


Figure 6-6 The mean velocity along the axial centerline direction for both diffusers (with and without conical insert) for (TI = 20% & ℓ= 10 cm) and (TI =30% & ℓ= 10 cm).

This rise in the pressure is also associated with flow rate the pressure gradient downstream of the flame. Therefore, together with vena contraction, the speeds downstream of the flame in the diffuser without conical inset is larger than at the centerline of the diffuser (Figure **6-7**).

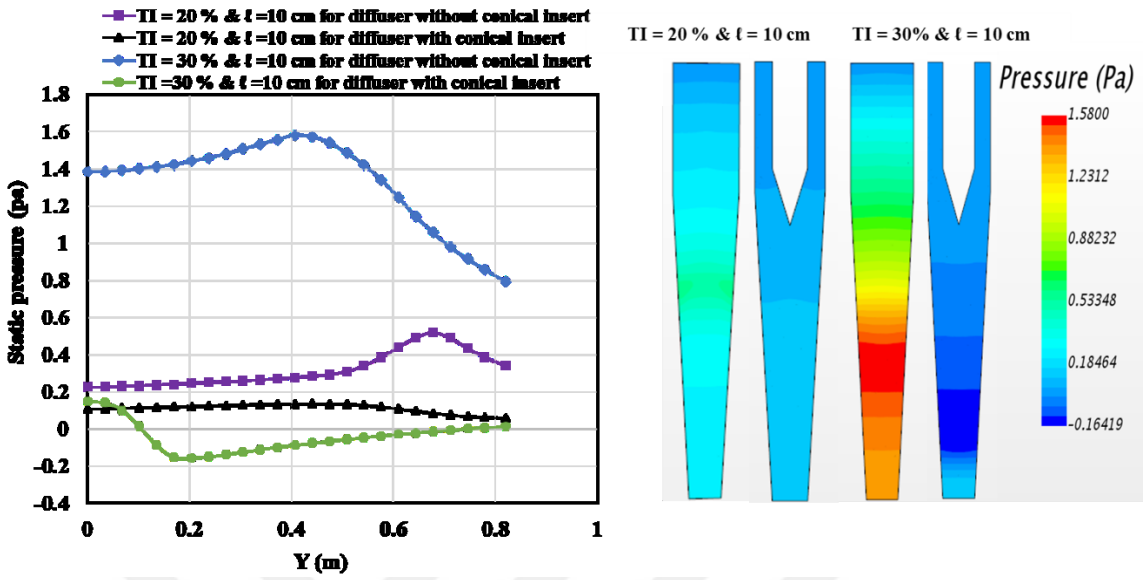


Figure 6-7 The static pressure along the axial centerline direction for both diffusers (with and without conical insert) for (TI = 20% & ℓ= 10 cm) and (TI =30% & ℓ= 10 cm).

The development of the TKE along the centerline of the diffuser is shown (Figure **6-8**). Interestingly, for TI = 20% & ℓ= 10 cm, TKE develops in the same behavior for both diffusers upstream of the flame, although the velocity field differs for both cases. This shows that the turbulence is not affected by the velocity gradient. Nevertheless, for TI = 30%, turbulence becomes strong enough to pull the flame towards the inlet of the diffuser with conical insert.

This analysis shows that the separation might cause changes in the pressure consequently the velocity field, which influences the flame location, more than the turbulence. The final of the flame location is determined by the local balance of the flame speed and the speed of the unburned gases. In the ongoing analysis, the diffuser with conical insert is used to show the sole effect of the turbulence.

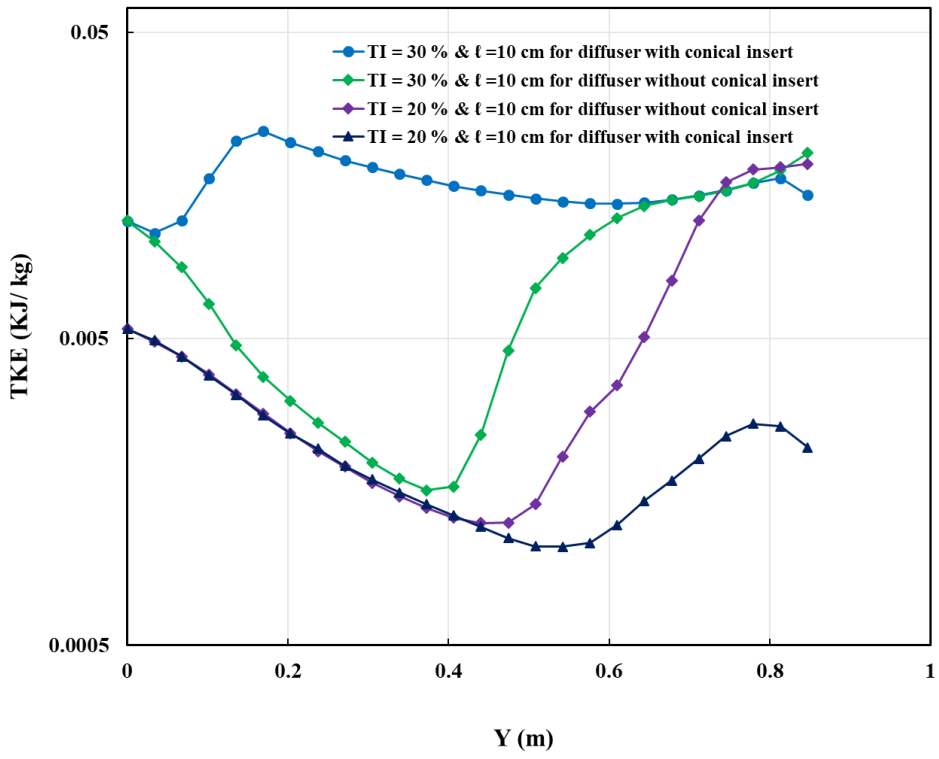


Figure 6-8 TKE along the axial direction for both diffusers (with and without conical insert) for (TI = 20% & ℓ= 10 cm).

## *6.4 The effect of the Taylor Reynolds number*

The Taylor-scale Reynolds number is a function of the turbulence intensity and length scale. Therefore, in order to understand the behavior of the flame location under the effect of the turbulence, the Taylor-scale Reynolds number is plotted as a function of the flame location and the temperature contours within the diffuser with the conical insert as shown in **Figures 6-9 & 6-10**. The Taylor-scale Reynolds number ($Re_\lambda$) is varied within wide ranges based on the values of the TI and ℓ.

Results show that the normalized flame location generally decreases with the increase of the Taylor-scale Reynolds number for high levels and that flame still stabilizes in low Taylor-scale Reynolds number (Figure **6-9**). Furthermore, investigation shows that flame shape also varies with the increase in $Re_{\lambda b}$ as shown in Figure **6-9**. Specifically, the flame shape changes from concave to convex shape after $Re_{\lambda b}$ =79.

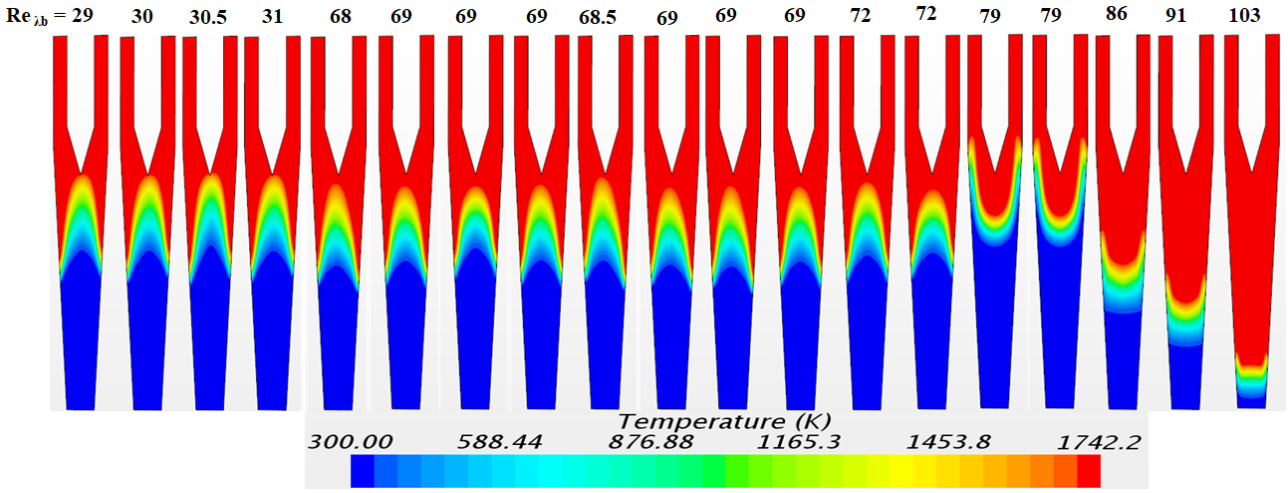


Figure 6-9 Temperature contours via Taylor-scale Reynolds number ($Re_{\lambda b}$) at the beginning of combustion for the diffuser combustor with conical insert.

Figure **6-10** shows the variations in a flame location with respect to the $Re_{\lambda i}$ and $Re_{\lambda b}$ for a diffuser with conical insert. Flame location generally travels gradually toward the inlet of the combustor with the increase in $Re_{\lambda i}$ and $Re_{\lambda b}$. Flame location is also observed to stabilize at the same location for the same low values of $Re_{\lambda i}$ and $Re_{\lambda b}$ as shown in Figure 6-10 especially for $Re_{\lambda i}$ 30 and 69. The flame location also decays rapidly toward the inlet of the diffuser after an increase in $Re_{\lambda i}$ greater than 79. Figure **6-10** shows that flame location is less sensitive to turbulence parameters at low-level of $Re_{\lambda b}$ and highly sensitive for $Re_{\lambda b} > 79$. In addition, the values of the $Re_{\lambda i}$ is less than of the $Re_{\lambda b}$ for the same values of the flame location especially for

the high values of the $Re_{\lambda i}$ and $Re_{\lambda b}$ which obvious in Figure **6-10**, for instance, $Re_{\lambda i}$ = 120 at the flame location = 0.48 while $Re_{\lambda b}$ at the same value of the flame location.

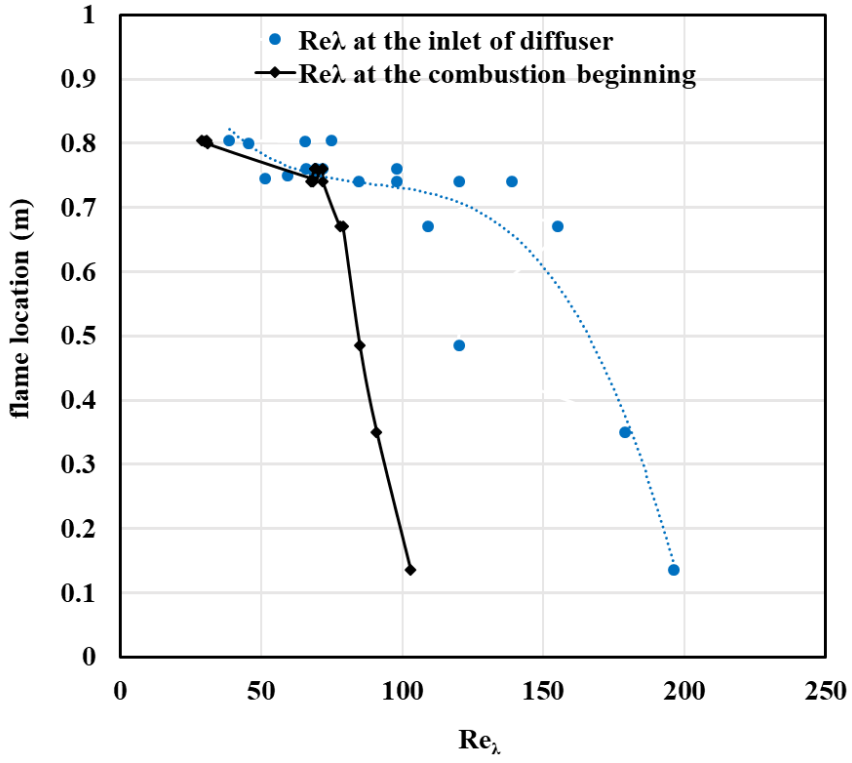


Figure 6-10 Flame location via $Re_{\lambda i}$ and $Re_{\lambda ib}$ for the diffuser combustor with conical insert.

The flame shape and area density are influenced by changes in flame turbulence intensity and turbulent length. In order to understand the trend of the flame location with a change in the Taylor-scale Reynolds number, turbulent kinetic energy is plotted along the axis of the diffuser, which will be explained in the turbulent kinetic energy section.

As can be seen in Figure **6-10**, increasing Taylor-scale Reynolds number at the beginning of the diffuser causes the flame to move towards the inlet of the diffuser. However, there are two distinct values for the same Taylor-scale Reynolds number at the beginning of the diffuser (Reλi = 120), the flame is located at a lower level in the diffuser with high turbulent kinetic energy (TI

= 30 % and ℓ = 5 cm) than that in the diffuser with low turbulent kinetic energy (TI = 15% and ℓ = 10 cm). This intriguing result needs to be explained. This can be understood clearly when velocity distribution along the X- axis of the diffuser from the centerline to the wall of the diffuser is explained (**Figures 6-11, 6-12 & 6-13**) for TI = 15% % & ℓ = 10 cm and TI=30% & ℓ =5 cm. As can be seen in the velocity distribution along the X- axis of the diffuser from the centerline to the wall of the diffuser, there is an interaction between the velocity and TKE next to the wall of the diffuser (**Figures 6-11, 6-12 & 6-13**). The increase in the turbulence intensity from 15% to 30% causes the velocity near the wall to increase and the velocity at the center to decrease. As a result, flame moves towards the inlet of the diffuser for the high turbulent kinetic energy. In addition, this increase in the turbulent kinetic energy cause to change in the shape of the flame from convex to a concave form.

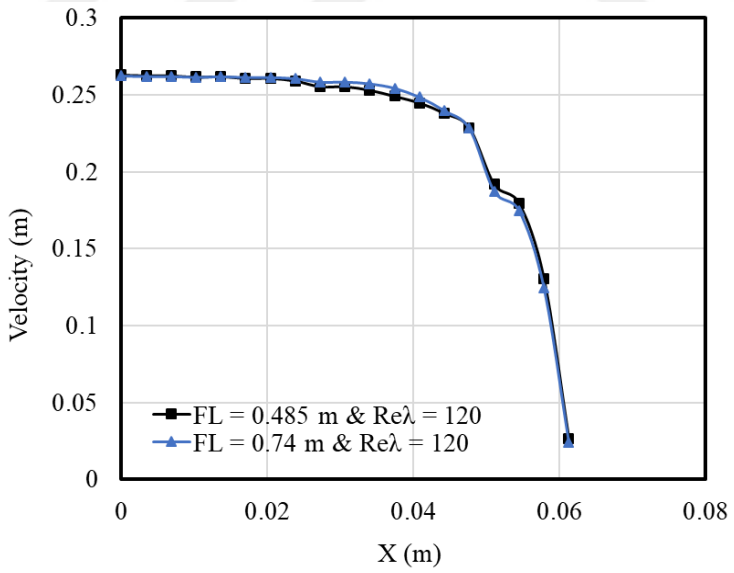


Figure 6-11 the velocity along the X –axis from the centerline of the diffuser to the wall for the level 0.2 m from the inlet of the diffuser.

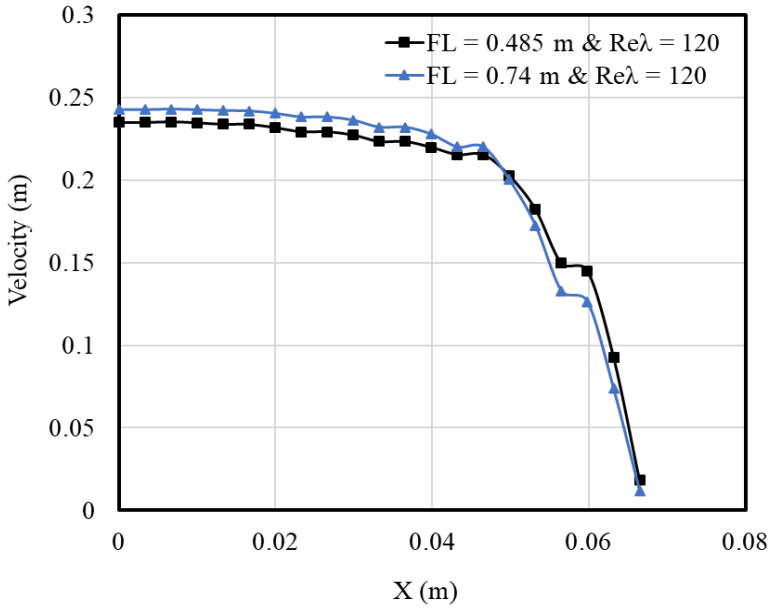


Figure 6-12 the velocity along the X –axis from the centerline of the diffuser to the wall for the level 0.3 m from the inlet of the diffuser.

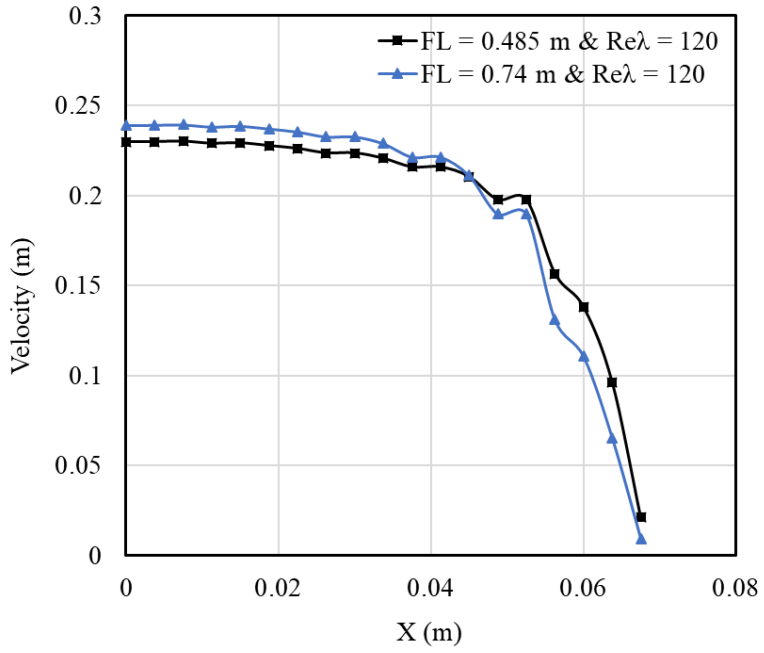


Figure 6-13 the velocity along the X –axis from the centerline of the diffuser to the wall for the level 0.32 m from the inlet of the diffuser.

## *6.5 Turbulent kinetic energy*

Turbulent kinetic energy (TKE) is the main parameter for understanding the behavior of flame location, which changes in the diffuser with a change in the turbulent length scale and turbulence intensity at the inlet of the diffuser. It should be noted the change in the turbulent length scale and turbulence intensity means also change in the Taylor-scale Reynolds number. Therefore, the development of the TKE should be illustrated to understand its effect on the flame.

**Figures 6-14, 6-15 & 6-16** illustrate the profiles of the TKE with different turbulence intensities and length scales of 1cm, 5 cm, and 10 cm, respectively, in the diffuser without the conical insert. The TKE changes with the increase in TI at the inlet and $\ell$ for all cases, as illustrated in **Figures 6-14, 6-15 & 6-16**. In all cases, the TKE initially decays from turbulence dynamics as expected, and then rises suddenly within the flame region. The increase of the TKE that occurs within the region of the combustion.

In addition, Figure **6-14** shows that the TKE for 10% TI is higher than for 5% TI within the combustion zone. Then, the TKE remains constant at TI > 10% and $\ell$ = 1 cm. This TKE trend explains the behavior of flame location for the turbulent length scale of 1 cm. **Figures 6-15 & 6-16** show that the peak rises in the TKE with the increasing TI from 25% and 30% at $\ell$ = 5 and 10 cm. This peak in the TI leads to a sharp drop in flame location toward the inlet of the combustor from 25% to 30% TI at 5-cm and 10-cm turbulent length scale as illustrated in Figure **6-3**. This TKE behavior is related to Eq. 2-64 Meanwhile, an increase in TKE means an increase in the value of the source term in terms of flame area density ($S_{\Sigma}$), which indicates that

the combustion region has become narrow, pushing the flame toward the diffuser inlet. This trend indicates that an interesting relationship exists between the flame location and the TKE under changing turbulence intensities and turbulent length scales.

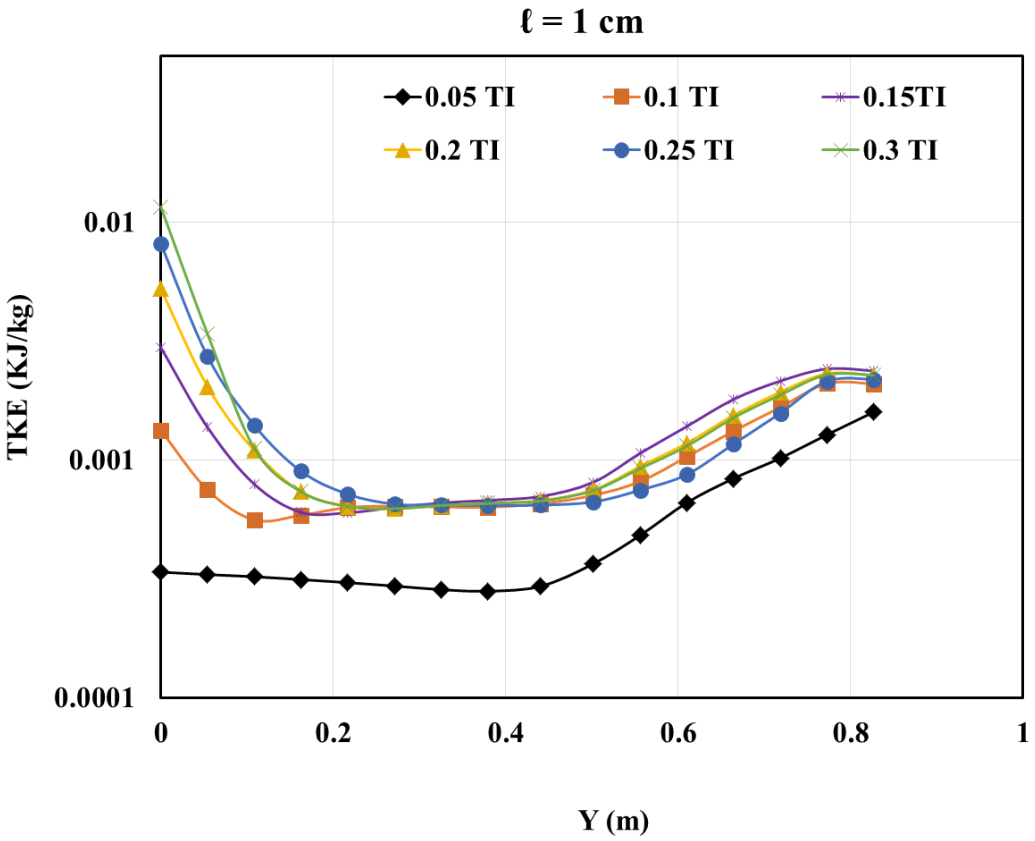


Figure 6-14 TKE along the axial direction of the current diffuser with conical insert for various turbulence intensities and at 1-cm turbulent length scale.

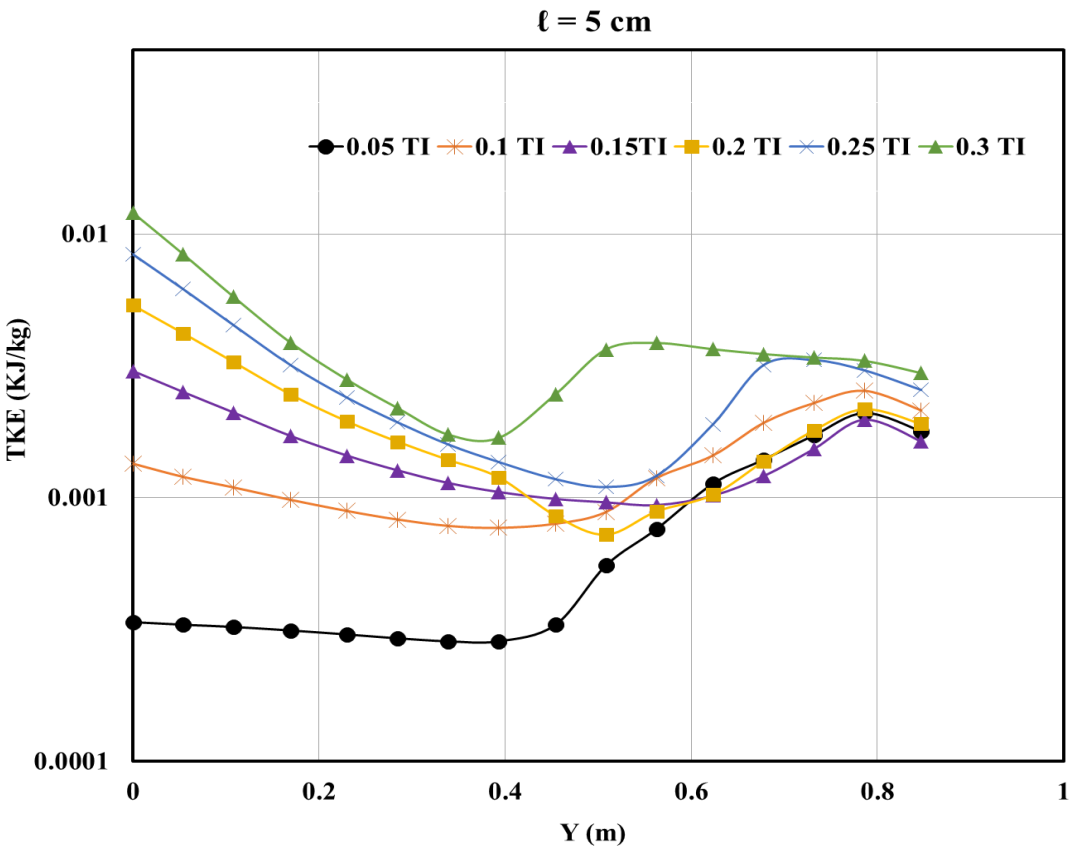


Figure 6-15 TKE along the axial direction of the current diffuser with conical insert for various turbulence intensities and at 5-cm turbulent length scale.

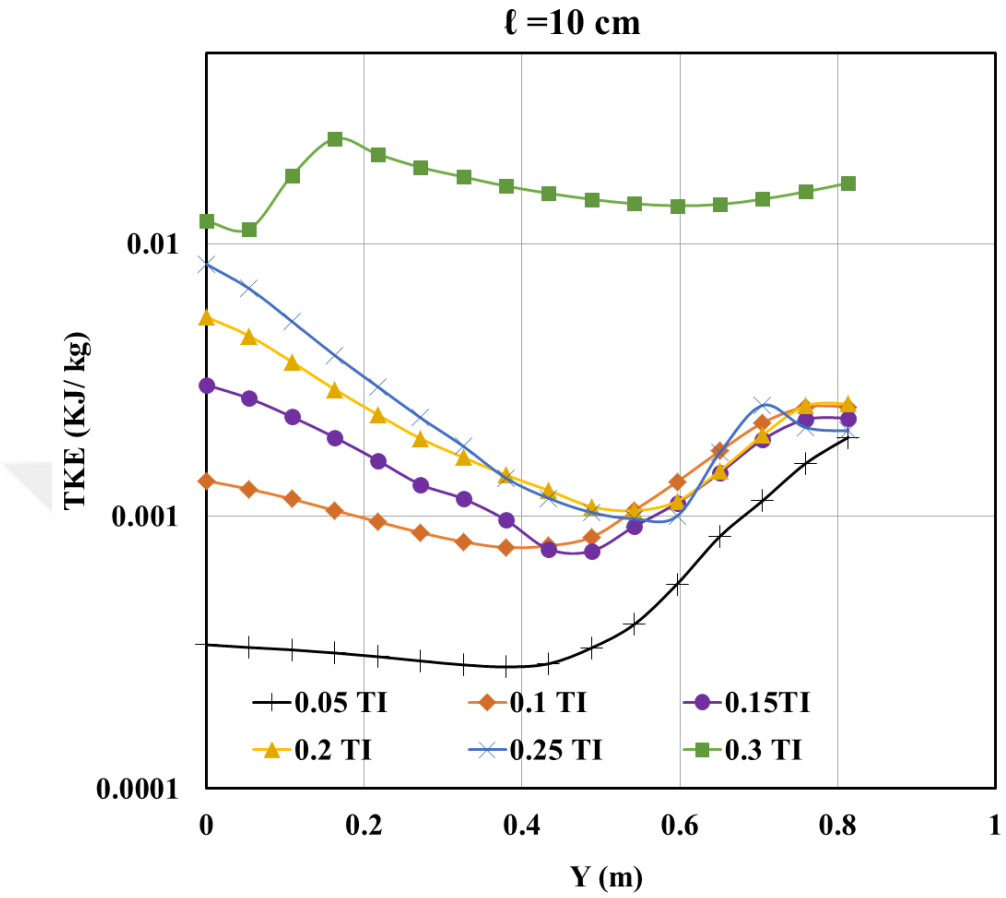


Figure 6-16 TKE along the axial direction of the current diffuser with conical insert for various turbulence intensities and at 10-cm turbulent length scale.

**Figure 6-17** portrays turbulent kinetic energy along the axial centerline of the diffuser at different $Re_{\lambda b}$. The behavior of turbulent kinetic energy changes with the increase in Taylor-scale Reynolds number at the beginning of the combustion. The trends of turbulent kinetic energy depend on turbulence intensity and length scale, that is, Taylor-scale Reynolds number at the beginning of combustion. Figure 6-17 shows that turbulent kinetic energy rises in the combustion region. In addition, Figure 6-17 also indicates a difference between the turbulent kinetic energy of all cases within the combustion zone. The turbulent kinetic energy at ($Re_{\lambda b}$ =103) is higher than that ($Re_{\lambda b}$ = 79). The highest turbulent kinetic energy is observed at the highest Taylor-scale

Reynolds numbers. Additionally, the flame location that sudden drops in the inlet is attributed to the peak that raises turbulent kinetic energy at $Re_{\lambda b}$ =103. This turbulent kinetic energy tendency is in accordance with Equation 2-64. Meanwhile, the values of turbulent kinetic energy increase relative to the source of flame area density $S_{\Sigma}$. This result indicates that the combustion zone narrowed resulting in the movement of the flame toward the inlet of the combustor. In summary, an interesting relationship exists among turbulent kinetic energy, Taylor-scale Reynolds numbers, and flame location.

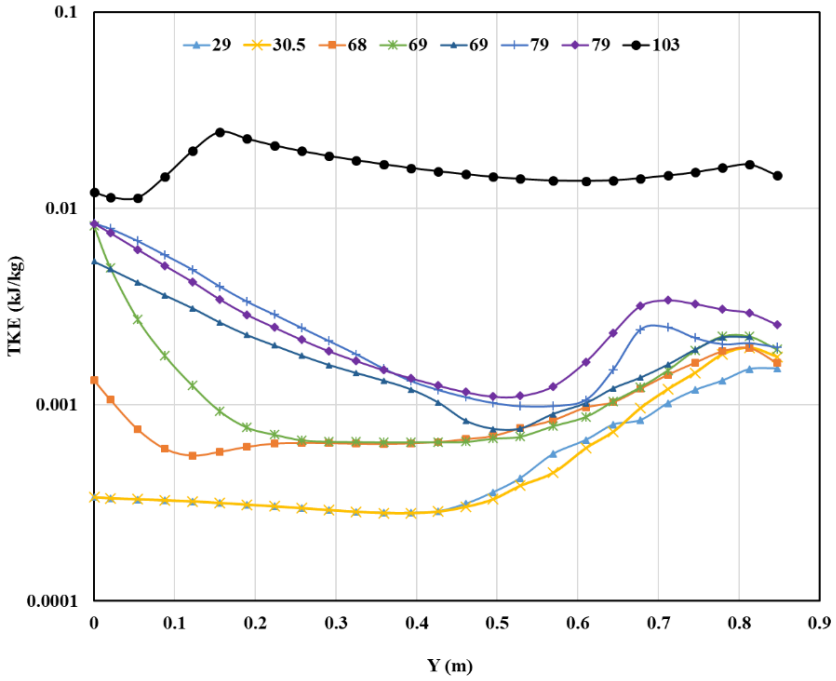


**Figure 6-17** TKE along the axial centerline of the diffuser with conical insert for different Taylor-scale Reynolds number (the number on the curve is the values of $Re_{\lambda b}$).

## *6.6 Flame area density*

The flame area density is the main parameter in the coherent flame model and the key for the interaction between turbulence and combustion in the coherent flame model. In this model,

flame area density relates to turbulent kinetic energy and turbulent dissipation within the term of the flame stretch as explained in Equations 2-66, 2-67 and 2-68. Therefore, flame area density is plotted with respect to Taylor-scale Reynolds number at the beginning of the combustion. In this section, the behavior of the flame area density under various Taylor-scale Reynolds number in the diffuser using a conical insert is explained.

Figure 45 indicates the contour of the flame area density as a function of the Taylor-scale Reynolds number at the beginning of the combustion for a diffuser with conical insert. Similar to the behavior of flame location, flame area density is less sensitive to low $Re_{\lambda i}$, and flame area increases rapidly with the increase in $Re_{\lambda b}$ higher than 79. Figure **6-18** also shows that flame area density has the highest value at the highest $Re_{\lambda b}$. The explanation of this behavior of the flame area density, an increase in turbulence intensity in the other word in TKE means an increase in $S_{\sum}$ in Eq. (2-67). The explanation of this behavior of flame area density is attributed to increases in TKE that means an increase in the source term of the flame area density in Equation (2-64). This increase in the source term of flame area density shows that the combustion zone became narrow. As a result, flame location pushed toward the combustor inlet, thereby increasing the value of the flame area density.

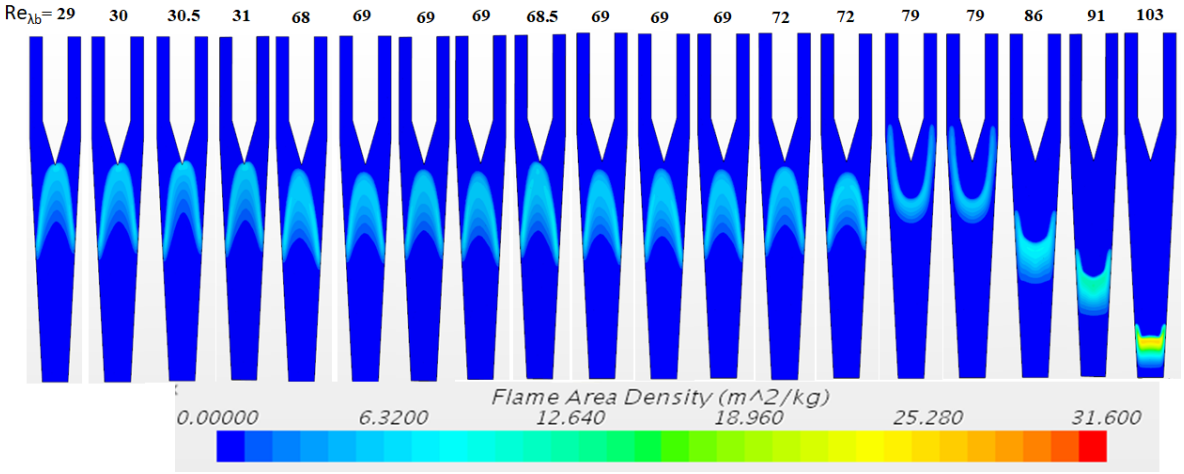

Figure 6-18 Contour of the flame area density via $Re_{\lambda b}$ for the diffuser combustor with conical insert.

The integral of the flame area within the combustor should be the same for all simulations. Therefore, the integrated flame area density is represented as a function of different turbulence intensities and turbulent length scales, as shown in Figure 6-19. For all cases of TI, ℓ, and $Re_{\lambda}$, the integrated flame has almost the same values, as illustrated in Figure 6-19.

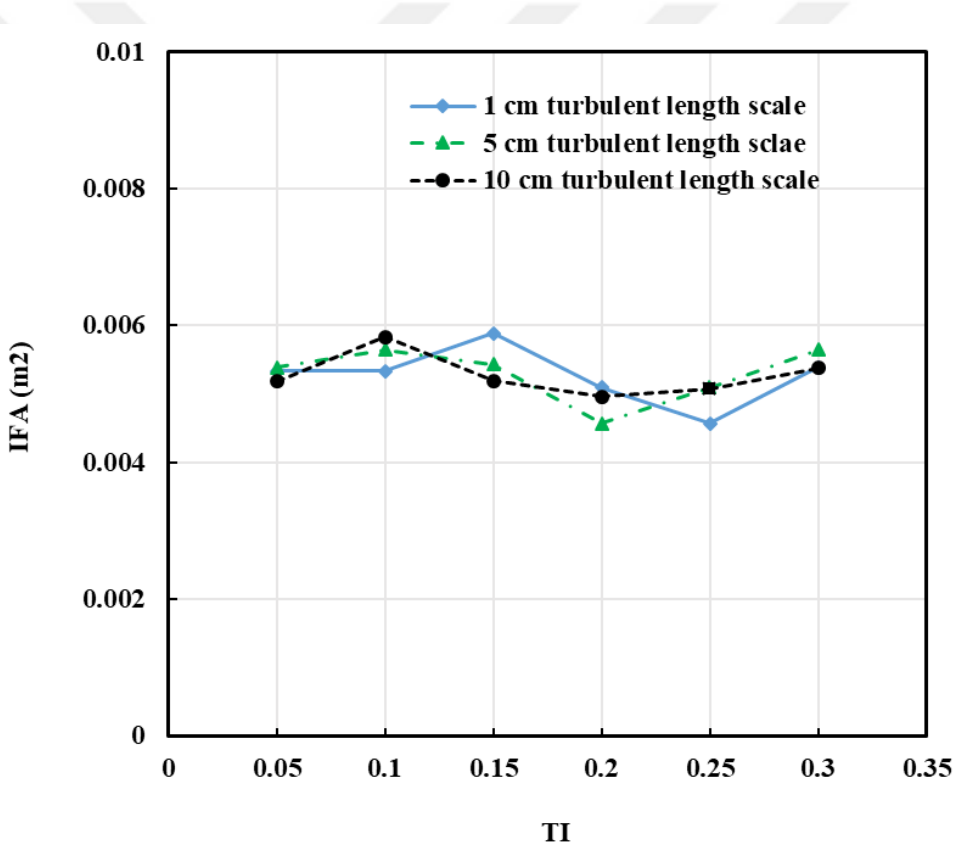


**Figure 6-19** The comparison of the integrated flame area density (IFAD) over the axial direction of the diffuser combustor with conical insert for various TI and ℓ.

Similar previous studies introduced on the flame area density by many researchers. For example Gülder and Smallwood [16] introduced study on the flame area density in a Bunsen burner at medium and high level of the turbulence intensities and indicated that the flame

surface density changes with increase in the turbulence intensity but this variation did not obey systematic correlation, as it is the case in the current study. Bagdanavicius et al.[17] also examined the response of the flame area density with change in a stretch rate in a turbulent premixed flame and indicated that the flame area density depends on the turbulent burning velocity and the flame stretch.

# CHAPTER VII

# 7 CONTROL OF FLAME LOCATION

## *7.1 Control algorithm*

In this section, the simulation methodology and its interaction with the algorithm for controlling flame location are explained. Flame location depends on turbulence intensity and length scale [172][175]. Therefore, the control strategy is based on changing the values of turbulence intensity and length scale at the inlet of the diffuser according to the current flame location and target flame location set by the user. The values of turbulence intensity and length scale depend on TKE and TDR according to equations 2-67 & 68. Therefore, TKE is used to control the characteristics of turbulent flow. To build the strategy for controlling flame location, establishing a relationship between flame location and the characteristics of turbulent flow is essential. The behavior of flame location at various TKEs and TDRs is first investigated. Flame location is related to TKE and TDR, as shown in Figure **7-1**. This figure is plotted based on the sets of simulations for wide ranges of TKEs and TDRs. Figure **7-1** clearly shows that flame location is affected by TKE and TDR. In general, flame location moves toward the inlet of the diffuser with an increase in TKE and TDR. Thereafter, an equation is derived based on the values in Figure **7-1**which relates flame location to TDE and TDR.

$$\boldsymbol{TkE = 0.0011 - (0.012 * Target\ flame\ location) + (0.079 * TDR)} \qquad (7\text{-}1)$$

This equation is utilized to introduce the initial value of TKE at the inlet of the diffuser combustor in the algorithm. Thus, the control algorithm is used to periodically adjust TKE and TDR at the inlet of the diffuser to hold the flame in the required location.

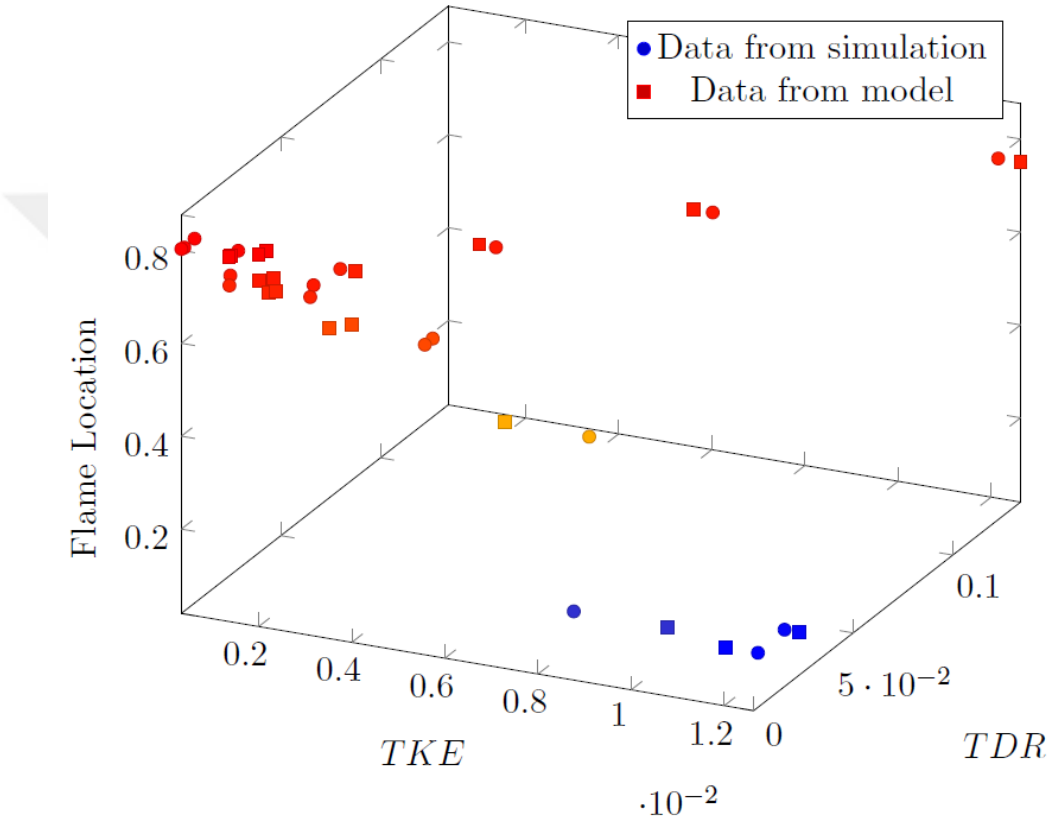


Figure 7-1 The scatter of turbulent kinetic energy, turbulent dissipation rate and fame location data and the model values.

Tuning the control parameters is crucial to match turbulence specifications to flame dynamics, thereby allowing flame to be located at the desired level as fast as possible without driving the system to an unstable state. The under relaxation factor (URF) is a parameter that controls the fluctuation of flame location. URF relates the current TKE and the difference between current flame location and target value as follows:

$$\boldsymbol{TKE_{new}} = \boldsymbol{(1 + URF * \Delta \ell) * TKE_{current}} \quad (7\text{-}2)$$

where Δl is the difference between the target flame location and the current location. Fluctuation in the flame location is damped by controlling URF. The control algorithm is introduced into simulations using a macro file, which is a program written in Java language. Macro files enable users to control almost all simulation factors. Starting a macro file in STAR-CCM+ program promotes target flame location for the user. On the basis of this value and using equation 9, an initial TKE value is set at the inlet boundary condition. Then, the program starts to run iterations based on the set parameters and checks flame location at every time step. Two turnover periods are allowed for the simulation to reach a steady-state value in flame location. After the two periods, flame location is compared with the target value, and modifications are made based on equation 10if necessary. However, to reach the target location within a short time, an additional condition is imposed on the algorithm. As mentioned previously, flame location is checked every time step. Hence, in case flame passes the target location, a modification in inlet TKE is implemented based on equation 10. . This additional condition helps the algorithm converge to the target flame location within a short time. A schematic of the control algorithm is provided in Figure 7-2.

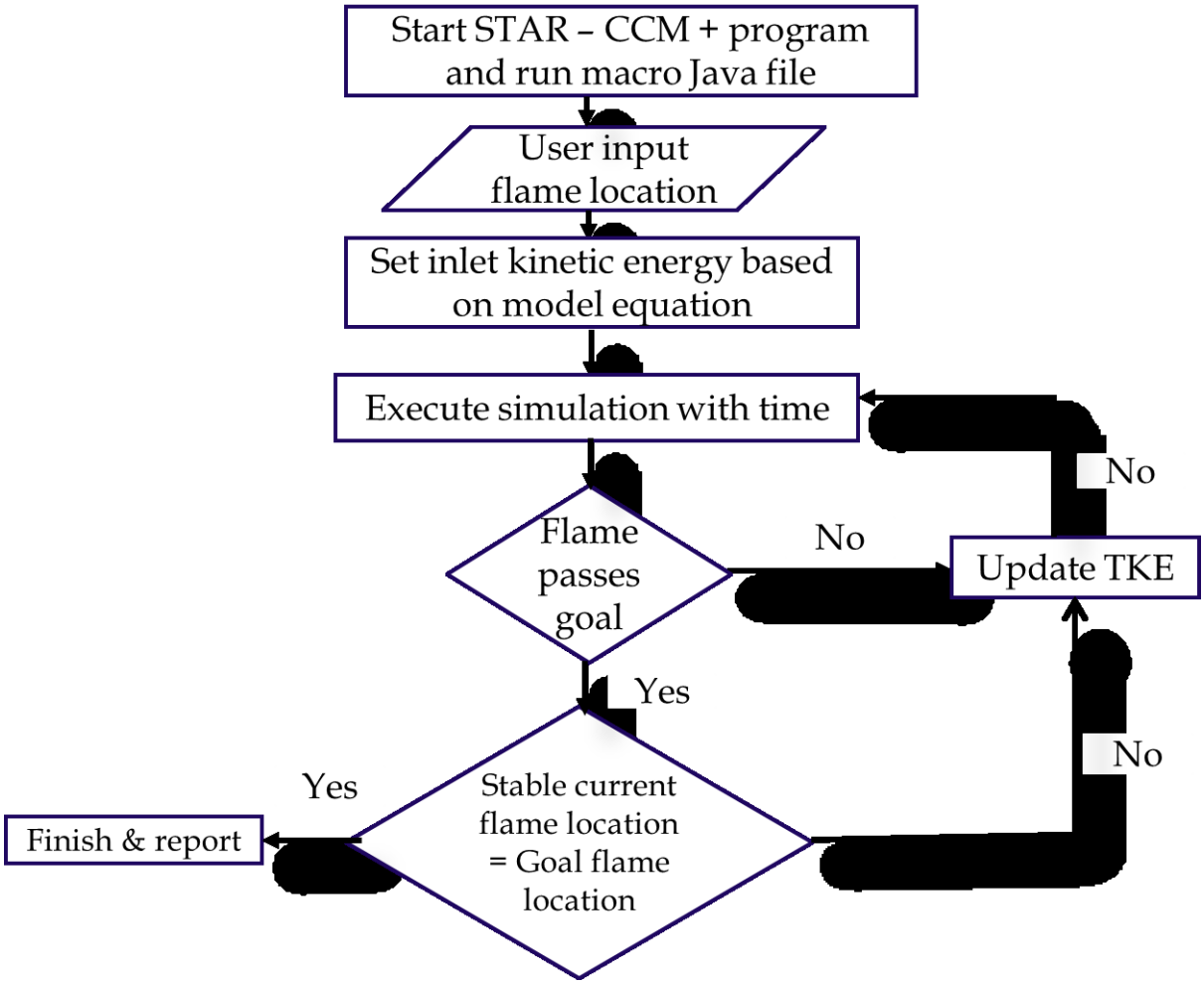


**Figure 7-2** The schematic view of the control system that considers at the combustor inlet section.

## *7.2 Control of the flame location*

In this section, we discuss the results and the robustness of the algorithm in controlling flame location (denoted as FL hereafter) at the desired level for various TKE ranges. In general, FL is a function of TKE according to equation 73. The results indicate how the algorithm controls FL by automatically changing the TKE value. The sensitivity of FL to URF is shown in

. This figure clearly indicates that flame reaches the target location at an earlier time when URF is reduced. In addition, the amount of fluctuations decreases with a reduction in URF.

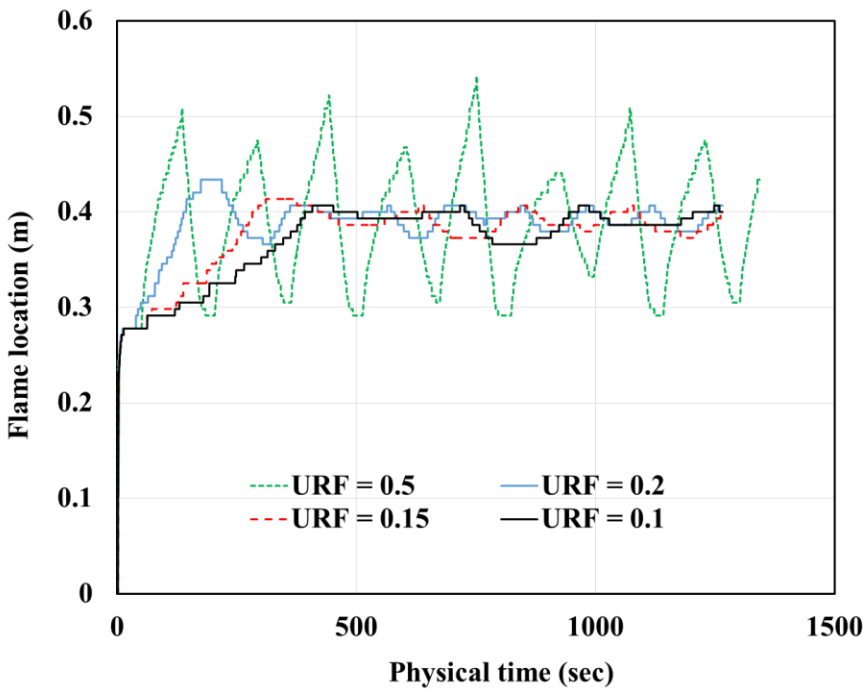


Figure 7-3 Flame Location Sensitivity to URF.

To show the behavior of TKE and FL with the algorithm for different URFs, two cases are presented in Figures 7- 4 and 7-5. These figures illustrate FL and TKE as functions of physical time for FL = 0.4 m and URFs of 0.20 and 0.15. Moreover, FL moves initially toward the target flame location with the given initial TKE value. When the flame front passes the target, TKE automatically and instantly adjusts to a new value by increasing its previous value. The increase in TKE pushes flame location toward the inlet of the combustor. Subsequently, TKE varies based on the difference in flame current and target location difference, which enables flame to reach the target value. Finally, FL fluctuates around the target FL with decreasing or

increasing TKE value. This oscillation decreases in time. The fluctuations are too small, which are approximately less than 2 cm, as evident in Figures 7- 4 and 7-5.

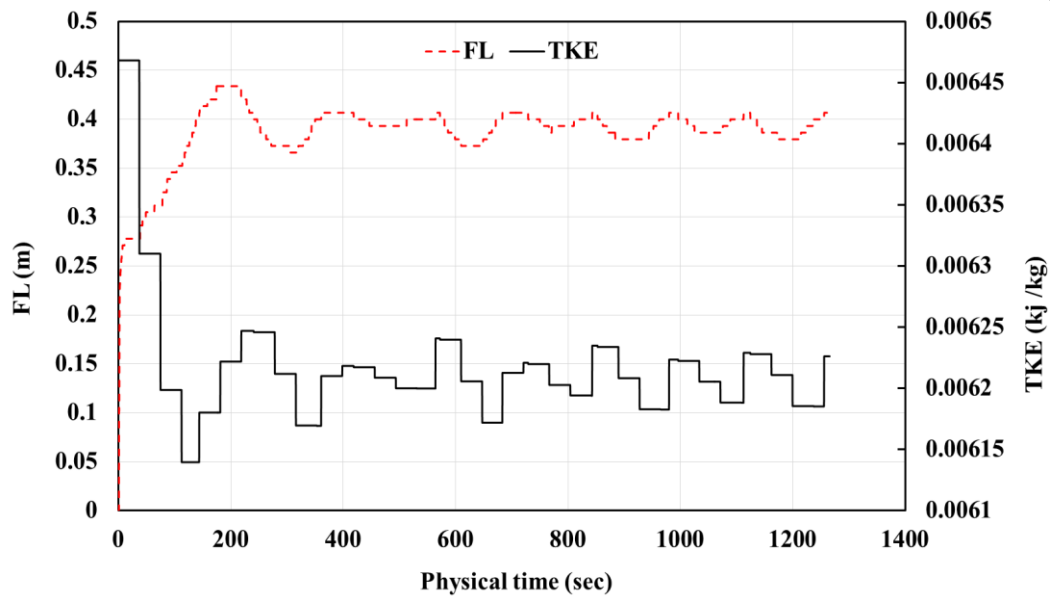


Figure 7-4 The flame location and TKE with physical time for the URF = 0.20.

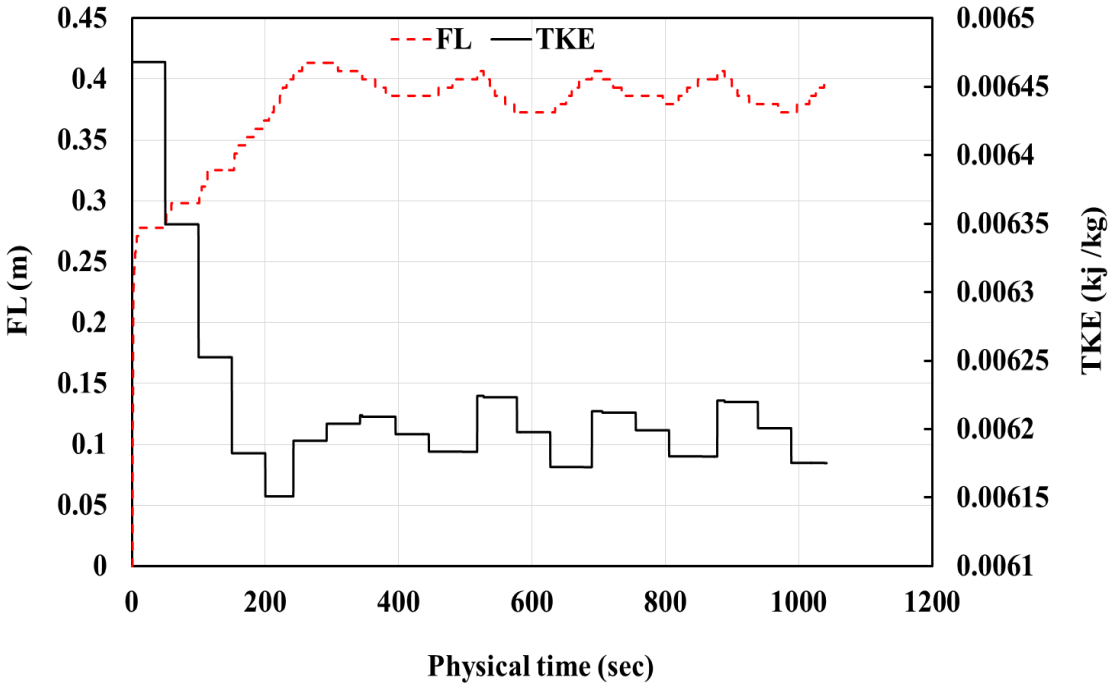

Figure 7-5 The flame location and TKE with physical time for the URF = 0.15.

To demonstrate the performance of the control algorithm for different target FLs, the results of two cases, with target flames of 0.34 m and 0.48 m, are presented in Figures 7- 6 and 7-7. These results illustrate the good performance of the algorithm for different target FLs. Different FLs are used to examine the robustness of the algorithm. FLs = 0.34, 0.4, and 0.48 m are selected to indicate the algorithm's performance in reaching the target location, as shown in Figure **7-8**. Figure **7-8** shows that FL starts with a high fluctuation around it and then reaches a low oscillation for the cases of FL= 0.4 m and 0.48 m. By contrast, the behavior for case FL= 0.34 m differs from that of the two previous cases (FL= 0.4 m and 0.48 m). That is, FL starts at a low position, reaches the target location, and stabilizes on it.

The dissimilarity among these cases in terms of the required time to reach the goal is that where the flame location with 0.4 m reach the goal location in the shortest time compared with other cases FL = 0.34 and 0.48 m respectively. Whilst the flame location with 0.48 m needed the longest time to reach the goal location. These behaviors of the flame location due to the behaviors of the TKE where FL and TKE are behaved in opposite proportion. In the beginning, TKE fluctuates with a high level of oscillation that leads to a high oscillation in FL = 0.48 m (Figure **7-7**). By contrast, TKE starts with less fluctuation in FL= 0.4 m, which leads to a low oscillation level.

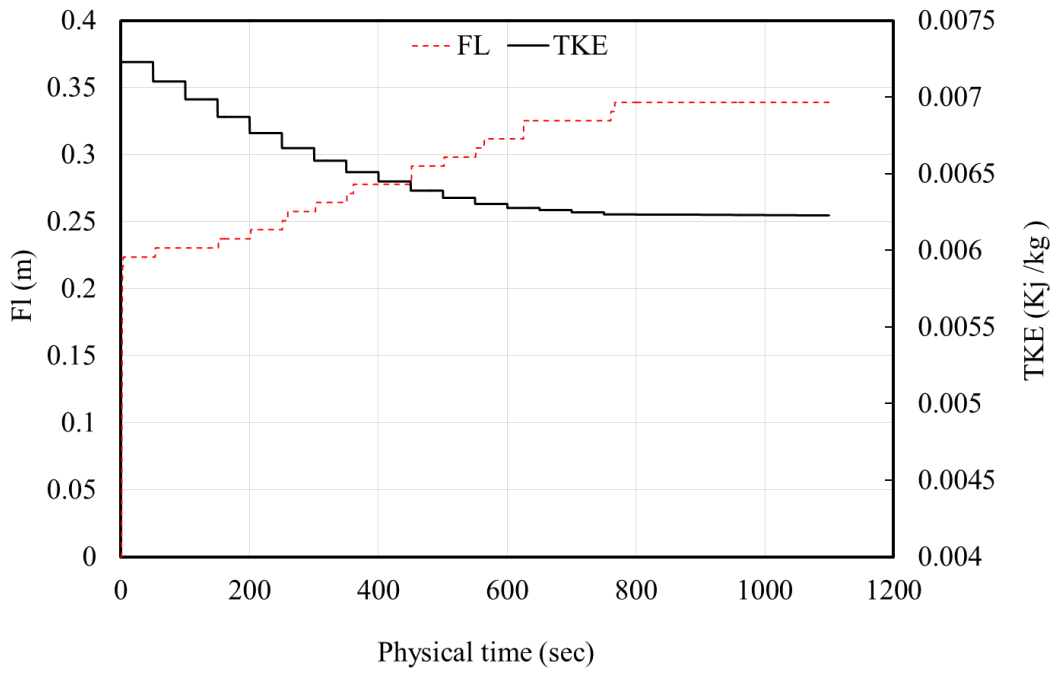


Figure 7-6 FL and TKE versus the physical time for the URF = 0.15 and at the flame location 0.34 m.

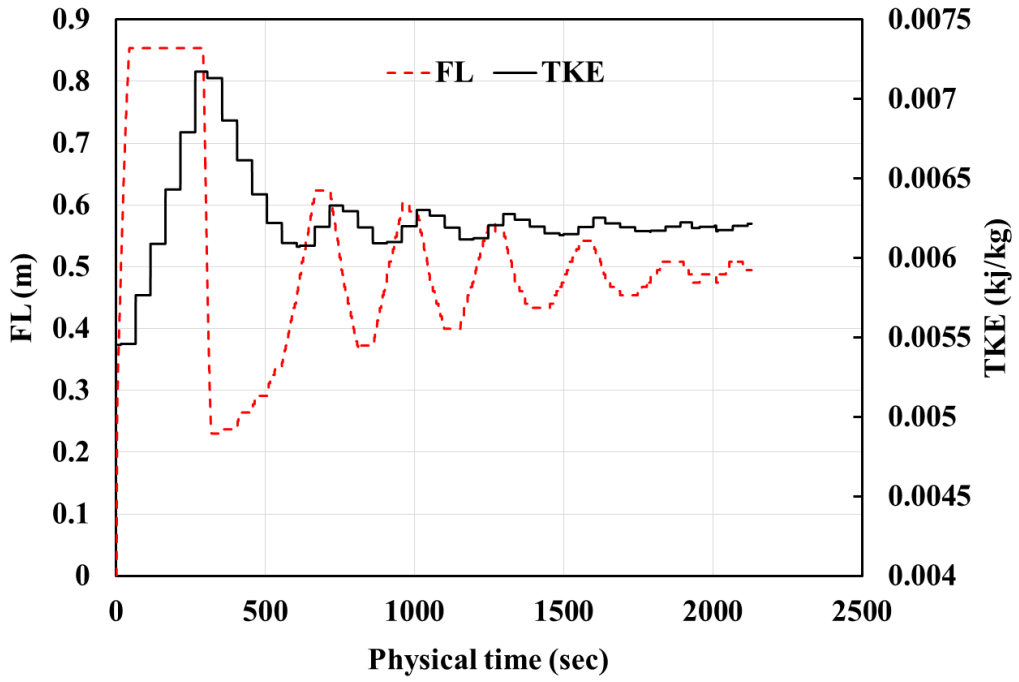


Figure 7-7 FL and TKE versus the physical time for the URF = 0.15 and at the flame location 0.48 m.

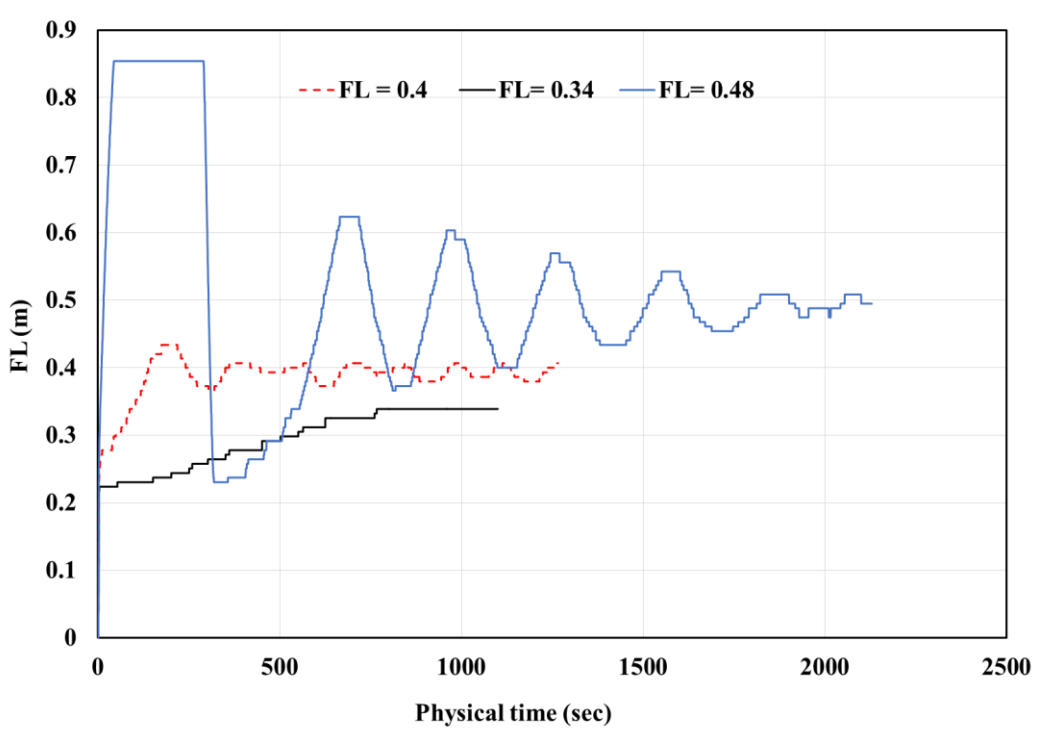


Figure 7-8 FL with physical various flame locations.

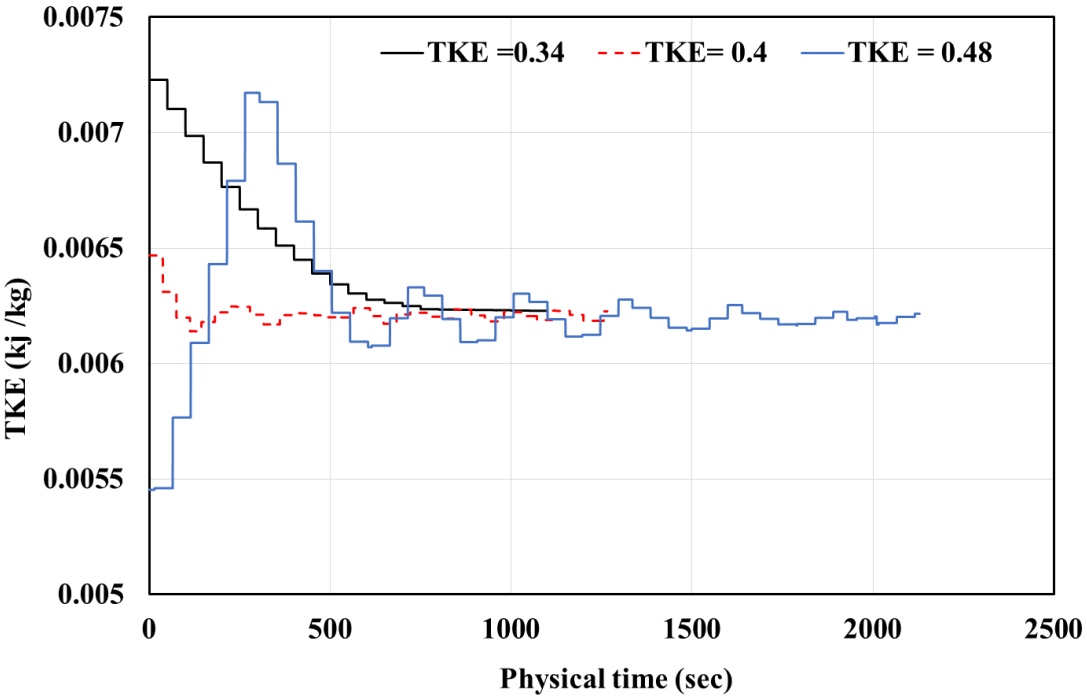


Figure 7-9 TKE with physical various flame locations.

FAD is also utilized to indicate the behavior of flame at various TKEs. Figure **7-10** shows the contour of FAD, TKE, and temperature at various FLs (FL = 0.34, 0.4, and 0.48 m). The maximum FAD increases with the movement of FL toward the inlet of the diffuser. In addition, the shape of the flame varies with changes in FL and TKE. Such behavior of FAD is attributed to an increase in TKE, which indicates an increase in the source term of FAD in equation 3. The increase in the source term of FAD shows that the combustion zone has become narrow. Consequently, FL pushes toward the combustor inlet, thereby increasing the value of FAD. Flame topology can be concave or convex. Nazzal and Ertun¸c [172][175] indicated that flame topology varies due to changes in turbulence intensity and length scale. In addition, Kerl, Lawn, and Beyrau [44] introduced a three-flame topology (parabolic, hyperbolic, and elliptic) in a diffuser burner with an annular swirling flow at the inlet. This previous investigation is the most similar study to the current work; hence, the flame shapes obtained in this previous work can be considered realistic.

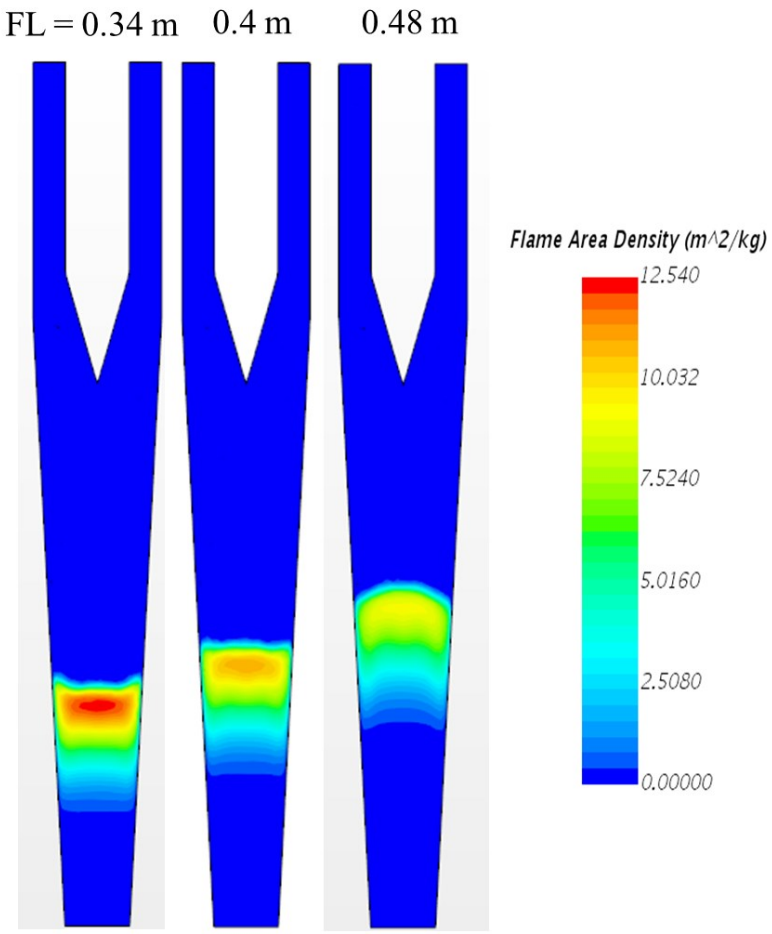


Figure 7-10 The flame area density distribution on the diffuser for different flame location.

# CHAPTER VIII

# 8 CONCLUSION AND FURTURE WORK

## *8.1 Conclusions*

The control of the flame location in the diffuser combustor is studied on the basis of the turbulent flow characteristics. For this purpose, the effects of turbulence intensity and turbulence length scale on flame location using a diffuser combustor for the steady- and unsteady-state conditions are explained.

The steady-state results indicate that turbulence intensities and turbulence length scales have a significant effect on the flame location of premixed combustion. The flame front generally moves towards the inlet of the combustor with the increase in turbulence intensity. For moderate and high turbulence length scales, the flame location initially decreases with the increase in turbulence intensity, and the flame location then stabilizes before decreasing at the inlet of the diffuser with an increase in turbulence intensities.

However, the behavior is different for low turbulence length scales. The flame location decreases with the increase in turbulence intensity from low turbulence intensities. Then, the flame location stabilizes with the increase in turbulence intensity. This behavior depends on the TKE. In addition, with the change in flame location, the flame shape changes with the increase in turbulence intensity to a high level at 5 and 10 cm turbulence length scales. We conclude that turbulence intensity and turbulence length scale simultaneously influence the flame location,

shape and area density. In addition, with the change in flame location, the flame shape might change when the turbulence intensity and the turbulence length scale are varied.

The results of the flame behavior are studied under unsteady-state conditions. The unsteady-state results indicate that turbulence intensity, length scale and flow separation also exert a significant effect on the flame location of premixed turbulent combustion. The flame front moves towards the diffuser inlet with increases in turbulence intensity and turbulence length scale. However, the effect of turbulence intensity is more visible than that of turbulence length scale within the tested range. An increase in turbulence length scale at a constant turbulence intensity decreases the flame location. Flow separation occurs behind the flame zones in most cases, thereby influencing the location and shape of the flame front. Therefore, the value of the flame location and the flame shape are influenced by flow separation, turbulence intensity and turbulence length scale. Flow separation was observed within the diffuser at the unsteady-state conditions. This flow separation effects on the flame location and prevent the sole effect of turbulence on flame location. In addition, this flow separation changes with a change in the turbulence intensity and turbulent length scale but not all cases. Therefore, a conical object is placed inside the diffuser. The conical object pushes the flow toward the wall, thus, the flow separation is eliminated.

In addition, the flame behavior is studied for the diffuser with a conical insert and compared with the results of the diffuser without a conical insert under the unsteady-state conditions. Results indicate that turbulence intensity, turbulence length scale and the Taylor-scale Reynolds number influence the flame location. The results for the diffuser (with conical insert) are compared with a diffuser without a conical insert. The flame location generally moves towards the inlet of the diffuser with the increase in turbulence intensities and turbulence length

scale for combustors with and without a conical insert. The main differences observed between the two diffuser cases are found at high turbulence intensities and turbulence length scales. The flame location drops rapidly at the inlet of the diffuser with a conical insert for high turbulence intensities (TI > 25%) and high turbulence length scales ($\ell$ > 5 cm). The flame location in the diffuser without conical insert [28] moves to the middle of the combustor before it stabilizes at TI > 25%. A similarity exists between the flame locations in the diffusers with and without a conical insert at low turbulence intensities (5%, 10% and 15%). However, the behavior of the flame location is based on the TI and the turbulence length scale.

In order to understand the flow structure for both cases of the diffusers (with and without conical insert), the flow fields within the diffusers for two cases (20% TI & $\ell$ = 10-cm) and (30% TI and $\ell$ = 10-cm) are compared. It is observed that a flow separation at the wall of the diffuser without conical insert behind the flame, which causes an increase in the velocity at the center. This increase in the velocity, which occurs in the combustion region, causes to occur deaccelerating in the velocity before the combustion region. For the case of the high turbulence intensity (30% TI and $\ell$ = 10-cm), flow separation, which occurs nearly at the wall of the diffuse and causes to push the flame away from the inlet. While with using the conical insert for 30% TI and $\ell$ = 10-cm, flow separation is eliminated, and the flame drops toward the inlet of the diffuser with the conical insert. As results, the flow separation causes the difference between the behavior flame locations in diffusers (with and without conical insert).

For the moderate turbulence intensity (20% TI & $\ell$ = 10-cm), the flow separation pushes the flame towards the middle of the diffuser without using a conical insert. In addition, flow separation is eliminated by using the conical insert, which pushes the flow toward the wall. The flame location moves towards the outlet of the diffuser. This behavior of the flame location for

the case of (20% TI & ℓ = 10-cm) attributes to the behavior of others parameters the turbulent kinetic energy, dynamic pressure and the mean velocity besides of the flow separation. It was observed two distinct tends for both diffusers, consider TI = 20% and ℓ = 10, the flame is located at a higher level in the diffuser with conical insert than that in the diffuser without the conical insert. A contrary state occurs when TI is set to 30%. This intriguing trend is explained by describing the flow separation, pressure drop, velocity and turbulent kinetic energy for both cases.

This flow separation causes extra deceleration of the velocity upstream of the flame, i.e. between the flame and the inlet. This is deceleration is partially due to the stagnation and due to the vena contraction effect in the diffuser. It is recognized that the static pressure rises in the diffuser without conical insert around the flame location. This rise creates a strong adverse pressure gradient, which reflects itself as the large deceleration of the flow velocity. As the local speed drops, flame penetrates towards the inlet more than that compared to the causes without conical insert, i.e. causes without flow separation at TI = 20% & ℓ = 10 cm. This rise in the pressure is also associated with flow rate the pressure gradient downstream of the flame. Therefore, together with vena contraction, the speeds downstream of the flame in the diffuser without conical inset is larger than at the centerline of the diffuser.

This analysis shows that the separation might cause changes in the pressure consequently the velocity field, which influences the flame location, more than the turbulence. The local balance of the flame speed and the speed of the unburned gases determines the final of the flame location.

We can conclude that at a low turbulence length scale (1 cm), the flame is less sensitive to the increase in turbulence intensities and remains constant with the increase in the turbulence intensities for a diffuser with a conical insert. Flame location is also observed to generally move towards the inlet of the combustor with the increase in the Taylor-scale Reynolds number. Results also show that flame location is less sensitive to low Taylor-scale Reynolds numbers and highly influenced by high Taylor-scale Reynolds numbers for a diffuser with a conical insert. However, after a Taylor-scale Reynolds number of 79, the flame location decreases rapidly to the inlet of the diffuser. In addition, the flame shape varies with the increase in the Taylor-scale Reynolds number, and the Taylor-scale Reynolds number affects the FAD. Results confirm that TKE, FAD, flame location and Taylor-scale Reynolds number are significantly related. This study indicates that the Taylor-scale Reynolds number is the main parameter in terms of the turbulence effect on flame location. This study shows that a diffuser combustor with a conical insert can generally be used to study the effect of turbulence on flame numerically and experimentally.

Finally, flame location is controlled according to the results of the unsteady-state conditions with a conical insert. The flame location in a diffuser combustor control is realized in CFD framework. Our study indicates that the algorithm appears to provide turbulent flow characteristics control that relatively controls the flame to the desired location. A new strategy for controlling the flame location is introduced by applying a feedback mechanism in a 3D diffuser geometry without distorting the geometric combustor. The turbulence is used to control combustion and, consequently, the flame location. A simple feedback control algorithm varied the turbulent flow characteristics at the inlet of the combustor to locate the flame at the desired

location. For high TKEs, the flame location stabilizes at the inlet of the diffuser, whilst the flame location stabilizes in the middle of the diffuser at moderate turbulence.

It can be observed the initial value of the TKE that start for the opposite flame location effect the time which needs to desired flame location. Whereas the TKE starts with closet value for the target flame location, the time required to reach the target location is less compare with that has farthest value, which need long time to reach the target location. The time required to reach the target location decrease for the low the sensitivity factors less than 0.2 compare with that occur for the sensitivity factor 0.5. In addition, this sensitivity factors lead to decrease the fluctuation in the flame location respect to the desired value.

In summary, a smart approach to controlling flame at a certain location within desirable levels is introduced by varying turbulent flow characteristics. This approach control the flame location using turbulence intensity and length scale without distorting the combustor geometry and without changing the mixture velocity, i.e., the thermal power.

## 8.2 *Future Work*

Although the outcomes of this work indicated that the turbulent flow characteristics influence the flame location, several characteristics and parameters should still be considered in the investigation of flame location. This work can be further expanded to investigate several other characteristics on the flame location, which are essential to indicate the behavior of the flame location in the diffuser combustor. Therefore, a brief of suggestions can be considered in any future investigation.

The combustion process produces hot products, thereby increasing the temperature of the mixture ahead of the flame front. Heating the mixture can affect the turbulent flame speed; that is, the flame location is influenced. In addition, the radiative heat from the walls can affect flame propagation. Therefore, the investigation on turbulent characteristic flows on the flame location needs to be expanded by considering the effect of radiation on the flame location in the diffuser combustor for any future study.

A smart approach to controlling flame at a certain location within desirable levels is achieved by varying turbulent flow characteristics. This study introduces the control of flame location in a diffuser combustor by actively changing turbulent flow characteristics at the inlet, and a control strategy is suggested for this purpose. A control algorithm written in Java language is adopted alongside commercial computations.

# APPENDIX

## *Control algorithm*

Control algorithm is built using macro java and STAR CCM++ in order to control flame location by varying the turbulent kinetic energy as shown:

```
// STAR-CCM+ macro: Step_1.java

// Written by STAR-CCM+ 11.02.010

// Version 1.0.1

package macro;

import java.util.*;

import star.turbulence.*;

import star.combustion.*;

import star.keturb.*;

import java.util.Scanner;

import java.io.*;

import java.io.BufferedReader;

import java.io.FileNotFoundException;

import java.io.FileReader;
```

```
import java.io.IOException;

import star.base.report.*;

import star.common.*;

import star.base.neo.*;

import star.vis.*;

public class Step_1 extends StarMacro {

public void execute() {

execute0();

  }

private void execute0() {

    Simulation simulation_0 =

      getActiveSimulation();

// Change the Turbulent Dissipation Rate and Turbulent Kinetic Energy

        Region region_0 =

      simulation_0.getRegionManager().getRegion("fluid");

    Boundary boundary_0 =

      region_0.getBoundaryManager().getBoundary("inlet");
```

```
        TurbulentDissipationRateProfile turbulentDissipationRateProfile_0 =
          boundary_0.getValues().get(TurbulentDissipationRateProfile.class);
        turbulentDissipationRateProfile_0.getMethod(ConstantScalarProfileMethod.class).getQu
antity().setValue(1.0);
        TurbulentKineticEnergyProfile turbulentKineticEnergyProfile_0 =
          boundary_0.getValues().get(TurbulentKineticEnergyProfile.class);
        turbulentKineticEnergyProfile_0.getMethod(ConstantScalarProfileMethod.class).getQua
ntity().setValue(2.0);
        // Field Function
        // Set Turbulent Dissipation Rate Field Function and assign it to B.C.
        UserFieldFunction userFieldFunction_0 =
          simulation_0.getFieldFunctionManager().createFieldFunction();
        userFieldFunction_0.getTypeOption().setSelected(FieldFunctionTypeOption.Type.SCAL
AR);
        userFieldFunction_0.setPresentationName("Turb_Diss_Rate");
        userFieldFunction_0.setFunctionName("Turb_Diss_Rate");
        double Turb_Diss_Rate = 0.0;
        String Turb_Diss_Rate_value = Double.toString(Turb_Diss_Rate);
```

```
        userFieldFunction_0.setDefinition(Turb_Diss_Rate_value);

        turbulentDissipationRateProfile_0.setMethod(FunctionScalarProfileMethod.class);


turbulentDissipationRateProfile_0.getMethod(FunctionScalarProfileMethod.class).setFieldFunct
ion(userFieldFunction_0);

        simulation_0.println("Turbulent Dissipation Rate " + Turb_Diss_Rate_value);

        // Set Turbulent Kinetic Energy Field Function and assign it to B.C.

        UserFieldFunction userFieldFunction_1 =

          simulation_0.getFieldFunctionManager().createFieldFunction();

      userFieldFunction_1.getTypeOption().setSelected(FieldFunctionTypeOption.Type.SCAL
AR);

        userFieldFunction_1.setPresentationName("Turb_Kinetic_Energy");

        userFieldFunction_1.setFunctionName("Turb_Kinetic_Energy");

        double Turb_Kinetic_Energy = 0.0030375;

        //String Turb_Kinetic_Energy_value = Double.toString(Turb_Kinetic_Energy);

        userFieldFunction_1.setDefinition(Double.toString(Turb_Kinetic_Energy));

        /*TurbulentKineticEnergyProfile turbulentKineticEnergyProfile_0 =

          boundary_0.getValues().get(TurbulentKineticEnergyProfile.class);*/
```

```
turbulentKineticEnergyProfile_0.setMethod(FunctionScalarProfileMethod.class);

turbulentKineticEnergyProfile_0.getMethod(FunctionScalarProfileMethod.class).setField
Function(userFieldFunction_1);

simulation_0.println("Turbulent Kinetic Energy " + Turb_Kinetic_Energy);

// Input the desired Flame location

double Goal_Flame_Loc = promptUserForInput("Desired Flame location", 0.400);

//

// Model based Turbulent kinetic energy

// p00=0.01154;

// p10=-0.01268;

// p01=0.07911;

// tke_model=0.01154-0.01268*fl+0.07911*0.01674;

// turbulent dissipation rate = 0.01674

double K = 1;

Turb_Kinetic_Energy = 0.01154-
(0.01268*Goal_Flame_Loc)+(0.07911*Turb_Diss_Rate);

userFieldFunction_1.setDefinition(Double.toString(Turb_Kinetic_Energy));

//
```

```
        double Time_control=0;
        double Current_Flame_Loc = 0.0;
        double diff_Loc = (Current_Flame_Loc - Goal_Flame_Loc);
        // Current Flame Location field function
        UserFieldFunction userFieldFunction_2 =
            simulation_0.getFieldFunctionManager().createFieldFunction();
        userFieldFunction_2.getTypeOption().setSelected(FieldFunctionTypeOption.Type.SCAL
AR);
            userFieldFunction_2.setPresentationName("Current_Flame_Loc");
            userFieldFunction_2.setFunctionName("Current_Flame_Loc");
            //String Turb_Kinetic_Energy_value = Double.toString(Current_Flame_Loc);
            userFieldFunction_2.setDefinition(Double.toString(Current_Flame_Loc));
        XyzInternalTable xyzInternalTable_0 =
              simulation_0.getTableManager().createTable(XyzInternalTable.class);
            PrimitiveFieldFunction primitiveFieldFunction_0 =
              ((PrimitiveFieldFunction)
simulation_0.getFieldFunctionManager().getFunction("Temperature"));
```

```
xyzInternalTable_0.setFieldFunctions(new NeoObjectVector(new Object[]
{primitiveFieldFunction_0}));

LinePart linePart_0 =

 ((LinePart) simulation_0.getPartManager().getObject("Line Probe"));

xyzInternalTable_0.getParts().setObjects(linePart_0);

// Open Plot for flame location

  ExpressionReport expressionReport_0 =

 simulation_0.getReportManager().createReport(ExpressionReport.class);

Units units_0 =

 simulation_0.getUnitsManager().getPreferredUnits(new IntVector(new int[] {0, 0, 0,
0, 0, 0, 0, 0, 0, 0, 0, 0, 0, 0, 0, 0, 0, 0, 0, 0, 0, 0, 0, 0, 0, 0, 0}));



expressionReport_0.setDefinition("${Current_Flame_Loc}");

simulation_0.getMonitorManager().createMonitorAndPlot(new NeoObjectVector(new
Object[] {expressionReport_0}), true, "%1$s Plot");

ReportMonitor reportMonitor_1 =

 ((ReportMonitor) simulation_0.getMonitorManager().getMonitor("Expression 1
Monitor"));
```

```
        MonitorPlot monitorPlot_1 =

          simulation_0.getPlotManager().createMonitorPlot(new NeoObjectVector(new
Object[] {reportMonitor_1}), "Expression 1 Monitor Plot");

        monitorPlot_1.open();

      // Open plot for inlet kinetic Energy

         ExpressionReport expressionReport_1 =

          simulation_0.getReportManager().createReport(ExpressionReport.class);

        Units units_1 =

          simulation_0.getUnitsManager().getPreferredUnits(new IntVector(new int[] {0, 0, 0,
0, 0, 0, 0, 0, 0, 0, 0, 0, 0, 0, 0, 0, 0, 0, 0, 0, 0, 0, 0, 0, 0, 0, 0}));

        expressionReport_1.setDefinition("${Turb_Kinetic_Energy}");



        simulation_0.getMonitorManager().createMonitorAndPlot(new NeoObjectVector(new
Object[] {expressionReport_1}), true, "%1$s Plot");

        ReportMonitor reportMonitor_2 =

          ((ReportMonitor) simulation_0.getMonitorManager().getMonitor("Expression 2
Monitor"));

        MonitorPlot monitorPlot_2 =
```

```
simulation_0.getPlotManager().createMonitorPlot(new NeoObjectVector(new
Object[] {reportMonitor_2}), "Expression 2 Monitor Plot");

monitorPlot_2.open();

// Control when flame passes goal location by diff_Loc_pass

double diff_Loc_pass;

while(Math.abs(diff_Loc) > 0.0000001 ){

// The 2500 steps changed to the 7500 4-15-2018

for(int iter_num = 0; iter_num < 10000; iter_num++){ // The number of
iteration to reach steady solution : iter_num

Time_control = Time_control + 0.005;

xyzInternalTable_0.extract();

xyzInternalTable_0.getTableDataItem(0, 0);

xyzInternalTable_0.export("D:\\Alireza Razeghi\\Combustion\\Temperature.csv", ",");

String csvFile = "D:\\Alireza Razeghi\\Combustion\\Temperature.csv";

BufferedReader br = null;

String line = "";

String cvsSplitBy = ",";

double numtoconv=0.0,cord=0.0;
```

```
try {
        br = new BufferedReader(new FileReader(csvFile));
        while ((line = br.readLine()) != null) {
           // use comma as separator
           String[] country = line.split(cvsSplitBy);
           //simulation_0.println("FIRST COL " + country[0] + "SECOND COL" + country[1] + "]"+ "THIRDD COL" + country[2] + "]");
     if(country[0].contains("1")||country[0].contains("2")||country[0].contains("3")||country[0].contains("4")||country[0].contains("5")||country[0].contains("6")||country[0].contains("7")||country[0].contains("8")||country[0].contains("9")||country[0].contains("0"))
           {
           numtoconv=Double.parseDouble(country[0]);
           cord=Double.parseDouble(country[2]);
             if(Math.abs((numtoconv-1400.0))<=20)
           {
            simulation_0.println("number = " + numtoconv+"cord = "+ cord );
            // Jump detection
            // if(Math.abs(Current_Flame_Loc-cord) > 0.05 && K!=1){
```

```
//                    Turb_Kinetic_Energy = 0.01154-
(0.01268*Goal_Flame_Loc)+(0.07911*Turb_Diss_Rate);

//
userFieldFunction_1.setDefinition(Double.toString(Turb_Kinetic_Energy));

//    iter_num = 0;

//     K = 1;

//}

// Passing Detection

if((Current_Flame_Loc-Goal_Flame_Loc)*(cord-Goal_Flame_Loc) < 0 &&
Time_control > 2.00){

 // The "(Math.abs(Current_Flame_Loc-cord)/0.01)" is used to adjust the
change beased on gradient of flame location

    diff_Loc_pass = (cord - Goal_Flame_Loc);

    Turb_Kinetic_Energy = (1+diff_Loc_pass)*Turb_Kinetic_Energy;


userFieldFunction_1.setDefinition(Double.toString(Turb_Kinetic_Energy));

    iter_num = 0;

    }

// Disable ignitor after 2 sec
```

```
            if(Time_control > 2.00){
            PhysicsContinuum physicsContinuum_0 =
              ((PhysicsContinuum) simulation_0.getContinuumManager().getContinuum("Physics
1"));
              FlameAreaDensityIgnitor flameAreaDensityIgnitor_0 =
               ((FlameAreaDensityIgnitor)
physicsContinuum_0.get(IgnitorManager.class).getIgnitor("FlameAreaDensityIgnitor 1"));
               flameAreaDensityIgnitor_0.getVolumeShapeGroup().setObjects();
        }
                    Current_Flame_Loc = cord;
                  }
                  }
                }
            } catch (FileNotFoundException e) {
              e.printStackTrace();
            } catch (IOException e) {
              e.printStackTrace();
            } finally {
```

```
            if (br != null) {
                try {
                    br.close();
                } catch (IOException e) {
                    e.printStackTrace();
                }
            }
        }
        //simulation_0.println("Hello");
        diff_Loc = (Current_Flame_Loc - Goal_Flame_Loc);
        //simulation_0.println("Desired Flame location is " + Goal_Flame_Loc);
        //simulation_0.println("Flame location is " + Current_Flame_Loc);
        //simulation_0.println("The difference is " + diff_Loc);
// Update the Current Flame location
        userFieldFunction_2.setDefinition(Double.toString(Current_Flame_Loc));
// Update the Tubulrnt Kinetic Energy & Turbulent Dissipation Rate
// Increase Turbulent Kinetic Energy to push Flame location towards inlet
```

```
//Turb_Diss_Rate = (1+diff_Loc)*Turb_Diss_Rate;

//userFieldFunction_0.setDefinition(Double.toString(Turb_Diss_Rate));

   simulation_0.println("+++++++++++++++++++++++++++++++++++++++++");

   simulation_0.println("Turbulent Kinetic Energy = " + Turb_Kinetic_Energy);

   simulation_0.println("Turbulent Diss Rate = " + Turb_Diss_Rate);

   simulation_0.println("+++++++++++++++++++++++++++++++++++++++++");

   // Start Update Temperature Table every time step

   // End Update Temperature Table every time step

   simulation_0.getSimulationIterator().step(1);

   diff_Loc = (Current_Flame_Loc - Goal_Flame_Loc);

   simulation_0.println("+++++++++++++++++++++++++++++++++++++++++");

   simulation_0.println("Goal Flame location is " + Goal_Flame_Loc);

   simulation_0.println("Current Flame location is " + Current_Flame_Loc);

   simulation_0.println("The difference is " + diff_Loc);

   simulation_0.println("+++++++++++++++++++++++++++++++++++++++++");

   //if(iter_num == 1){

     //  Turb_Kinetic_Energy = (1+diff_Loc)*Turb_Kinetic_Energy;
```

```
                //}

            }

            Turb_Kinetic_Energy = (1+0.2*diff_Loc)*Turb_Kinetic_Energy;


//+++++++++++++++++++++++++++++++++++++++++++++++++++++++++++++++++++++++++++++++++
+++++++++

            // Parameter to eliminate change in every time step

        //+++++++++++++++++++++++++++++++++++++++++++++++++++++++++++++++++++++++++++++
+++++++++++++++

            userFieldFunction_1.setDefinition(Double.toString(Turb_Kinetic_Energy));

            simulation_0.println("++++++++++++++++++++++++++++++++++++++++++");

            simulation_0.println("Turbulent Kinetic Energy = " + Turb_Kinetic_Energy);

            simulation_0.println("Turbulent Diss Rate = " + Turb_Diss_Rate);

            simulation_0.println("++++++++++++++++++++++++++++++++++++++++++");

        }
```

# REFERENCES


[1] S. R. Turns, *An Introduction To Combustion: Concepts and Applications*, Second edi. pennsylvania: Mcgraw-Hill series in mechanical engineering, 2000.

[2] K. K. Kuo, *Principles of combustion*, Secomd Edi. New York, United States: Wiley, 1986.

[3] A. Lipatnikov, *Fundamentals of Premixed Turbulent Combustion*. London, U.K: CRC Pres, 2012.

[4] Yu Shi and Rolf Reitz, *Modelling Diesel Combustion*. India: Springer Dordrecht Heidelberg London New York, 2010.

[5] C. G. Gatski, Thomas B., Sarkar, Sutanu, Speziale, *Studies in Turbulence*. New York: Springer-Verlag New York, 1992.

[6] A. R. Kerstein, "Turbulence in combustion processes: Modeling challenges," *Proc. Combust. Inst.*, vol. 29, no. 2, pp. 1763–1773, 2002.

[7] P. A. Durbin and And B. A. Pettersson Reif, *Statistical Theory and Modeling for Turbulent Flows*, Second Edi. A John Wiley and Sons.

[8] P. Bradshaw, *an itroduction to turbulence and its measurement*, First Edit. pergamon, 1985.

[9] N. Swaminathan and K. N. C. Bray, *Turbulent premixed flames*, Cambridge. cambridge , London: cambridge university press, 2011.

[10] N. Peters, *turbulent combustion*, Second edi. Cambridge, U.K: Cambridge University, 2004.

[11] D. Dunn-Rankin, *Lean Combustion Technology and control*, Second Edi. Irvine, USA: Elsevier, Inc. All, 2011.

[12] S. S. Rashwan, M. A. Nemitallah, and M. A. Habib, "Review on premixed combustion technology : Stability , emission control , applications and numerical case study Review on premixed combustion technology : Stability , emission control , applications and numerical case study," *Energy & Fuels*, vol. 30, no. 12, pp. 9981–10014, 2016.

[13] C. T. Eichler, "Flame Flashback in Wall Boundary Layers of Premixed Combustion Systems," Münih Teknik Üniversitesi, Germany, 2011.

[14] M. S. Mansour *et al.*, "Effect of the mixing fields on the stability and structure of turbulent partially premixed flames in a concentric flow conical nozzle burner," *Combust. Flame*, vol. 175, pp. 180–200, 2017.

[15] J. G. Strahman, "Flame stability of an ultra-lean premixed low-swirl burner," Carleton University, Ottawa, Ontario, Canada, 2007.

[16] T. Poinsot and D. Veynante, *Theoretical and Numerical Combustion*, Second edi., vol. second edi. Edwards, 2005.

[17] D. Veynante and L. Vervisch, "Turbulent combustion modeling," *Prog. Energy Combust. Sci.*, vol. 28, no. 3, pp. 193–266, 2002.

[18] R. Borghi, "Turbulent combustion modelling," *Prog. Energy Combust.*, vol. 14, pp. 245–292, 1989.

[19] R. G. Abdel-Gayed Derek Bradley F. K.- K. Lung, "Combustion Regimes and the Straining of Turbulent Premixed Flames," *Combust. Flame*, vol. 76, pp. 213–218, 1989.

[20] N. Peters, “Length and time scales in turbulent combustion,” *Turbul. React. flows*, pp. 242–256, 1989.

[21] Ö. L. Gülder, “Turbulent premixed flame propagation models for different combustion regimes,” *Symp. Combust.*, vol. 23, no. 1, pp. 743–750, 1991.

[22] T. Poinsot, D. Veynante, and S. Candel, “Diagrams of premixed turbulent combustion based on direct simulation,” *Symp. Combust.*, vol. 23, no. 1, pp. 613–619, 1991.

[23] E. Tangermann, R. Keppeler, and M. Pfitzner, “Premixed turbulent combustion models for large eddy and RANS simulations,” *Proc. ASME Turbo Expo 2010 Power Land, Sea Air*, 2010.

[24] V. Sankaran and S. Menon, “Structure of premixed turbulent flames in the thin- reaction-zones regime,” *Proc. Combust. Inst.*, vol. 28, no. 1, pp. 203–209, 2000.

[25] P. Clavin and G. Joulin, “Premixed flames in large scale and high intensity turbulent flow,” *J. Phys. Lettres*, vol. 44, no. 1, pp. 1–12, 1983.

[26] R. C. Aldredge and F. a. Williams, “Influence of wrinkled premixed-flame dynamics on large-scale, low-intensity turbulent flow,” *J. Fluid Mech. Digit. Arch.*, vol. 228, pp. 487–511, 1991.

[27] S. Zhang and C. J. Rutland, “Premixed flame effects on turbulence and pressure-related terms,” *Combust. Flame*, vol. 102, no. 4, pp. 447–461, 1995.

[28] E. Giacomazzi, V. Battaglia, and C. Bruno, “The coupling of turbulence and chemistry in a premixed bluff-body flame as studied by LES,” *Combust. Flame*, vol. 138, no. 4, pp. 320–335, 2004.

[29] J. Yuan, Y. Ju, and C. K. Law, “Effects of turbulence and flame instability on flame front evolution,” *Phys. Fluids*, vol. 18, no. 10, pp. 1–9, 2006.

[30] B. H. Y. Tang and C. K. Chan, “Simulation of flame surface density and burning rate of a premixed turbulent flame using contour advection,” *Combust. Flame*, vol. 147, pp. 49–66, 2006.

[31] Ö. Gülder and G. Smallwood, “Flame Surface Densities in Premixed Combustion At Medium To High Turbulence Intensities,” *Combust. Sci. Technol.*, vol. 179, no. 1–2, pp. 191–206, 2007.

[32] I. Han and K. Y. Huh, “Roles of displacement speed on evolution of flame surface density for different turbulent intensities and Lewis numbers in turbulent premixed combustion,” *Combust. Flame*, vol. 152, no. 1–2, pp. 194–205, 2008.

[33] G. Hartung, J. Hult, C. F. Kaminski, J. W. Rogerson, and N. Swaminathan, “Effect of heat release on turbulence and scalar-turbulence interaction in premixed combustion,” *Phys. Fluids*, vol. 20, no. 3, pp. 1–16, 2008.

[34] A. N. Lipatnikov and J. Chomiak, “Effects of premixed flames on turbulence and turbulent scalar transport,” *Prog. Energy Combust. Sci.*, vol. 36, no. 1, pp. 1–102, 2010.

[35] G. Fru, D. Thévenin, and G. Janiga, “Impact of turbulence intensity and equivalence ratio on the burning rate of premixed methane-air flames,” *Energies*, vol. 4, no. 6, pp. 878–893, 2011.

[36] Y. Minamoto, N. Fukushima, M. Tanahashi, T. Miyauchi, T. D. Dunstan, and N. Swaminathan, “Effect of flow-geometry on turbulence-scalar interaction in premixed

flames," *Phys. Fluids*, vol. 23, no. 12, pp. 2–12, 2011.

[37] A. Y. Poludnenko and E. S. Oran, "The interaction of high-speed turbulence with flames: Turbulent flame speed," *Combust. Flame*, vol. 158, no. 2, pp. 301–326, 2011.

[38] P. E. Hamlington, A. Y. Poludnenko, and E. S. Oran, "Interactions between turbulence and flames in premixed reacting flows," *Phys. Fluids*, vol. 23, no. 12, 2011.

[39] M. Matalon and F. Creta, "The 'turbulent flame speed' of wrinkled premixed flames," *Comptes Rendus Mec.*, vol. 340, no. 11–12, pp. 845–858, 2012.

[40] A. M. Steinberg, J. F. Driscoll, and N. Swaminathan, "Statistics and dynamics of turbulence-flame alignment in premixed combustion," *Combust. Flame*, vol. 159, no. 8, pp. 2576–2588, 2012.

[41] S. Chaudhuri, A. Saha, and C. K. Law, "On flame-turbulence interaction in constant-pressure expanding flames," *Proc. Combust. Inst.*, vol. 35, no. 2, pp. 1331–1339, 2014.

[42] A. Bagdanavicius, P. J. Bowen, D. Bradley, M. Lawes, and M. S. Mansour, "Stretch rate effects and flame surface densities in premixed turbulent combustion up to 1 . 25 MPa," *Combust. Flame*, vol. 162, no. 11, pp. 4158–4166, 2015.

[43] A. J. Aspden, M. S. Day, and J. B. Bell, "Turbulence-chemistry interaction in lean premixed hydrogen combustion," *Proc. Combust. Inst.*, vol. 35, no. 2, pp. 1321–1329, 2015.

[44] J. Kerl, C. Lawn, and F. Beyrau, "Three-dimensional flame displacement speed and flame front curvature measurements using quad-plane PIV," *Combust. Flame*, vol. 160, no. 12, pp. 2757–2769, 2013.

[45] J. P. Mcgarry and K. A. Ahmed, “Flame – turbulence interaction of laminar premixed deflagrated flames,” *Combust. Flame*, vol. 176, pp. 439–450, 2017.

[46] Z. Wang and J. Abraham, “Effects of Karlovitz number on flame surface wrinkling in turbulent lean premixed methane-air flames,” *Combust. Sci. Technol.*, vol. 190, no. 3, pp. 362–391, 2018.

[47] E. E. S. and A. S. S. A. I. Krikunova, “Premixed conical flame stabilization,” in *International Conference on Equations of State for Matter*, 2016, pp. 1–6.

[48] S. A. Filatyev, J. F. Driscoll, C. D. Carter, and J. M. Donbar, “Measured properties of turbulent premixed flames for model assessment , including burning velocities , stretch rates , and surface densities,” *Combust. Flame*, vol. 141, no. 1–12, pp. 1–21, 2005.

[49] S. Pfadler, A. Leipertz, and F. Dinkelacker, “Systematic experiments on turbulent premixed Bunsen flames including turbulent flux measurements,” *Combust. Flame*, vol. 152, no. 4, pp. 616–631, 2008.

[50] P. Tamadonfar and Ö. L. Gülder, “Effect of burner diameter on the burning velocity of premixed turbulent flames stabilized on Bunsen-type burners,” *Exp. Therm. Fluid Sci.*, vol. 73, pp. 42–48, 2016.

[51] S. Boukebbab, “The turbulence effect on a lean premixed methane-air flame in a Bunsen burner,” *WIT Trans. Ecol. Environ.*, vol. 186, no. 2014, pp. 719–727, 2014.

[52] J. B. Bell, R. K. Cheng, M. S. Day, J. F. Grcar, and V. E. Beckner, “Numerical Simulation of a Laboratory-Scale Turbulent V-Flame,” *pnas*, vol. 102, no. 29, pp. 10006–10011, 2005.

[53] S. and Ö. L. G. Kheirkhah, "Turbulent premixed combustion in V-shaped flames :Characteristics of flame front," *Phys. Fluids*, vol. 25, no. 5, pp. 1–23, 2013.

[54] C. B. D. D. Dovizio, A. Debbagh, "RANS Simulations of a Series of Turbulent V-Shaped Flames using Conditional Source-term Estimation," *Flow, Turbul. Combust.*, vol. 96, no. 4, pp. 891–919, 2016.

[55] R K. Cheng, "Velocity and Scalar Characteristics of Premixed Turbulent Flames Stabilized by Weak Swirl," *Combust. Flame*, vol. 101, pp. 1–14, 1995.

[56] S. S. Sattler, D. A. Knaus, and F. C. Gouldin, "Determination Of Three-Dimensional Flamelet Orientation Distributions In Turbulent V-Flames From Two-Dimensional Image Data," *Proc. Combust. Inst.*, vol. 29, no. 2, pp. 1785–1792, 2002.

[57] J. H. Frank, P. A. M. Kalt, and R. W. Bilger, "Measurements of Conditional Velocities in Turbulent Premixed Flames by Simultaneous OH PLIF and PIV," *Combust. Flame*, vol. 116, no. 1–2, pp. 220–232, 1999.

[58] A. Soika, F. Dinkelacker, and A. Leipertz, "Measurement Of The Resolved Flame Structure Of Turbulent Premixed Flames With Constant Reynolds Number And Varied Stoichiometry," in *Twenty-Seventh Symposium (International) on Combustion/The Combustion Institute*, 1998, pp. 785–792.

[59] D. Most, F. Dinkelacker, and A. Leipertz, "Lifted Reaction Zones In Premixed Turbulent Bluff-Body Stabilized Flames," *Proc. Combust. Inst.*, vol. 29, no. 2, pp. 1801–1808, 2002.

[60] B. Coriton, J. H. Frank, and A. Gomez, "Effects of strain rate, turbulence, reactant stoichiometry and heat losses on the interaction of turbulent premixed flames with

stoichiometric counterflowing combustion products," *Combust. Flame*, vol. 160, no. 11, pp. 2442–2456, 2013.

[61] D. Luff, E. Korusoy, P. Lindstedt, and J. H. Whitelaw, "Counterflow flames of air and methane , propane and ethylene , with and without periodic forcing," *Exp.*, vol. 35, pp. 618–626, 2003.

[62] E. Yasari, S. Verma, and a. N. Lipatnikov, "RANS Simulations of Statistically Stationary Premixed Turbulent Combustion Using Flame Speed Closure Model," *Flow, Turbul. Combust.*, vol. 94, no. 2, pp. 381–414, 2014.

[63] L. W. Kostiuk, K. N. C. Bray, and T. C. Chew, "Premixed Turbulent Combustion In Counterflowing Streams," *Combust. Sci. Technol.*, vol. 64, pp. 233–241, 1989.

[64] P. Moreau, "Turbulent Flame Development in a High Velocity Premixed Flow," in *American Institute of Aeronautics and Astronautics, Aerospace Sciences Meeting,* 1977.

[65] A. Guessab, A. Aris, M. Cheikh, and T. Baki, "Combustion of Methane and Biogas Fuels in Gas Turbine Can-type Combustor Model," vol. 9, no. 5, pp. 2229–2238, 2016.

[66] A. Yoshida, *Smart Control of Turbulent Combustion*. Tokyo Denki University,Tohyo, Japan: springer, 2001.

[67] N. Docquier and S. Candel, "Combustion control and sensors: A review," *Prog. Energy Combust. Sci.*, vol. 28, no. 2, pp. 107–150, 2002.

[68] M. Gad-el-Hak, *Flow control: passive, active, and reactive flow management*, vol. 37, no. 2. 2000.

[69] L. Cai and H. Pitsch, *Active Flow and Combustion Control*. london: Springer International Publishing Switzerland, 2015.

[70] C. E. Johnson, "Adaptive Control of Combustion Instabilities Using Real-Time Modes Observation Adaptive Control of Combustion Instabilities Using Real-Time Modes Observation," Georgia Institute of Technology, 2006.

[71] M. a Richard, O. W. Bynum, D. R. Sheridan, P. H. Mark, G. Morrison, and L. T. Brewer, "Sensor Technology for Advanced Combustion Control and Monitoring Instrumentation," no. 1, pp. 1155–1158, 1992.

[72] X. Zhou, X. Liu, J. B. Jeffries, and R. K. Hanson, "Development of a sensor for temperature and water concentration in combustion gases using a single tunable diode laser," *Meas. Sci. Technol.*, vol. 14, pp. 1459–1468, 2003.

[73] M. Annaswamy and a F. Ghoniem, "Active control of combustion instability: Theory and practice," *IEEE Control Syst. Mag.*, vol. 22, no. 6, pp. 37–54, 2002.

[74] D. Bhattacharjee, "Experimental Studies of Active Combustion Control," vol. 3, no. 6, pp. 629–634, 2013.

[75] C. Seywert, G. Isella, and F. E. C. Culick, "Active Feedback Control of Combustor Dynamics with Time Delay and Noise," *AIAA/ASME/SAE/ASEE Jt. Propuls. Conf. Exhib.*, vol. 36, no. May, p. 10, 2000.

[76] A. Coker, Y. Neumeier, T. Lieuwen, B. T. Zinn, and S. Menon, "Studies of Active Instability Control Effectiveness in a High Pressure , Liquid Fueled Combustor," in *41st AIAA Aerospace Sciences Meeting and Exhibit 6-9 January 2003 Reno, NV*, 2003, no.

AIAA-1009.

[77] A. Banaszuk, K. B. Ariyur, M. Krstić, and C. a. Jacobson, “An adaptive algorithm for control of combustion instability,” *Automatica*, vol. 40, no. 11, pp. 1965–1972, 2004.

[78] T. Yi and E. J. Gutmark, “Dynamics of a High-Frequency Fuel Actuator and its Applications for Combustion Instability Control,” *J. Eng. Gas Turbines Power*, vol. 129, no. 3, p. 648, 2007.

[79] J. B. Bell, M. S. Day, J. F. Grcar, and M. J. Lijewski, “Active Control for Statistically Stationary Turbulent Premixed Flame Simulations,” *Commun. Appl. Math. Comput. Sci.*, vol. 1, no. 1, pp. 29–51, 2006.

[80] A. L. Birbaud, S. Ducruix, D. Durox, and S. Candel, “The nonlinear response of inverted ‘ V ’ flames to equivalence ratio nonuniformities,” *Combust. Flame*, vol. 154, pp. 356–367, 2008.

[81] S. H. and T. L. Shreekrishna, “Premixed flame response to equivalence ratio perturbations,” *Combust. Theory Model.*, vol. 14, no. 5, pp. 681–714, 2010.

[82] V. L. Zimont, W. Polifke, M. Bettelini, and W. Weisenstein, “An Efficient Computational Model for Premixed Turbulent Combustion at High Reynolds Numbers Based on a Turbulent Flame Speed Closure,” *J. Gas Turbines Power*, vol. 120, no. 3, pp. 526–532, 1998.

[83] M. L. Hack, “Joint Probability Density Function PDF Closure of Turbulent Premixed Flames,” Eth Zurich, 2011.

[84] T. E. Break, U. Model, P. Combustion, and F. R. Further, “Eddy break - up model for

combustion," pp. 12–15, 2016.

[85] Marble and Broadwell, "Coherent Flame Model for Turbulent chemical Reactions," Purdue Unversity, Indiana, USA, 1977.

[86] S. B. Pope, "computations of turblent combustion: progress and challenges," in *Twenty-Third Symposium (International) on Combustion/The Combustion Institute*, 1990, pp. 591–612.

[87] R. Prosser and R. S. Cant, "Turbulent Combustion Modeling," *Fluid Mech. its Appl.*, vol. 95, pp. 331–351, 2011.

[88] G. M. &J. B. M. K. N. C. Bray, Paul A. Libby, "Turbulence Production in Premixed Turbulent Flames," *Combust. Sci. Technol.*, vol. 25, no. 3–4, pp. 127–140, 1981.

[89] P. A. L. and J. B. M. C. Bray, K N C, "Unified Modeling Approach for Premixed Turbulent CombustionmPart I : General Formulation," *Combust. Flame*, vol. 61, pp. 87–102, 1985.

[90] K. N. C. Bray and J. B. Moss, "A unified statistical model of the premixed turbulent flame," *Acta Astronaut.*, vol. 4, no. 3–4, pp. 291–319, 1977.

[91] K. N. C. BRAY, "Studies of the turbulent burning velocity," *Math. Phys. Sci.*, vol. 431, no. 1882, pp. 315–335, 1990.

[92] B. Y. D. Bradley, A. K. C. Lau, and M. Lawes, "Flame stretch rate as a determinant of turbulent burning velocity," in *Mathematical , Physical and Engineering Sciences*, 1992, no. 13, pp. 359–387.

[93] W. Polifke, P. Flohr, and M. Brandt, “Modeling of Inhomogeneously Premixed Combustion With an Extended TFC Model,” *J. Eng. Gas Turbines Power*, vol. 124, no. 1, p. 58, 2002.

[94] V. L. Zimont, “Gas premixed combustion at high turbulence. Turbulent flame closure combustion model,” *Exp. Therm. Fluid Sci.*, vol. 21, no. 1–3, pp. 179–186, 2000.

[95] V. L. and A. N. L. Zimont, “A numerical model of premixed turbulent combustion of gases,” *Chem. Phys. Reports*, vol. 14, no. 7, pp. 993–1025, 1995.

[96] D. B. Spalding, “Mixing And Chemical Reaction In Steady Confined Turbulent Flames,” *Symp. Combust.*, vol. 13, no. 1, pp. 649–657, 1971.

[97] R. Said and R. Borghi, “A Simulation With A ‘Cellular Automaton’ For Turbulent Combustion Modelling,” *Twenty-Second Symp. Combust. Combust. Inst.*, vol. 22, no. 1, pp. 569–577, 1988.

[98] S. I. Möller E. Lundgren C. Fureby, “Large eddy simulation of unsteady combustion ¨,” in *Twenty-Sixth Symposium (International) on Combustion/The Combustion Institute*, 1996, pp. 241–248.

[99] W. Kim, J. J. Lienau, R. E. Malecki, and R. E. M. and S. S. Slooten, Paul R Van, Meredith B. Colket, “Towards Modeling Lean Blow Out In Gas Turbine Flameholder Applications,” *J. Eng. Gas Turbines Power*, vol. 128, no. 1, pp. 40–48, 2004.

[100] A. W. Cook and J. J. Riley, “A subgrid model for equilibrium chemistry in turbulent flows,” *Phys. Fluids*, vol. 6, no. 28, pp. 2868–2870, 1994.

[101] S. B. Pope, “PDF methods for turbulent reactive flows,” *progess Energy Combust.*, vol.

11, pp. 119–192, 1985.

[102] P. Givi, “Model-free simulations of turbulent reactive flows,” *progess Energy Combust.*, vol. 15, pp. 1–107, 1989.

[103] A. W. Cook, J. J. Riley, and G. K. O. S. Y, “A laminar flamelet approach to subgrid-scale chemistry in turbulent flows,” *Combust. Flame*, vol. 109, no. 3, pp. 332–341, 1997.

[104] Andrew W. Cook And James J. Riley, “Subgrid-Scale Modeling for Turbulent Reacting Flows,” *Combust. Flame*, vol. 112, pp. 593–606, 1998.

[105] A. Trouve and T. Poinsot, “The evolution equation for the flame surface density in turbulent premixed combustion,” *J. Fluid Mech.*, vol. 278, pp. 1–31, 1994.

[106] S. A. Pope, “the evolution of surface in turbulence,” *Int. J. Eng. Sci.*, vol. 26, no. 5, pp. 445–469, 1988.

[107] E. M. and S. M. C. D. Veynante, F. Lacas, “Coherent flame model for non-uniformly premixed turbulent flames,” in *Turbulent Shear Flows 7*, Stanford, USA: Springer-Verlag Berlin Heidelberg, 1993, pp. 367–379.

[108] A. Trouv and T. Poinsot, “evolution in equation turbulent for the flame surface density in turbulent premixed combustion premixed,” *J. Fluid Mech.*, vol. 278, pp. 1–13, 1994.

[109] J. M. Duclos, D. Veynante, and T. Poinsot, “A Comparison of Flamelet Models for Premixed Turbulent Combustion,” *Combust. Flame*, vol. 95, pp. 101–117, 1993.

[110] R. O. S. Prasad and J. P. Gore, “An Evaluation of Flame Surface Density Models for Turbulent Premixed Jet Flames,” *Combust. Flame*, vol. 116, pp. 1–14, 1999.

[111] C. De Recherche and C. Turbulente, “Direct Numerical simulations Analyis of Flame Surface Density Concept For Large Eddy simulation Of Turbulent,” *Twenty-Seventh Symp. Combust. Combust. Inst.*, vol. 27, no. 1, pp. 917–925, 1998.

[112] S. Candel, D. Veynante, and F. Lacas, “Coherent Flamelet Model : Applications And Recent Extensions,” *Recent Adv. Combust. Model.*, vol. 6, pp. 19–64, 1990.

[113] C. R. Choi and K. Y. Huh, “Development of a Coherent Flamelet Model for a Spark-Ignited Turbulent Premixed Flame in a Closed Vessel,” *Combust. Flame*, vol. 114, no. 3–4, pp. 336–348, 1998.

[114] B. Deschamps, A. Boukhalfa, C. Chauveau, and I. Gokalp, “An Experimental Estimation Of Flame Surface Density And Mean Reaction Rate In Turbulent Premixed Flames,” *Twenty-Fourth Symp. Combust. Combust. Institute,* vol. 24, no. 1, pp. 469–475, 1992.

[115] M. Zhang, J. Wang, W. Jin, Z. Huang, H. Kobayashi, and L. Ma, “Estimation of 3D flame surface density and global fuel consumption rate from 2D PLIF images of turbulent premixed flame,” *Combust. Flame*, vol. 162, no. 5, pp. 2087–2097, 2015.

[116] U. Ahmed and R. Prosser, “Modelling flame turbulence interaction in RANS simulation of premixed turbulent combustion,” *Combust. Theory Model.*, vol. 20, no. 34–57, 2016.

[117] B. E. Launder, G. J. Reece, and W. Rodi, “Progress in the development of a Reynolds-stress turbulence closure,” *J. Fluid Mech.*, vol. 68, no. 3, pp. 537–566, 1975.

[118] W. Rodi, “Experience Wlth Two-Layer Models Combining The K-E Model Wlth A One-Equation Model Near The Wall,” in *29th Aerospace Sciences Meeting*, 1991.

[119] J. E. Bardina, M. Field, P. G. Huang, T. J. Coakley, M. Field, and N. Aeronautics,

*Turbulence Modeling Validation , Testing , and Development*. Ames Research Center; Moffett Field, CA United States: National Aeronautics and Space Administration, 1997.

[120] D. C. Haworth and S. B. Pope, "Turbulent Combustion Modeling," vol. 95, pp. 38–53, 2011.

[121] D. C. Wilcox, *Turbulence_modeling for CFD*, Sesond Edi. california, 1994.

[122] V. Yakhot and S. A. Orszag, "Renormalization-Group Analysis of Turbulence," vol. 57, no. 14, pp. 0–2, 1986.

[123] V. Yakhot and L. M. Smith, "The Renormalization Group , the e-Expansion and Derivation of Turbulence Models," *J. Sci. Comput.*, vol. 7, no. l, pp. 35–61, 1992.

[124] J. Smagorinsky, "General Circulation Experiments With the Primitive Equations," *Mon. Weather Rev.*, vol. 91, no. 3, pp. 99–164, 1963.

[125] K. K. Kuo and R. Acharya, *Fundamentals of Turbulent Multi-Phase Combustion*. Hoboken, New Jersey, Canada: John Wiley & Sons, 2012.

[126] M. F. Modest and D. C. Haworth, *Radiative Heat Transfer in Turbulent Combustion Systems Theory and Applications*. Minneapolis, Minnesota, USA: SpringerBriefs in Applied Sciences and Technology, 216AD.

[127] M. F. M. S. Mazumder, "Turbulence-Radiation Interactions in Nonreactive Flow of Combustion Gases," *J. heat Treans.*, vol. 121, no. 726–729, 1999.

[128] P.J. Foster, "Relation of time-mean transmission of turbulent flames to optical depth," *J. Inst. Fuel*, vol. 340, no. 13, p. 179, 1969.

[129] S. W. W. Krebs, R. Koch, H.J. Bauer, R. Kneer, “Effect of turbulence on radiative heat transfer inside a model combustor,” in *Proceedings of Eurotherm Seminar No. 37—Heat Transfer in Radiating and Combusting Systems*, 1994, vol. 2, pp. 349–362.

[130] S. J. Fischer, B. I. N. I. D. Hardouin-duparc, and W. L. Grosshandler, “The Structure and Radiation of an Ethanol Pool Fire,” *Combust. Flame*, vol. 70, no. 3, pp. 291–306, 1987.

[131] S. Jeng, M. Lai, and G. M. Faeth, “Nonluminous Radiation in Turbulent Buoyant Axisymmetric Flames Nonluminous Radiation in Turbulent Buoyant,” *Combust. Sci. Technol. ISSN*, vol. 40, pp. 41–53, 1984.

[132] J. P. Gore, S. Jeng, and G. M. Faethj, “Spectral and Total Radiation Properties of Turbulent Carbon Monoxide / Air Diffusion Flames,” *AIAA J.*, vol. 25, no. 2, pp. 339–345, 1987.

[133] G. Li and M. F. Modest, “Importance of Turbulence-Radiation Interactions in Turbulent Diffusion Jet Flames,” *J. Heat Transfer*, vol. 125, no. 5, p. 831, 2003.

[134] J. P. Gore and G. M. Faeth, “Spectral and Total Radiation Properties of Turbulent Hydrogen / Air Diffusion Flames,” *J. Heat Transf*, vol. 109, pp. 165–171, 1978.

[135] P. J. Ã. Coelho, “Numerical simulation of the interaction between turbulence and radiation in reactive flows,” *Prog. Energy Combust. Sci. 33*, vol. 33, pp. 311–383, 2007.

[136] P. J. Coelho, O. J. Teerling, and D. Roekaerts, “Spectral radiative effects and turbulence/radiation interaction in a non-luminous turbulent jet diffusion flame,” *Combust. Flame*, vol. 133, no. 1–2, pp. 75–91, 2003.

[137] P. J. Coelho, “Detailed numerical simulation of radiative transfer in a nonluminous

turbulent jet diffusion flame," *Combust. Flame*, vol. 136, no. 4, pp. 481–492, 2004.

[138] R. S. Yuan Zheng, Barlow and J. P. Gore, "Spectral Radiation Properties of Partially Premixed Turbulent Flames," *J. Heat Transfer*, vol. 125, pp. 1065–1073, 2003.

[139] J. P. Yuan Zheng, Gore and M. J. Z. Laboratories, "Measurements and Calculations of Spectral Radiation Intensities for Turbulent Non-Premixed and Partially Premixed Flames," *J. Heat Transfer*, vol. 125, 2003.

[140] A. Wang, M. F. M. Ã, D. C. Haworth, and L. Wang, "Monte Carlo simulation of radiative heat transfer and turbulence interactions in methane / air jet flames," *J. Quant. Spectrosc. Radiat. Transf.*, vol. 109, no. 2, pp. 269–279, 2008.

[141] Y. Yunardi, D. Darmadi, H. Hisbullah, and M. Fairweather, "Predictions of Soot Formation in Turbulent Propane Non-Premixed Flames With and Without Air Preheat," pp. 1–5, 2011.

[142] I. Kennedy, "Models of soot formation a n d oxidation," *Prog. Energy Combust. Sci.*, vol. 23, no. 2, pp. 95–132, 1997.

[143] H. G. G. Wagner, "SOOT FORMATION IN COMBUSTION," *Symp. Combust.*, vol. 17, no. 1, pp. 3–19, 1979.

[144] Ranjan S. Mehta, "Detailed Modeling of Soot Formation and Turbulence – Radiation Interactions in Turbulent Jet Flames," Pennsylvania State University, 2008.

[145] R. J. Santoro and H. G. Semerjian, "Soot Formation in diffusions Flames : Flow Rate , Fuel Species and Temperature Effects," in *Twentieth Symposium (International) on Combustion/The Combustion Institute*, 1984, pp. 997–1006.

[146] A. Ciajolo, A. D. Anna, R. Barbella, A. Tregrossi, A. Violi, and I. R. Combustione, "The Effect of Temperature on Soot Inception in Premixed Ethylene Flames," in *Twenty-Sixth Symposium (International) on Combustion/The Combustion Institute*, 1996, pp. 2327–2333.

[147] F. Mauss, B. Trilken, and H. Breitbach, "Soot Formation in Partially Premixed Diffusion Flames at Atmospheric Pressure," in *Soot Formation in Combustion*, 1994, pp. 325–349.

[148] R. S. Mehta, M. F. Modest, and D. C. Haworth, "Radiation characteristics and turbulence-radiation interactions in sooting turbulent jet flames," *Combust. Theory Model.*, vol. 14, no. 1, pp. 105–124, 2010.

[149] M. R. Busupally and A. De, "Numerical modeling of Soot formation in a turbulent C2H4/air diffusion flame," *Int. J. Spray Combust. Dyn.*, vol. 8, no. 2, pp. 67–85, 2016.

[150] M. Sirignano, J. Kent, and A. D. Anna, "Modeling Formation and Oxidation of Soot in Nonpremixed Flames," 2013.

[151] A. Kronenburg, R. W. Bilger, and J. H. Kent, "Modeling Soot Formation in Turbulent Methane – Air Jet Diffusion Flames," *Combust. Flame*, vol. 121, no. 2, pp. 21–24, 2000.

[152] L. F. Richardson, *Weather Prediction by Numerical Process*. cambridge , London: Cambridge University Press, 1922.

[153] N. Peters, "Multiscale combustion and turbulence," *Proc. Combust. Inst.*, vol. 32, no. 1, pp. 1–25, 2009.

[154] L. Mydlarski and Z. Warhaft, "On the onset of high-Reynolds number grid-generated wind tunnel turbulence," *J. Fluid Mech.*, vol. 320, pp. 331–368, 1996.

[155] L. Mydlarski and Z. Warhaft, “Passive scalar statistics in high-Peclet-number grid turbulence,” *J. Fluid Mech.*, vol. 358, pp. 135–175, 1998.

[156] N. Peters, “Length Scales in Laminar and Turbulent Flames,” in *Turbulent Reactive Flows*, 1991, pp. 155–182.

[157] J. G. Gens, F. Mauss, and N. Peters, “Analytic Approximations of Burning Velocities and Flame Thicknesses of Lean Hydrogen, Methane, Ethylene, Ethane, Acetylene, and Propane Flames,” in *Twenty-Fourth Symposium (International) on Combustion/The Combustion Institute*, 1992, pp. 129–135.

[158] G. J. Gibbs And H. F. Calcote, “Effect of Molecular Structure on Burning Velocity,” *J. Chem. Eng. Data*, vol. 4, no. 3, pp. 226–237, 1959.

[159] G. E. Andrews and D. Bradley, “Determination of Burning Velocities : A Critical Review,” *Combust. Flame*, vol. 18, no. 1, pp. 133–153, 1972.

[160] I. Glassman and R. A. Yetter, *Combustion*, Fourth edi. London: Elsevier Inc., 2008.

[161] M. Metghalchi and J. C. Keck, “Burning Velocities of Mixtures of Air with Methanol , Isooctane , and Indolene at High Pressure and Temperature,” *Combust. Flame*, vol. 48, pp. 191–210, 1982.

[162] J. Sellmann, J. Lai, and A. M. Kempf, “Flame surface density based modelling of head-on quenching of turbulent premixed flames,” *Proc. Combust. Inst.*, vol. 36, no. 2, pp. 1817–1825, 2016.

[163] T. Echekki and E. Mastorakos, *Turbulent Combustion Modeling*. London New York: Springer-Verlag Berlin Heidelberg, 2011.

[164] F. M. Series, “Equations des gaz turbulents compressibles,” *j. de. Mec.*, vol. 4, no. 361, 1956.

[165] M. Katragadda, “Development of Flame Surface Density Closure for Turbulent Premixed Flames Based on A Priori Analysis of Direct Numerical Simulation Data,” Newcastle University, 2013.

[166] M. M. Kamal *et al.*, “Favre- and Reynolds-averaged velocity measurements : interpreting PIV and LDA measurements in combustion,” *Proc. Combust. Inst.*, vol. 35, no. 3, pp. 3803–3811, 2015.

[167] C. Chen, J. J. Riley, and P. A. Mcmurtry, “A Study of Favre Averaging in Turbulent Flows with Chemical Reaction,” *Combust. Flame*, vol. 87, no. 3–4, pp. 257–277, 1991.

[168] C. Meneveau and T. Poinsot, “Stretching and quenching of flamelets in premixed turbulent combustion,” *Combust. Flame*, vol. 86, no. 4, pp. 311–332, 1991.

[169] S. C. CD-adapco, *documentation and user guide*. Melville, USA: Version 11.02.009-R8, 2016.

[170] S. B. Pope, *Turbulent Flows*, First edit. London: Cornell University, New York, 2000.

[171] H. K. V. and W. Malalasekera, *Introduction to Computational Fluid Dynamics*, Second Edi. Harlow, UK: Pearson Education Limited, 1995.

[172] I. T. Nazzal and Ö. Ertunc, “Effects of turbulence intensity and length scale on the flame location of premixed turbulent combustion in a diffuser combustor,” *J. Therm. Sci. Technol.*, vol. 12, no. 2, p. JTST0029, 2017.

[173] N. Chakraborty and R. S. Cant, “Effects of strain rate and curvature on surface density function transport in turbulent premixed flames in the thin reaction zones regime,” *Phys. Fluids*, vol. 17, no. 6, pp. 1–15, 2005.

[174] B. Cabral and L. C. Leedom, “Imaging Vector Fields Using Line Integral Convolution,” in *Proceedings of the 20st Annual Conference on Computer Graphics and Interactive Techniques, SIGGRAPH 102*, 1993, pp. 263–270.

[175] Ibrahim Thamer Nazzal and Özgür Ertunc, “Numerical investigation of the flame location of turbulent premixed combustion in a diffuser burner exposed to various turbulence intensities and turbulence length scales,” *Isı Bilim. ve Tek. Dergisi, J. Therm. Sci. Technol.*, vol. 38, no. 1, pp. 55–64, 2018.

# VITA

Ibrahim Thamer Nazzal was born in Iraq. He joined to Tikrit University in Tikrit, Iraq in 1997. He received his bachelor and M.SC in Mechanical engineering department from Tikrit University, Tikrit, Iraq in 2001 and 2004 respectively. In February 2013, he jointed to Ozyegin University in Istanbul, Turkey. He started with English Preparatory School in Ozyegin University. In February 2014, he joined to study Ph.D. in Mechanical Engineering Department, Graduate School of Engineering and Science with Assistant Professor Özgür Ertunç at the Ozyegin University, Istanbul, Turkey.

His previous research interests included rotary heat exchanger and alternative fuel of internal combustion engines. His current research interests include turbulence and flame interaction for the flame location control in diffuser combustor. He published two journal and one-conference papers and two journal papers are pending as shown below:

| No | Paper title | Paper status | Journal name | Data |
|---|---|---|---|---|
| 1. | Diffuser combustor to study the ınfluence of turbulence on turbulent lean premixed flame. | *Published* | 6th International conference on Renewable , Fuel Combustion and Fire. | 2017 |
| 2. | Effects of turbulence intensity and length scale on the flame location of premixed turbulent | *Published* | *Journal of Thermal Science and Technology*, vol. 12, | 2017 |

| | | | | |
|---|---|---|---|---|
| | combustion in a diffuser combustor | | no. 2, p. JTST0029. | |
| 3. | Numerical ınvestigation of the flame location of turbulent premixed combustion in a diffuser burner exposed to various turbulence ıntensities and turbulence length scales. | *Published* | *Isı Bilimi ve Tekniği Dergisi, J. of Thermal Science and TechnologyTechnology*, vol. 38, no. 1, pp. 55–64. | 2018 |
| 4. | Influence of the turbulent flow characteristics on flame behaviour in a diffuser combustor. | Submitted to journal | Energy. | 2018 |
| 5. | Control of ame location for turbulent premixed flame. | Submitted to journal | Combustion Science and Technology. | 2018 |